11-1-2008

Polymer Supported Optical Biosensors

Ignacio Joseph Garcia
University of Denver

POLYMER SUPPORTED OPTICAL BIOSENSORS

_____

A Dissertation

Presented to

the Faculty of Natural Science and Mathematics

University of Denver

_____

In Partial Fulfillment

of the Requirements for the Degree

Doctor of Philosophy

_____

by

Ignacio Joseph Garcia

November 2008

Advisor: Todd A. Wells

Author: Ignacio Joseph Garcia
Title: POLYMER SUPPORTED OPTICAL BIOSENSORS
Advisor: Todd A. Wells
Degree Date: October 2008

ABSTRACT

The use of various polymer supports adhering phospholipid multibilayers to an internal reflection element have been investigated. The polymer supports studied range from polystyrene (PS), and 100 nm wide PS nanospheres to triethylaminated poly(vinyl benzyl chloride) (PVBC). The PS nanospheres showed the most promise as an adhesion layer since they appear to be the most robust with repeated washings. They also appear to stabilize their adjacent phospholipid multibilayer by increasing the lipid melting temperature. The triethylaminated DVBC also provided an increase of lipid melting temperature, but not quite to the same degree as the PS nanospheres. The cooperativity of such systems is much greater than without an adhesion layer. It is believed that in the case of PS nanospheres, a slight negative charge interacts with the polar head groups of the phospholipid multibilayer, thus leading to an increase in cooperativity. The triethylaminated DVBC is believed to interdigitate between the phospholipid molecules in a way such that the positively charged nitrogen atom interacts directly with the negatively charged phosphate group located on the phospholipid molecules, thus giving rise to its relatively high cooperativity and lower melting temperature than the uncharged polymers and nanobeads. The PS nanosphere polymer support was shown to be an effective platform for biosensors. Myoglobin based biosensors, using PS nanosphere supports, showed that myoglobin retains its native ligand binding ability.

Table of Contents

Figure List:

Equation List:

Table List:

Chapter 1: Introduction

1.0 Introduction
1.1 Biosensors

A general example of a *sensor* would be litmus paper for acids and bases. A qualitative indication of the presence of either base or acid is provided by a simple color change. Special indicator solutions can also provide a more precise indication of acidity or basicity. However, the most accurate method of measuring acidity is the use of a pH meter. [1]

The sensor is the part that responds to the degree of acidity. In the case of litmus paper, the sensor is the dye litmus. In the case of using indictor solutions, it is the indicator solution itself that provides the sensing element. Using a pH meter, the sensor would be the hydronium ion permeable glass electrode. [1]

In a sensor, the chemical or electrical response needs to be converted into a signal which can be analytically measured. The case with litmus is simple: a visible color change is observed. With a pH meter, the electrical response of the glass electrode needs to be *transduced* into a change in the digital display (or a movement of the needle in the case of more antiquated pH meter). The *transducer* is responsible for this conversion. [1]

A *biosensor* incorporates a recognition element that is biological in nature. This is known as a selective biological element (SBE) or also as a molecular recognition element (MRE). This recognition element needs to be connected to a transducer in order

to form an observable response. Biosensors are generally concerned with sensing and measuring particular chemicals which need not be biological components themselves, although sometimes they are. We shall usually refer to them as the substrate, although the more general term analyte is often used. Figure 1.1 shows schematically the general arrangement of a biosensor. [1]

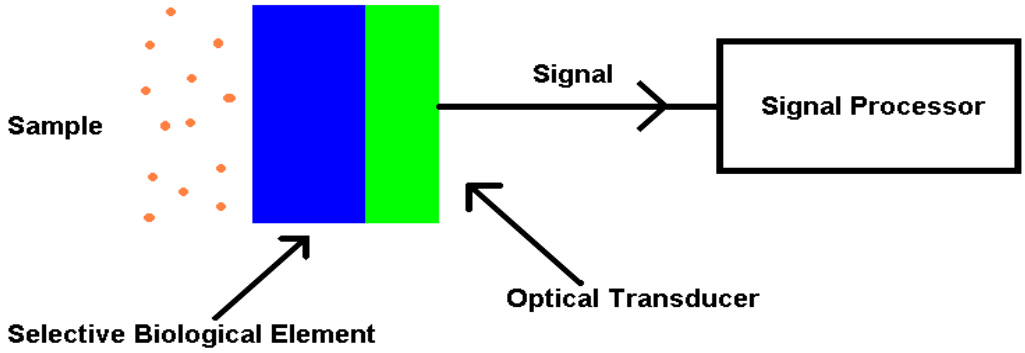

Figure 1.1 Schematic layout of a biosensor

Biological elements provide the major (selective) recognition element in biosensors. A good recognition element will bind only to an analyte of interest. Four main groups of materials can do this: [1]

(i) Enzymes.

(ii) Antibodies.

(iii) Nucleic acids.

(iv) Receptors.

Enzymes are proteins which catalyze specific chemical reactions *in vivo* [2]. Like all catalysts, they accelerate the rate of reaction of a particular substrate without being consumed in the process. Enzymes are found in all types of cells. A given cell will typically contain many hundreds of enzymes, though the exact distribution and quantity of enzymes present varies considerably according to the cell's natural function. The structure of individual enzymes varies immensely within the basic framework of a polypeptide structure and determines the catalytic role of the molecule. [3]

The two most important properties of any proposed biosensor are: (a) its specificity and (b) its sensitivity towards the target analyte(s). The specificity of a biosensor is entirely governed by the properties of the biological component because this is where the analyte interacts with the sensor. The sensitivity of the integrated device, however, is dependent on both the biological component and the transducer. In comparison with chemical sensors, an inherent advantage that can be exploited in biosensor technology is the significantly higher specificity that can generally be achieved as a direct result of biologically-optimized molecular recognition. [3]

The high specificity of biomolecules and biological systems with respect to intermolecular interactions of interest can be successfully exploited in biosensor devices only if there is highly efficient coupling between the biological and transducer components. The range of potential biological component and similar range of transducer technology available for use in biosensors necessitates a truly multi- and interdisciplinary approach to research and development in this area. [3]

Since relatively small changes in the conformation of key amino acids at the active site of enzymes can cause dramatic changes in enzymatic activity and substrate specificity, it follows that factors which influence protein structure and conformation will also influence the stability of enzymatic action – a property of significance with regard to biosensor applications. Denaturation is the term given to the process where enzyme activity is lost by largely irreversible disruption and perturbation of the secondary, tertiary, and quaternary protein structure. Denaturation can be caused by changes in pH, temperature and pressure, or exposure to UV radiation, detergents, organic solvents or certain chemicals such as urea or guanidinium salts. [3]

Isolation of enzymes and subsequent incorporation into an *in vitro* operating environment will generally result in a loss of some of the enzymatic activity and an increase in the Michaelis constant "K_m". However, this decrease in activity can be minimized by recreating suitable pH, temperature and co-factor conditions; this does tend to restrict the operating abilities of certain enzyme-based biosensors with respect to sample type. Though every enzyme has an optimum operating temperature and pH, it is possible to obtain acceptable rates of reaction and substrate specificities under conditions which permit greater flexibility of analysis conditions in a sensor format. [3]

Virtually any self-replicating biological entity can be discriminated on the basis of nucleic acid sequences unique to that particular organism. The most obvious exception are prions, which have no nucleic acid associated with them. For lower eukaryotes and prokaryotes, a number of different strategies have been explored to identify unique sequences, typically as a prelude to the development of an assay. These well-documented approaches justify the claim that an assay can be developed for virtually any organism

given a sufficient effort to identify specific sequences unique to the target organism. The challenge is to make these assays totally inclusive and thus make it recognize all potential biological variants. [4]

Antibodies are serum proteins which are produced by two types of blood cells, B lymphocytes and plasma cells, in response to a foreign substance. The foreign substance is termed an "antigen," so defined because it evokes an immune response. In most instances, an individual antibody will only recognize one particular substance; this substance is termed the "antigen." In biosensors based on antibodies, the analyte is either the corresponding antigen of the antibody used or a part of it – known as a "hapten". An antibody-antigen interaction is characterized by two major properties that may be exploited for sensing or detection purposes: [3]

(i) it has very high affinity constant; up to 10-18 M of antigen can be detected in certain laboratory assays based on antibodies (immunoassays); and

(ii) it has low cross-reactivity; relatively minor changes in the structure of a given antigen can render it almost invisible to an antibody produced in response to the original unmodified structure.

For this dissertation, the focus on receptors as a molecular recognition element is emphasized since myoglobin was used during the research phase. Molecular receptors are cellular proteins (often membrane-bound) which bind specific chemicals in a matter which results in a conformational change in the protein structure. [2] The conformational change triggers a cellular response, for example, opening an ion-channel or secreting an enzyme. In general, molecular receptors are distinct from receptors (which include larger

multi-component systems) on the basis of their composition, which is a single protein structure, though possibly containing more then one subunit. Among the important receptors found to date are receptors for hormones, amino acids, insulin, and neurochemical transmitters (which are able to bind synthetic bioactive chemicals such as drugs). [3]

Molecular receptors have two important properties relevant to their possible incorporation into biosensor devices, namely their intrinsic signal amplification properties and their high specificity. The former are a direct result of the biochemical consequences triggered by even a single receptor-ligand interaction. This may consist of the initiation of a flow of ions along a gradient or the production/consumption of cellular chemicals. Major limitations in the studies and use of molecular receptors are:

(i) the relatively difficult experimental procedures necessary to isolate the receptor proteins which are both time-consuming and expensive,

(ii) the inability, at present, to obtain more then very small amounts of pure receptor, and

(iii) the rapid loss of biological function which, in most cases follows isolation.

Molecular biology has enabled progress to be made in the first two areas while advances in artificial membrane technology and reconstitution are reducing the latter problem. [3]

A *transducer* is a device, usually electrical, electronic, electro-mechanical, electromagnetic, photonic, or photovoltaic that converts one type of energy or physical attribute to another for various purposes including measurement or information transfer.

The term transducer is commonly used to describe phases of signal transduction in two respects; the sensor, used to detect a parameter in one form and the device used reports it in another (usually an electrical or digital signal). [5]

In order to make a viable biosensor, the biological component needs to be properly attached to a transducer. This process is known as *immobilization*. There are five regular methods of doing this: [1]

(i) Adsorption

(ii) Microencapsulation

(iii) Entrapment

(iv) Cross-Linking

(v) Covalent Binding

Adsorption is the simplest method and involves the least preparation. However, since the bonding is weak this method is only suitable over a short lifetime. [1]

Early biosensors used *microencapsulation* as the mode for immobilization. Close contact between the biological element and the transducer was achieved through the use of a membrane. It is adaptable. The reliability of the biological element is retained. Contamination and degradation are limited. It is stable towards changes in temperature, pH, ionic strength and chemical composition. Materials such as small molecules, gas molecules and electrons can be permeable to particular membranes. [1]

A good example of this permeability may be a polyethylene membrane, which is permeable to oxygen. A cellulose acetate membrane is permeable to both oxygen and

glucose. For these reasons, both of these membranes were used in early glucose biosensors. [1]

With *entrapment*, the biomaterial is trapped when it is mixed with a monomer solution to form a gel. The barriers formed by polymerization can limit the diffusion of the substrate, thus slowing the reaction. Biological elements can also diffuse and escape through pores in the gel, thus resulting in a loss of bioactivity. The most commonly used gel is polyacrylamide, although starch gels, nylon and silastic gels have been used. Conducting polymers such as polypyrroles are particularly useful with electrodes. [1]

When using *cross-linking*, the selective biological element is chemically bonded to solid supports or to other supporting materials such as a gel. In this method, bifunctional reagents such as glutaraldehyde are used. Again there is some diffusion limitation and there can be damage to the biomaterial. Also, the mechanical strength is poor. It is a useful method to stabilize adsorbed biomaterials. [1]

One interesting application of *cross-linking* was to immobilize urease and penicillinase, as very fine films, directly on the sensitive ends of glass pH electrodes. A tyrosinase biosensor for polyphenols was made by pretreating the electrode by polymerizing pyrrole in 0.1 M tetraethylammonium sulphonate on the surface. The tyrosinase solution was then repetitively coated on the surface alternating with glutaraldeyde solution. This cross-linked the enzyme to the polypyrrole surface. [1]

Covalent binding involves a carefully designed bond between functional groups in the biomaterial to the support matrix. Nucleophilic groups in the amino acids of the biomaterials, which are not essential for the catalytic action of enzyme, are suitable.

Many examples are known. One example of this is as follows: a carboxyl group on the support is reacted with a carbodiimide. This then couples with an amine group on the biomaterial to form an amide bond between the support and the enzyme. [1]

The reaction must be performed under mild conditions: low temperature, low ionic strength, and neutral pH. The enzyme will not be lost from the biosensor during use with this method. [1]

Let us survey the more common range of optical techniques that could potentially be used in such sensors. Figure 1.3 shows the electromagnetic spectrum, showing the relative wavelengths of important types of radiation such as visible, ultraviolet and infrared.

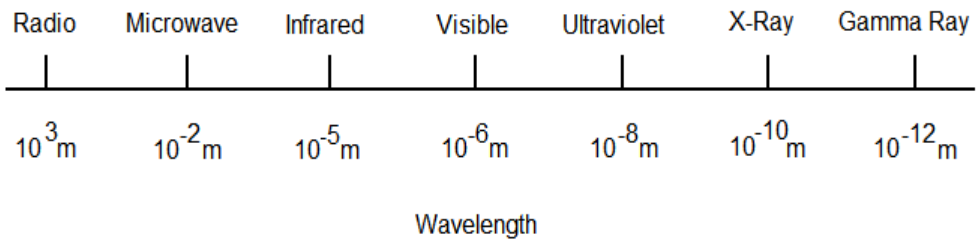

Figure 1.2 The electromagnetic spectrum

The main types of photometric behavior which have been exploited in biosensors are as follows: [1]

(i) Ultraviolet – visible absorption

(ii) Fluorescence (and phosphorescence) emission

(iii) Bioluminescence

(iv) Chemiluminescence

(v) Internal reflection spectroscopy (IRS)

(vi) Laser light scattering methods

The most widespread example of a commercial biosensor is the blood glucose biosensor. This particular biosensor uses an enzyme to break down blood glucose. In doing so it first oxidizes glucose and uses two electrons to reduce the FAD (a component of the enzyme) to $FADH_2$. This in turn is oxidized by the electrode (accepting two electrons from the electrode) in a number of steps. The resulting current is a measure of the concentration of glucose. In this case, the electrode is the transducer and the enzyme is the biologically active component. [1]

There are many potential applications of biosensors of various types [1]

- Glucose monitoring in diabetes patients
- Environmental applications e.g. the detection of pesticides and river water contaminants
- Remote sensing of airborne bacteria e.g. in counter-bioterrorist activities
- Detection of pathogens
- Determining levels of toxic substances before and after bioremediation
- Detection and determining of organophosphate
- Routine analytical measurement of folic acid, biotin, vitamin B12 and pantothenic acid as an alternative to microbiological assay
- Determination of drug residues in food, such as antibiotics and growth promoters, particularly meat and honey.

- Drug discovery and evaluation of biological activity of new compounds.

Fundamental studies in biosensor development can be divided into three fields – molecular recognition elements (MREs) (also known as selective biological elements [SBEs]), techniques and tools for biosensor construction, and basic biosensor devices. In the development of MREs, enzymes, microbes, antibodies, receptors, plant or animal cells, organelles, or tissues have been used. In addition, new MREs of engineered biomaterials such as enzymes, microbes, antibodies, antibody recognition elements, receptors and aptamers, etc., and of artificial materials such as peptide nucleic acids (PNAs) and molecularly imprinted polymers (MIPs) have been studied and applied to biosensor development in recent years. Current techniques and tools for biosensor construction, microfabrication techniques, including nanoscale fabrication, are most significant for miniaturization of biosensing chips or devices, because they enable reduction of cost by mass production, reduction of sample volume, etc. [6]

1.2 Myoglobin

Myoglobin was chosen as the selective biological element during this course of investigation because its ability to bind several analytes. Myoglobin is a single-chain globular protein of 153 amino acids, has a molecular weight of 16.7 kDa, and is responsible for the storage of diatomic oxygen in muscle tissue. [7] Each myoglobin protein molecule contains a single heme (iron-containing porphyrin) near its center, about which, the remaining apoprotein folds. Unlike hemoglobin, to which myoglobin is

structurally related, [8] myoglobin does not demonstrate cooperative binding of oxygen. Positive cooperativity is a property of multimeric/oligomeric proteins. Instead, the binding of oxygen by myoglobin is unaffected by the oxygen pressure in the surrounding tissue. The structure of myoglobin, by high-resolution X-ray crystallography, was determined by John Kendrew and associates in 1958.[9]

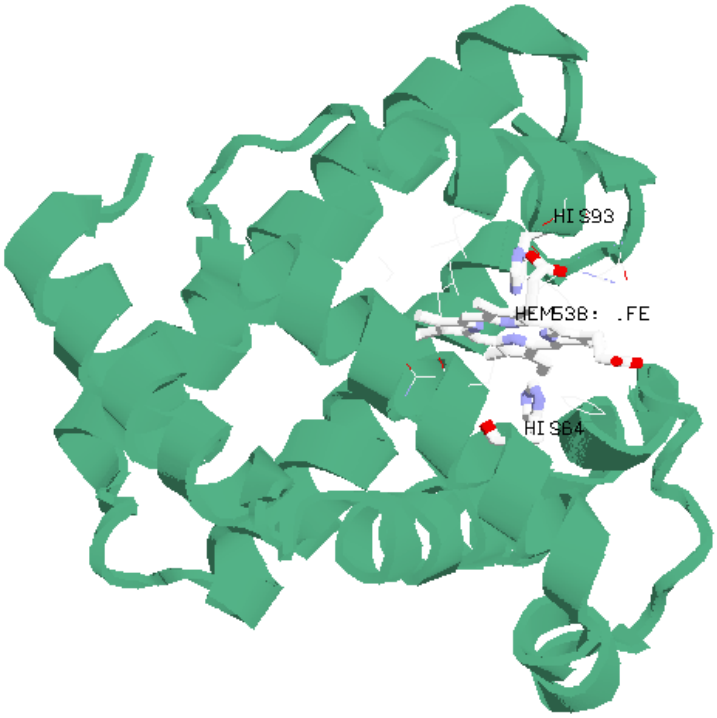

Figure 1.3: Myoglobin Structure

A porphyrin ring with an iron center is contained within myoglobin. A *proximal histidine* group is attached directly to the iron center, and a *distal histidine* group is present on the opposite face which is not bonded to the iron.

Many functional models of myoglobin have been studied. One of the most important is that of *picket fence porphyrin* by James Collman. This model was used to show the importance of the distal prosthetic group. As such, it serves three functions. First is that it forms hydrogen bonds with the dioxygen moiety, subsequently increasing the O_2 binding constant, while simultaneously preventing the binding of carbon monoxide. Carbon monoxide binds to iron in an end-on fashion, and is hindered by the presence of the distal histidine, which forces it into a bent conformation. Carbon monoxide binds to the heme 23,000 times better than O_2, but only 200 times better when incorporated into hemoglobin and myoglobin. Oxygen binds in a bent fashion, which corresponds well with the distal histidine. [4] Irriversible dimerization of oxymyoglobin with deoxymyoglobin species is also prevented by the distal histidine.

1.3 Lipids and Membranes

The lipid bilayer is the principal structural component of all biomembranes. The mimetic membrane is critical to biosensor design and molecular device development. Mimetic membrane-based biosensors have a number of practical advantages over other film systems. These are simplicity of construction, ease of modification, electrical methods of detection and fast response time. [11]

Lipids may be broadly defined as hydrophobic or amphiphilic small molecules that originate entirely or in part from two distinct types of biochemical subunits or "building blocks": ketoacyl and isoprene groups.[6] Using this approach, lipids may be divided into eight categories : fatty acyls, glycerolipids, glycerophospholipids, sphingolipids,

saccharolipids and polyketides (derived from condensation of ketoacyl subunits); and sterol lipids and prenol lipids (derived from condensation of isoprene subunits).

The glycerophospholipids are the main structural component of biological membranes, such as the cellular plasma membrane and the intracellular membranes of organelles. In animal cells the plasma membrane physically separates the intracellular components from the extracellular environment. All eukaryotic cells are compartmentalized into membrane-bound organelles which carry out different functions. These glycerophospholipids are amphipathic molecules that contain a glycerol core linked to two fatty acid-derived "tails" by ester or, more rarely, ether linkages and to one "head" group by a phosphate ester linkage. While glycerophospholipids are the major component of biological membranes, other non-glyceride lipid components such as sphingomyelin and sterols (mainly cholesterol in animal cell membranes) are also found in biological membranes.

A biological membrane is a form of lipid bilayer, as is also a liposome. The formation of lipid bilayers is an energetically-preferred process when the glycerophospholipids described above are in an aqueous environment. In an aqueous system, the polar heads of lipids orientate towards the polar, aqueous environment, while the hydrophobic tails minimize their contact with water. The lipophilic tails of lipids tend to cluster together, forming a lipid bilayer, or a micelle. Micelles and bilayers form in the polar medium by a process known as the hydrophobic effect. [12] Other aggregations are also observed and form part of the polymorphism of amphiphile (lipid) behavior. When dissolving a lipophilic or amphiphilic substance in a polar environment, the polar molecules (i.e. water in an aqueous solution) become more ordered around the dissolved lipophilic

substance, since the polar molecules cannot form hydrogen bonds to the lipophilic areas of the amphiphile. So in an aqueous environment the water molecules form an ordered "clathrate" cage around the dissolved lipophilic molecule. [12]

1.4 Infrared spectroscopy

Infrared (IR) spectroscopy is an information rich technique which can monitor the subtle selective molecular recognitions between biological molecules. Infrared spectroscopy was used extensively throughout the research conducted for this dissertation. For this reason, a general introduction into IR spectroscopy will be provided, as well as for Fourier-transform IR spectroscopy and attenuated total reflectance. All of which were techniques that were indispensable.

The infrared portion of the electromagnetic spectrum is divided into three regions. These regions are known as the near-, mid- and far-infrared, and are named as such for their relation to the visible spectrum. The far-infrared, approximately 10-400 cm^{-1} (1000–30 μm), lying adjacent to the microwave region, has low energy and may be used for rotational spectroscopy. The mid-infrared, approximately 400-4000 cm^{-1} (30–1.4 μm) may be used to study the fundamental vibrations and associated rotational-vibrational structure. The higher energy near-IR, approximately 4000-4000 cm^{-1} (1.4–0.8 μm) can excite overtone or harmonic vibrations. The names and classifications of these subregions are merely conventions. There are neither strict divisions based on exact molecular nor electromagnetic properties.

The infrared spectra of a sample are collected by passing a beam of infrared light through the sample. Examination of the transmitted light reveals how much energy was absorbed at each wavelength. This can be done with a monochromatic beam, which changes in wavelength over time, or by using a Fourier transform instrument to measure all wavelengths at once. From this, a transmittance or absorbance spectrum can be produced, showing at which IR wavelengths the sample absorbs. Analysis of these absorption characteristics reveals details about the molecular structure of the sample.

This technique works almost exclusively on samples with covalent bonds. Simple spectra are obtained from samples with few IR active bonds and high levels of purity. More complex molecular structures lead to more absorption bands and more complex spectra. The technique has been used for the characterization of very complex mixtures.

A net change in the dipole moment of a molecule during vibration or rotation must take place in order for that molecule to absorb IR radiation. Only in the presence of a net dipole can the oscillating electric field of the radiation interact with the molecule and cause a change in the amplitude of one of its vibrational modes. For example, the charge distribution around a molecule such as carbon dioxide is symmetric even though the oxygen atoms have a higher electron density then the central carbon atom. However, asymmetric stretching and bending modes result in a net dipole moment. Absorption of the radiation takes place when the frequency of the radiation exactly matches a natural vibrational frequency of the molecule. It should be noted that the symmetric vibrational modes found in CO_2 do not result in a dipole moment, and thus are not IR active. [13]

Homonuclear species such as O_2 or N_2 are completely symmetric about their covalent bonds. Since this is the case, no net change in dipole moment can occur during vibration or rotation. As a result, such compounds cannot absorb IR radiation. With these few exceptions, all other molecular species with covalent bonds absorb IR radiation. [13]

Only wavelengths greater then 100 μm have the energy required to trigger a change in a rotational level. The far-IR absorption of gases results in discrete, well-defined absorption bands since rotational modes are quantized. In liquids or solids, these well-defined lines are widened into a broad continuum due to intramolecular collisions and interaction. [13]

The energy differences between vibrational quantum states typically match that of the mid-IR region. Since there are numerous rotational energy levels for each vibrational level, the IR spectra of gases commonly consist of a sequence of narrowly gapped lines. However, since rotation is greatly constrained in liquids and solids, these discrete vibrational-rotational lines become somewhat broadened vibrational bands. [13]

Due to the great variety of vibrational and rotational modes among molecules, the relative position of an atom in a particular molecule is not fixed. For a simple molecules (diatomic or even triatomic molecules), it is straightforward to define the number and nature of such vibrations and assign an energy of absorption. An analysis of this type becomes impractical for molecules made up of a large number of atoms due to the great number of vibrating centers. A complete analysis must not only take into account the large number of vibrating centers, but the interactions between them as well. [13]

There are two basic types of vibrations. These are known as stretches and bends. A stretching vibration involves a constant change in the distance between two bonded atoms. Bending vibrations are distinguished by a change in the angle between two bonded atoms. There are four types of bends: scissoring, rocking, wagging, and twisting. These are shown schematically in Figure 1.5. [13]

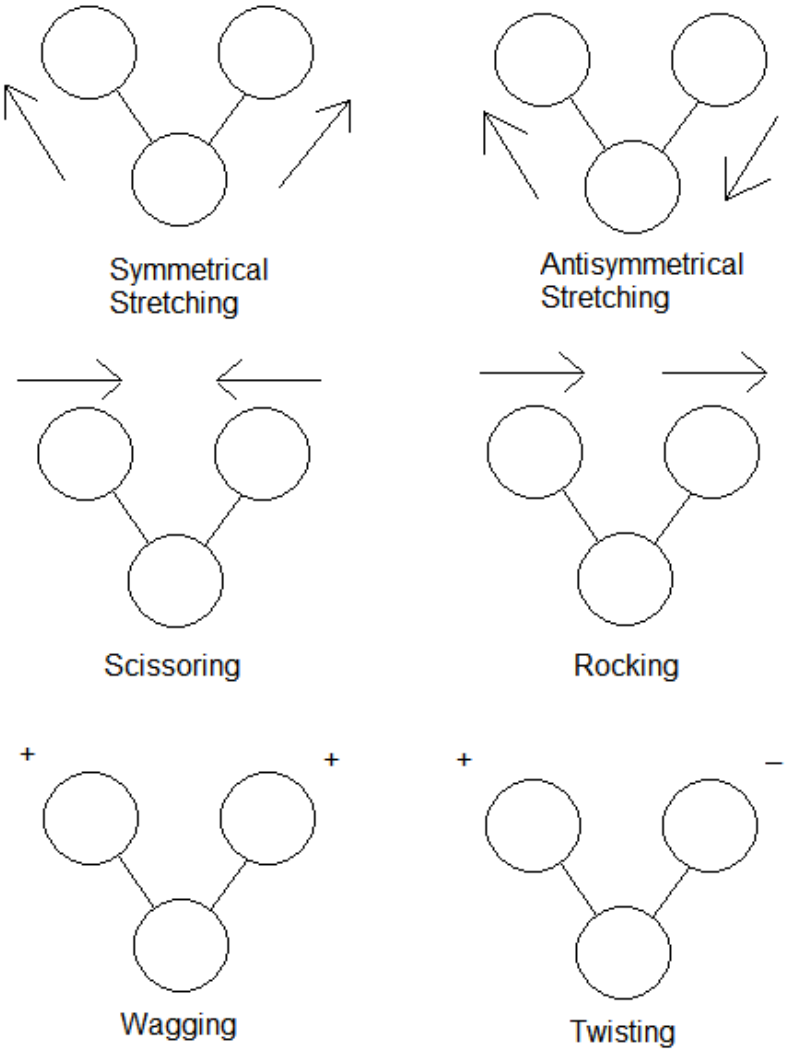

Figure 1.4: Types of Molecular Vibrations.

All six types of vibrations shown in Figure 1.4 are viable in a molecule containing three or more atoms. Furthermore, there can be interactions (or coupling of vibrations) that can occur if the vibrations involve bonds to a single central atom. The resulting change is characteristic of the comprised vibrations. [13]

A classic mechanical model approach, consisting of two masses connected by a spring, can approximate the characteristics of an atomic stretching vibration. A *simple harmonic motion* results from the movement of one of the masses along the axis of the spring. [13]

Let us consider *simple harmonic motion*. In this example, a single mass vibrates across a spring fastened to an immovable object. If the mass is displaced (from its equilibrium) a distance "y" along the axis of the spring by the employment of force, the restoring force "F" is then directly proportional to the displacement (Hooke's law). That is,

$$F = -ky \qquad \text{Eqn 1.4 - 1}$$

where "k" is the force constant, which has a value that depends on the rigidity of the spring. The more rigid the spring is, the higher is the value of "k." The negative sign signifies that "F" is a restoring force, meaning that the force is bringing the mass back toward equilibrium. [13]

When this system is at equilibrium, a value of zero can be assigned to the potential energy "E" of the mass and spring. As the spring is compacted or extended, the potential energy of this system is augmented by a quantity equal to the work required to

move the mass. Thus, if the mass is displaced from "y" to position "y + dy," the rise in potential energy "dE" is equal to the force "F" times the distance "dy." Thus, [13]

$$dE = -Fdy \qquad \text{Eqn 1.4 - 2}$$

Combining Equations 1.4-1 and 1.4-2 bears,

$$dE = ky\, dy$$

Integrating between the equilibrium position "y = 0" and "y" provides

$$\int_0^E dE = \int_0^y ydy$$

$$E = (1/2)\, ky^2 \qquad \text{Eqn 1.4-3}$$

As depicted in the following figure (fig. 1.5), the potential-energy curve for a simple harmonic oscillation (as derived from equation 1.4-3) is a parabola. The potential energy is at a maximum when the spring is stretched or compressed to its maximum amplitude, and decreases to zero as it approaches the equilibrium position. [13]

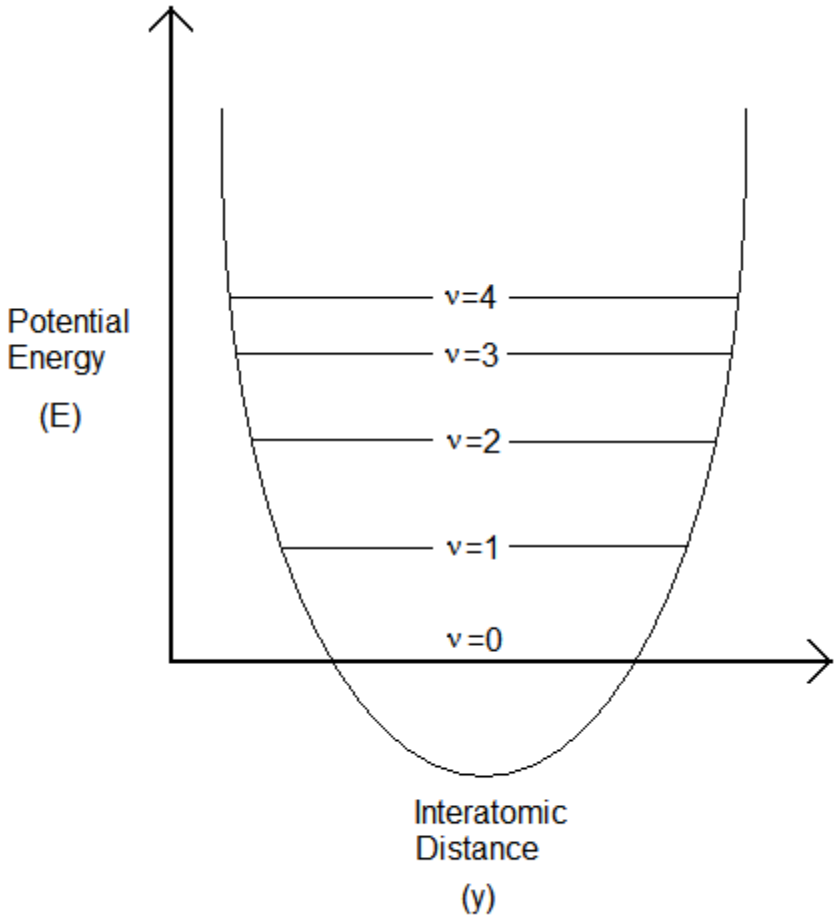

Figure 1.5: Potential-energy diagram

The motion of the mass as a function of time "t" can be reasoned from classical mechanics. Newton's second law states that force equals mass times acceleration:

$$F = ma$$

where "m" is the mass and "a" is its acceleration. However, acceleration is the second derivative of distance with respect to time. Hence,

$$a = \frac{d^2 y}{dt^2}$$

Substituting these equations into equation 1.4-1 provides [13]

$$m\frac{d^2y}{dt^2} = -ky \qquad \text{Eqn 1.4 - 4}$$

A cosine relationship, such that its second derivative is equal to the original function times "-k/m," is a solution to this equation. Thus, the displacement of the mass "y" at time "t" can be written as

$$y = A\cos 2\pi\nu_m t \qquad \text{Eqn 1.4 - 5}$$

where "ν_m" is the natural vibrational frequency and "A" is the maximum amplitude of the motion. The second derivative of equation 1.4-5 is

$$\frac{d^2y}{dt^2} = -4\pi^2\nu_m{}^2 A\cos 2\pi\nu_m t \qquad \text{Eqn 1.4 - 6}$$

Substitution of equations 1.4-5 and 1.4-6 into equation 1-4 gives

$$A\cos 2\pi\nu_m t = \frac{4\pi^2\nu_m{}^2 m}{k} A\cos 2\pi\nu_m t$$

The terms "A cos $2\pi\nu_m t$" then cancels out of each side of the equation, leaving the natural frequency of the oscillation as

$$\nu_m = \frac{1}{2\pi}\sqrt{\frac{k}{m}} \qquad \text{Eqn 1.4 - 7}$$

where "ν_m" is the natural frequency of the mechanical oscillator. It should be noted that though the natural frequency of the spring and mass depends on the force constant, the amplitude "A" independently changes as energy is imparted to the system. [13]

Equation 1.4-7 may be adapted to illustrate the behavior of a system of two masses "m_1" and "m_2" connected by a spring. It is necessary to substitute the reduced mass "μ" for the single mass "m" such that [13]

$$\mu = \frac{m_1 m_2}{m_1 + m_2} \qquad \text{Eqn 1.4 - 8}$$

Thus, the vibrational frequency for such a system is determined as

$$v_m = \frac{1}{2\pi}\sqrt{\frac{k}{\mu}} = \frac{1}{2\pi}\sqrt{\frac{k(m_1 + m_2)}{m_1 m_2}} \qquad \text{Eqn 1.4 - 9}$$

The classical mechanical equations provided for thus far do not completely describe the quantized behavior of atomic particles. The quantized nature of molecular vibrational energies, as well as other atomic and molecular energies, does not appear in classical equations. In order to compensate for this and develop the harmonic oscillator further, one must call upon the wave equations of quantum mechanics. Quantum mechanical solutions for these equations of potential energies have the form

$$E = \left(v + \frac{1}{2}\right)\frac{h}{2\pi}\sqrt{\frac{k}{\mu}} \qquad \text{Eqn 1.4 - 10}$$

where "*h*" is Planck's constant, and "*v*" is the *vibrational quantum number*. The vibrational quantum number can only have positive integer values (including zero). Thus, in contrast to classical mechanics where vibrators can assume a continuum of values, quantum mechanical vibrators can only take on certain discrete energy levels. [13]

Substituting equation 1.4-9 into 1.4-10, we find

$$E = \left(v + \frac{1}{2} \right) h\nu_m \qquad \text{Eqn 1.4 - 11}$$

where "ν_m" is the vibrational frequency of the classical model. [13]

The absorption of radiation results in the transition of vibrational energy levels. This can only happen when the energy of radiation exactly matches the difference in energy levels, "ΔE," between vibrational quantum states. Also, the vibration must cause a change in dipole moment. It should be noted that "ν" in equations 1.4-10 and 1.4-11 can only assume whole numbers, thus the difference in energy levels is always identical between pairs of adjacent levels, that is: [13]

$$\Delta E = h\nu_m = \frac{h}{2\pi}\sqrt{\frac{k}{\mu}} \qquad \text{Eqn 1.4 - 12}$$

Substituting "v = 0," since the majority of molecules are in the ground state at room temperature, from equation 1.4-11 provides: [13]

$$E_0 = \frac{1}{2} h\nu_m$$

Substituting "v = 1" into equation 1.4-11 corresponds to the energy from promotion to the first excited state:

$$E_1 = \frac{3}{2} h\nu_m$$

The energy of radiation required for such a transition is such that:

$$\left(\frac{3}{2} h\nu_m - \frac{1}{2} h\nu_m \right) = h\nu_m$$

As discussed above, the frequency of radiation "ν" used for such a transition is equal to the classical vibrational frequency of the bond "ν_m." This may be illustrated as follows:

$$E_{radiation} = h\nu = \Delta E = h\nu_m = \frac{h}{2\pi}\sqrt{\frac{k}{\mu}}$$

or,

$$\nu = \nu_m = \frac{1}{2\pi}\sqrt{\frac{k}{\mu}} \qquad \text{Eqn 1.4 –13}$$

Should we desire to express the radiation in wavenumbers, simply substitute into the following equation and rearrange:

$$\bar{\nu} = k\nu$$

$$\bar{\nu} = \frac{1}{2\pi c}\sqrt{\frac{k}{\mu}} = 5.3\times10^{-12}\sqrt{\frac{k}{\mu}} \qquad \text{Eqn 1.4 – 14}$$

where "$\bar{\nu}$" is the wavenumber of an absorption maximum (cm^{-1}), "k" is the force constant for the bond in Newtons per meter (N/m), "c" is the velocity of light in a vacuum ($cm\ s^{-1}$), and "μ" is the reduced mass (kg) defined by equation 1.4-8.[13]

1.5 Fourier Transform Spectroscopy

Fourier transform techniques of spectral detection and analysis are almost always used by modern spectrometers, especially those operating in the infrared. The core of a Fourier transform spectrometer is a *Michelson interferometer*, which is a device for analyzing the frequencies present in a composite signal. If the total signal from a sample

is like white light, then the Fourier transform of the signal is equivalent to the separation of the white light into its individual colors, or spectrum. [14]

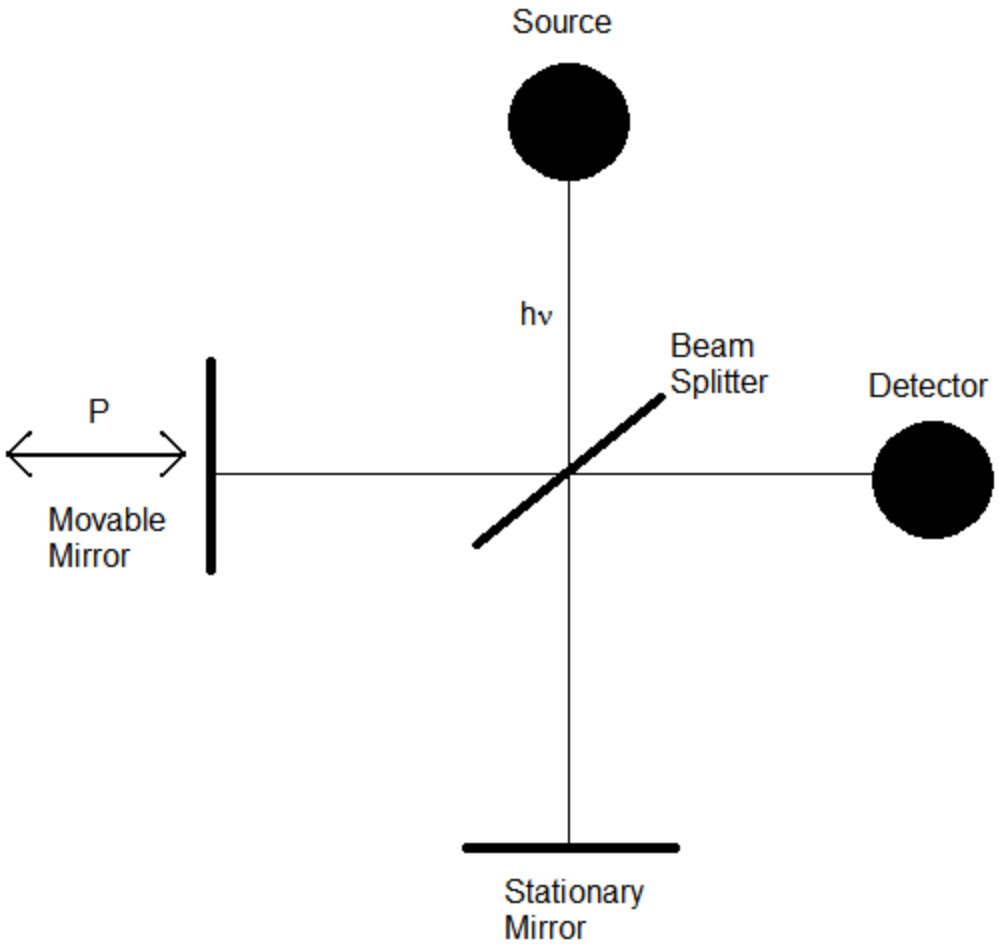

Figure 1.6: A Michelson Interferometer

A Michelson interferometer works by splitting the beam from the sample into two beams, while simultaneously introducing a varying path difference, "p", into one of the two split beams. When the two beams recombine, the resulting phase differences between them interfere either constructively or destructively depending on the difference in path lengths. The signal received by the detector oscillates as the two beams alternately come into and out of phase as the path difference is changed. Should the radiation have

wavenumber "$\bar{\nu}$", the intensity of the detected signal due to radiation in the range of wavenumbers from "$\bar{\nu}$" to "$\bar{\nu} + \mathrm{d}\bar{\nu}$", can be denoted: [14]

$$\mathrm{I}(p,v)dv = \mathrm{I}(v)(1+\cos 2\pi vp)dv \qquad \text{Eqn 1.5 – 1}$$

Thus, the interferometer translates the presence of a particular wavenumber component in the signal into a variation in intensity of the radiation reaching the detector. In actuality a signal is made of radiation extending a broad range of wavenumbers, and the total intensity at the detector, is the sum of all contributions from the wavenumbers present in the signal, and is denoted "I(p)." [14]

$$I(p) = \int_0^\infty \mathrm{I}(p,v)dv = \int_0^\infty \mathrm{I}(v)(1+\cos 2\pi vp)dv \qquad \text{Eqn 1.5 - 2}$$

The question is how to find "I(v)" which is the variation of intensity with respect to wavenumber, and is the required spectrum, from the recorded values of "I(p)." This step is a regular technique of mathematics, and is the 'Fourier transformation' step from which this type of spectroscopy takes its name. Specifically: [14]

$$I(v) = 4\int_0^\infty \{I(p) - \frac{1}{2}I(0)\}\cos 2\pi vpdp \qquad \text{Eqn 1.5 – 3}$$

"I(0)" is provided for by equation 1.5 – 2. The integration is executed on a computer interfaced to a spectrometer. The resulting output, also known as "I(v)," is the samples transmission spectrum. [14]

A key benefit of the Fourier transform process is that the whole of the radiation sent out by the source is overseen simultaneously. This is in distinction to a monochromatic spectrometer that disposes of most of the emitted radiation. Since this is the case, Fourier transform spectrometers are more sensitive then the now outmoded spectrometer models. The maximum resolution attainable is inversely proportional to the maximum path length difference, "p_{max}," of the interferometer: [14]

$$\Delta v = \frac{1}{2p_{\max}} \qquad \text{Eqn 1.5 - 4}$$

1.6 Attenuated Total Reflectance

Attenuated total reflectance (ATR) is a mode of infrared spectroscopy that can be used to study materials adsorbed on or forced down next to an optical surface. For this dissertation, the material is adhered to different optical surfaces through the utilization of phospholipid multibilayers. This technique is also appropriate for use with immunoassays. [1]

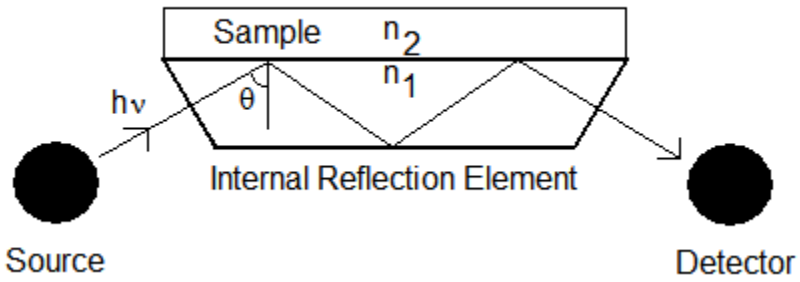

Figure 1.7: Attenuated Total Reflection

As soon as a photon reaches the interface of two media with two different refractive indices, here described as "n_1" and "n_2," then *total internal reflection* takes place when the reflection angle, "θ," is described as follows: (Snell's Law): [1]

$$\sin\theta_c = n_2/n_1 \text{ and } n_1 > n_2$$

Should $\theta > \theta_c$, where θ_c is the critical angle, there will be an *evanescent wave* that is refracted perpendicular to the interface ("Z" direction) which then passes through the second medium, "n_2," a penetration depth of "d_p," which has a length on the order of wavelength. The following equation shows how a waves electrical field vector, "E," is greatest at the interface, noted as "E_0,"and then exponentially decays along the length of the "Z" axis: [1]

$$E = E_0\exp(Z/d_p) \qquad \text{Eqn 1.6 - 1}$$

The penetration depth, "d_p," may also be associated to a number of factors in the following equation: [1]

$$d_p = \frac{\lambda / n_1}{2\pi\left[\sin^2\theta - \left(n_2 / n_1\right)^2\right]^{1/2}} \qquad \text{Eqn 1.6 – 2}$$

Observing equation 1.6 – 2 indicates that "d_p" diminishes in value in conjunction with an enlarging "θ" and also intensifies as "n_2/n_1" moves toward unity. Thus, one can decide on a value for "d_p" by selecting suitable quantities for "θ", "n_1" and "λ." [1]

The depth of penetration, "d_p," is the first of several aspects influencing the reflections attenuation. Additional factors include electric field intensity located adjacent to the reflecting surface, which is dependant on polarization; the size of the area used for sampling; and how well the two refractive indices match. The effective depth, "d_e," is determined from a traditional transmission experiment in which absorption due to the film thickness matches the absorption using ATR. [1]

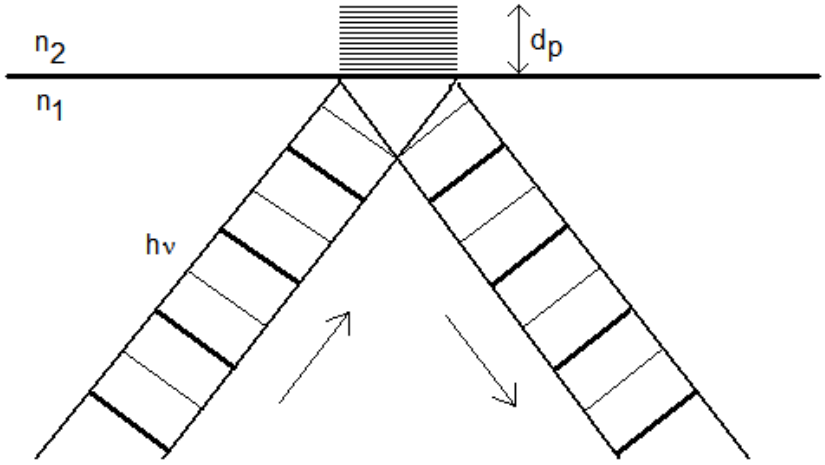

Figure 1.8: Generation of the evanescent wave at an interface between two optical media.

Multiple reflections are employed to augment the sensitivity of this type of system. The number of reflections is referred to as "N," and is a function of length "L," the thickness of the waveguide "T," and the angle of incidence "θ," and may be described as follows: [1]

$$N = (L/T)\cos\theta \qquad \text{Eqn 1.6 – 3}$$

"N" becomes larger as the waveguide becomes both longer and thinner. As a consequence of a larger "N," the evanescent wave will interact more repeatedly with the interfacing surface layer. Should "R" be the reflectivity, then the following equation may be invoked,

$$R = 1 - \alpha d_e$$

where the absorption coefficient is "α," and "d_e" is the effective depth. The following is then true for "N" number of reflections:

$$R^N \cong 1 - N\alpha d_e$$

This application of this equation is utilized in Chapter 4 where nine-reflection internal reflection elements are used. The materials used for the IREs are diamond, germanium and zinc selenide.

References:

1. Eggins, B. 1996. *Biosensors: An Introduction.* Chichester: John Wiley & Sons.
2. Leninger, A.L. 1977. B*iochemistry*, Second Edition. New York: Worth Publishers.
3. Abuknesha, R.A and Myfield, M.P., 1994. Biochemical Aspects of Biosensors. Biosensors and Bioelectronics 9: 373-400.
4. Iqbal, S.S, Mayo, M.W., Bruno, J.G., Bronk, B.V., Batt, C.A. and Chambers, J.P. 2000. A Review of Molecular Recognition Technologies for Detection of Biological Threat Agents. Biosensors and Bioelectronics 15: 549-578.
5. Allocca, J. and Stuart, A. 1984. *Transducers: Theory and Application*, Reston.
6. Nakamura, H. and Karube, I. 2003. Current Research Activities in Biosensors Anal Bioanal Chem 377: 446-468.
7. Ordway, G.A. and Garry, D. J. 2004. Myoglobin: an essential hemoprotein in striated muscle. Journal of Experimental Biology 207: 3441–3446.

8. Lodish, H., Berk, A., Zipursky, L.S, Matsudaira, P., Baltimore, D. and Darnell, J. 2000. Evolutionary tree showing the globin protein family members myoglobin and hemoglobin. Molecular Cell Biology. Fourth Edition, W. H. Freeman.

9. Kendrew, J.C., Bodo, G., Dintzis, H.M., Parrish, R.G., Wyckoff, H., and Phillips, D.C 1958. A Three-Dimensional Model of the Myoglobin Molecule Obtained by X-Ray Analysis. Nature 181: 662-666.

10. Collman, J. P., Brauman, J. I., Halbert, T. R., and Suslick, K. S. 1976. Nature of Oxygen and Carbon Monoxide Binding to Metalloporphyrins and Heme Proteins. Proceedings of the National Academy of Sciences of the United States of America 73 (10): 3333-3337.

11. Huang, W., Yang, X. and Wang, E. 2005. Mimetic Membrane for Biosensors. Analytical Letters 38: 3-18.

12. Wiggins, P.M. 1990. Role of Water in Some Biological Processes. Microbiol. Rev. 54 (4): 432-49.

13. Skoog, D, Holler, F.J. and Crouch, S. 2007. Principles of Instrumental Analysis. 6th ed. Thomson Brooks/Cole Publishing

14. Atkins, P., 1998. Physical Chemistry, 6th *ed. Oxford: Oxford University Press.*

Chapter 2: Formation of polymer cushioned lipid films

1.0 Introduction

1.1 Supported Lipid Membranes

1.1.1 Types of Layers

1.1.1.1 Monolayers

Monolayers come in *heads-up* and *heads-down* varieties (see Figure 2.1). *Heads-down monolayers* are prepared by using the Langmuir-Blodgett technique. In this technique, a hydrophilic support surface is withdrawn from the aqueous subphase of a trough up through a lipid *monolayer* at the air-water interface into the air. The ensuing preparation contains phospholipid headgroups, which are adjacent to the support surface. These phospholipids are arranged such that the hydrophobic tails are open to the air. [1, 2] In order to prepare the other, or *heads-up* variety of monolayers, either a hydrophobic support is required, or a hydrophilic support that has been treated with alkyl-silane. The heads-up *monolayers* are prepared using the Langmuir-Blodgett technique in one of two ways: either the support is dipped through a lipid *monolayer* at the air-water interface, or the support surface is applied flat onto a monolayer at the air-water interface. [3]

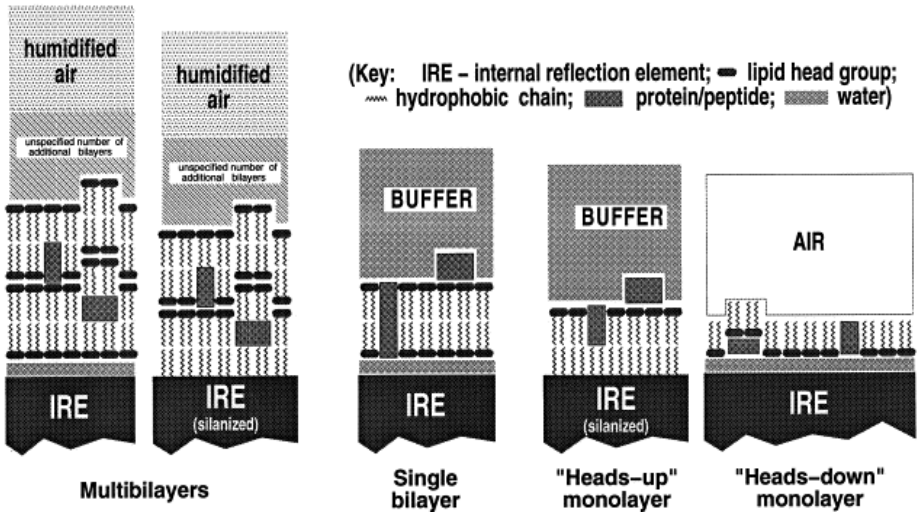

Figure 2.1: "Schematic illustration comparing the structures of supported multibilayers, single bilayers and monolayers." [3]

Monolayer preparations have several unique advantages. The primary advantage is the ability to control membrane pressure. This is to contrast *multibilayers* or *bilayers*, where there is no control over lipid surface pressure. When examining the thermodynamics of membrane insertion, the ability to control the lipid pressure is also an advantage. A third advantage to *monolayer* preparation versus bilayers is that highly active membrane peptides tend to disrupt supported bilayers. Due to the covalent linkages attaching the alkyl-silane to the hydrophilic support, *monolayers* tend to resist disruption. This then permits the study of how peptides interact with the outer half of the *monolayer*. Additionally, the preparation of *monolayers* is a swift process. A description of monolayer preparations may be found in Figure 2.2. Also, there is no uncertainty about the thoroughness of support surface coverage, nor its topology. The buffer phase composition neighboring the membrane can also be manipulated, and non-lipid constituents may be introduced to membranes from this buffer phase. [3]

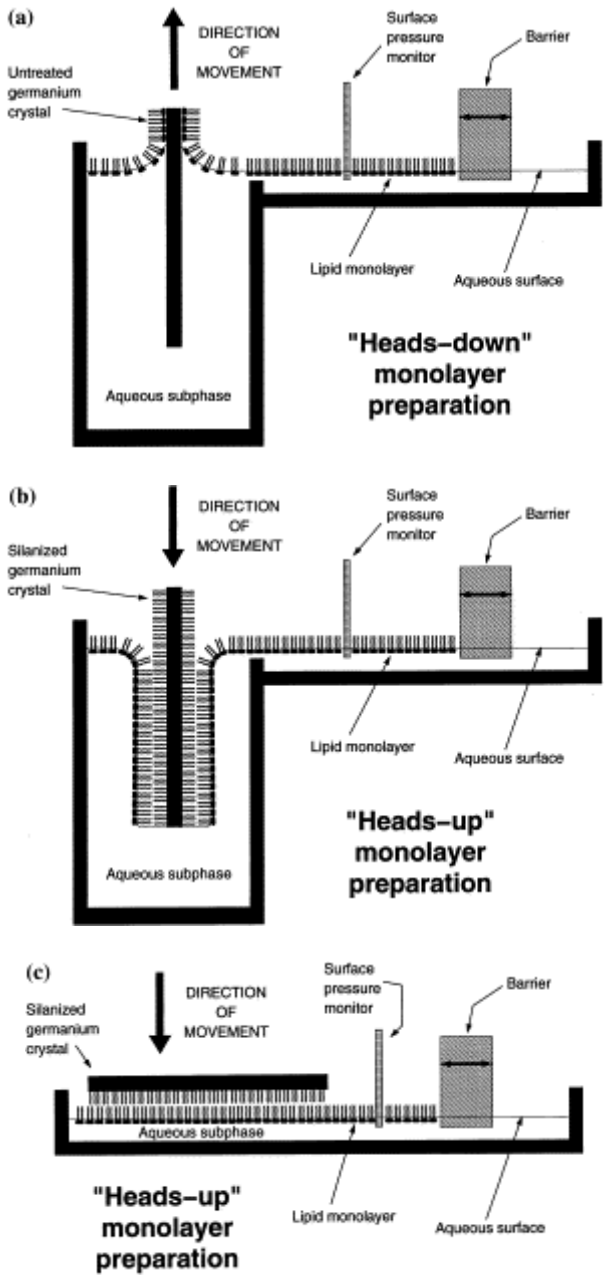

Figure 2.2: "Monolayer preparation using Langmuir-Blodgett techniques (a, b) and application of a flat hydrophobic crystal to the surface of a Langmuir trough (c)." [3]

The major disadvantage to heads-up *monolayers* is the cost and complexity of the instrumentation involved in such procedures. A custom and integrated trough is required for the formation of monolayers, thus making the Langmuir trough a necessity. [4] The inability to study transmembrane proteins is also another disadvantage. [3]

1.1.1.2 Single Bilayer

Supported *bilayers* are also prepared by first applying one *monolayer* to a support surface by means of the Langmuir-Blodgett technique as discussed above. It is not possible to add a heads-up *monolayer* by re-immersion into the trough. When the layers are composed of ordinary phospholipids, adhesion of the first monolayer to the support surface is not sufficient. Re-immersion also typically disrupts the first *monolayer* resulting in the failure for the second monolayer to apply. [3]

Adding a second monolayer can be achieved by exposing a *heads-down monolayer* preparation into a suspension of unilammelar lipid vesicles. After excess vesicles have been washed away, these vesicles will fuse spontaneously to produce highly ordered single bilayers. [5, 6] Some success can come by fusing whole vesicles composed of zwitterioinic lipid directly to a hydrophilic support surface [5, 7]. Utilizing the presence of divalent cations, vesicles composed of anionic lipids can be fused directly to hydrophilic supports. [3]

An important issue for single *bilayers* is how well it is covered by the second monolayer. This issue is important since one cannot use spectroscopy to distinguish whether materials are binding to the membrane surface, or to the uncovered patches. A

minor number of adherent unfused vesicles remain in these types of preparations, [5] though the end result depends on technique. [3]

There are several advantages of single *bilayer* preparation versus *multibilayer* preparation. The principle advantage is having the ability to control the buffer phase composition that is located adjacent to the membrane. Another key advantage is having the ability to introduce non-lipid components to the preformed bilayer membrane from the buffer phase. Some unnatural structural features from *multibilayer* preparations are removed under these conditions. The electrostatic double-layer is also preserved. The lateral diffusion rate of both monolayers of a supported bilayer membrane is nearly normal [8-11]. It is presumed that the pressure of the second half of the *bilayer* is in equilibrium with that of vesicles. Non-lipid components can be added to vesicles prior to fusion, in which case they are incorporated into the supported *bilayer*. However, the resulting transmembrane segments of such non-lipid components should be examined thoroughly. [3]

There are a few disadvantages to consider for the single *bilayer* technique. For each preparation the coverage of the support surface needs to be confirmed, which is a difficult process. It is also difficult to confirm that all unfused lipid vesicles have been washed away. In addition, it is difficult to determine whether there is equilibrium between the surface pressure and the pressure of the vesicles. For studies involving time restrictions, the formation of the second half of the bilayer requires 1-2 hours time. Finally, for proteins with large hydrophilic domains oriented toward the substrate, there may not be enough water between the membrane and substrate surfaces to demonstrate native structure or properties. [3]

1.1.1.3 Multibilayers

Multibilayers are multiple sheets of coplanar bilayers stacked one on top of another. They may be formed on either hydrophobic or hydrophilic surfaces. This can be done in one of two ways: either an aqueous suspension of lipid vesicles is evaporated [12-19], or an organic solution of lipid monomers is evaporated [20]. Such a preparation consists largely of stacked *bilayers* immediately upon evaporation; however, better bilayer characteristics are demonstrated by re-hydrating the preparation [21]. This is easily done by equilibrating the samples with an atmosphere of high relative humidity. [3]

The major advantage of *multibilayers* is their ease of preparation. Other then a basic internal reflection element to form the *multibilayers on*, no special equipment is required. Also, non-lipid components may be readily incorporated into the membrane before evaporation takes place to form the *multibilayers*. Thirdly, solid-state NMR may be used to study the same *multibilayers* [22-24]. The final advantage is beneficial for kinetic studies since H_2O and D_2O vapor readily equilibrates with exchangeable protons throughout a formed *multibilayer* [25].

Multibilayers do have several distinct disadvantages. Among these include whether or not normal bilayer structure is preserved in the region immediately surrounding any non-lipid components. Another possibility is that kinetically or thermodynamically improbable protein conformations may arise by adding components prior to evaporation as compared to when the same matter is added to preformed *bilayers*. Added components may also produce local structures of a non-bilayer motif. All of these

disadvantages are of particular concern when surface-associated proteins interact together with two adjacent membranes. Additionally, there are a few factors that cannot be known about *multibilayers*. These three-fold factors include the concentrations of various components in the aqueous phase, whether the *multibilayer* has uniform composition, or even whether or not the surface tension of the *multibilayer* membrane is analogous to that of a vesicle or cell membrane. [3]

1.1.2 Support Materials

1.1.2.1 Black Lipid Membranes

The term *black lipid membrane* (or BLM), which is illustrated in Figure 2.3, originates from this type of membranes appearance during optical microscopy. When first observed from extracted brain lipids [26, 27], interference bands were noticed, thus providing for the color of the membrane. It is believed that when this interference-effect vanishes during thinning signifies the formation of a single bilayer membrane as shown in Figure 2.3 [28]

There are several modes to produce BLMs. All modes require the membrane to be developed over a small aperture, usually between 100 μm and 1 mm in diameter. The aperture is prepared from hydrophobic materials and is usually part of a barrier separating two reservoirs. These reservoirs can then be filled with aqueous solutions, each with their own reference electrode. Of the several modes that exist, there are two popular modes of BLM formations. The first mode entails the painting of a lipid solution over an aperture. The second entails the formation of a folded bilayer [29]. Both modes result in two aqueous reservoirs separated by a suspended bilayer [28].

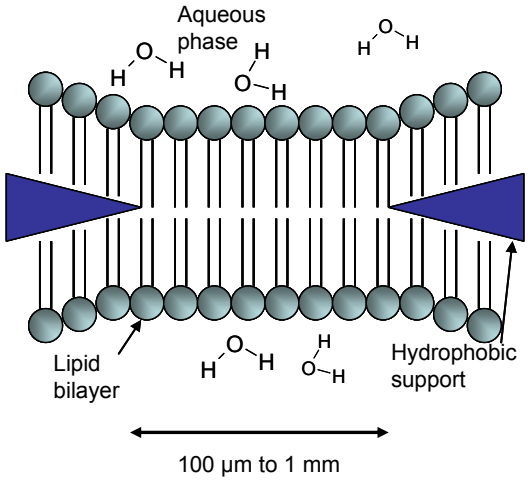

Figure 2.3: "Illustration of a black lipid membrane." [28]

A small artists' paintbrush is used to paint BLMs. While under aqueous solution, a solution of organic solvent containing 1% - 2% phospholipid is painted across an aperture. The accumulated lipid mass then spreads out and thins, forming the BLM. This methodology has been used unchanged for the most part, since the 1960s [26].

Creating a BLM using folded lipid bilayer requires a chamber in which two compartments are separated by a small aperture. The solution levels in each compartment must be controlled independently. Both compartments are filled with a desired aqueous solution, and then a monolayer of phospholipid material is spread on top of one of the compartments. The solution containing the lipid monolayer is then slowly lowered below the aperture and then elevated again to a level above the aperture. Upon each pass of the aperture, one monolayer is deposited, thus among two passes a complete bilayer membrane is formed. [29]

1.1.2.2 Solid Supported Lipid Bilayers

Solid supported phospholipid bilayers are more robust then BLMs. An illustration of *solid supported phospholipid* bilayers may be found in Figure 2.4. Solid supports also invite the use of surface specific analytical techniques that cannot be used for BLMs. The fluidity of such a solid supported membrane is maintained by a 1 -2 nm layer of water which is trapped between the substrate and the bilayer as seen in Figure 2.4 [30, 31].

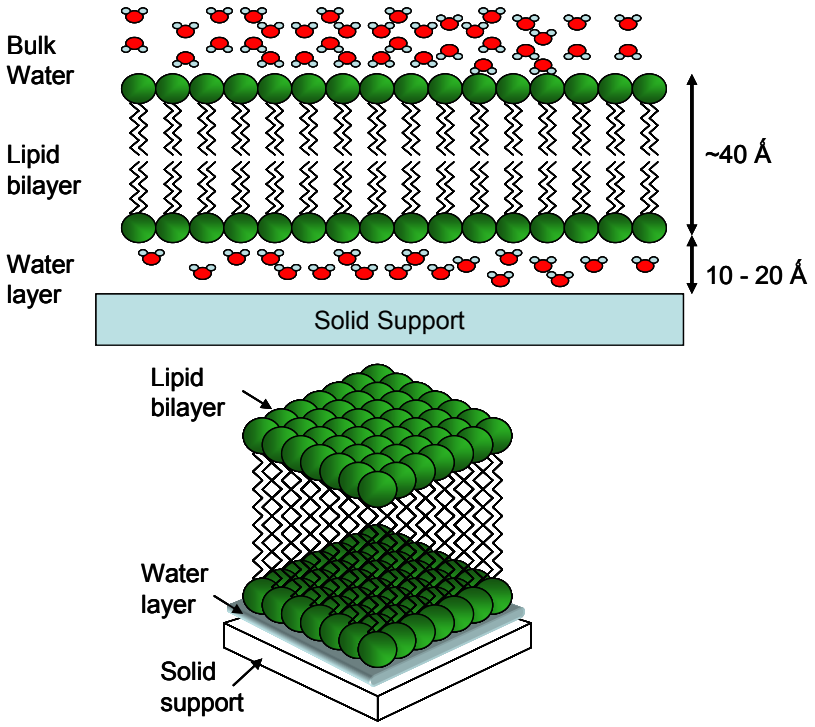

Figure 2.4: "Schematic Diagram of Solid Supported Bilayers." [28]

The selection of substrates with the ability of supporting phospholipid bilayers is limited to a certain extent. In order to produce a high quality membrane that contains

little to no defects, while retaining high lipid mobility, the substrate surface should be hydrophilic, smooth and clean. Fused silica, borosilicate glass, mica and oxidized silicon are among the best substrates [28].

As far as biosensor applications are concerned, there are three principle modes for the formation of supported phospholipid bilayers on planar supports. The first mode involves the combination of two techniques: first is the Langmuir-Blodgett technique followed by the Langmuir-Schaefer technique. First a lower leaflet of lipids is transferred from the air-water interface as per the Langmuir-Blodgett technique. This is then followed by the transfer of an upper leaflet by horizontally immersing the substrate to create the second layer (Figure 2.5a) [30]. The adsorption and fusion of vesicles from aqueous solution to a substrate surface (Figure 2.5b) constitutes the second mode of supported bilayer formation [32, 33]. The third mode also involves a combination of techniques. A monolayer of phospholipid is prepared using the Langmuir-Blodgett technique, which is then followed by the fusion of vesicles to form the top half of the bilayer (Figure 2.5c) [34].

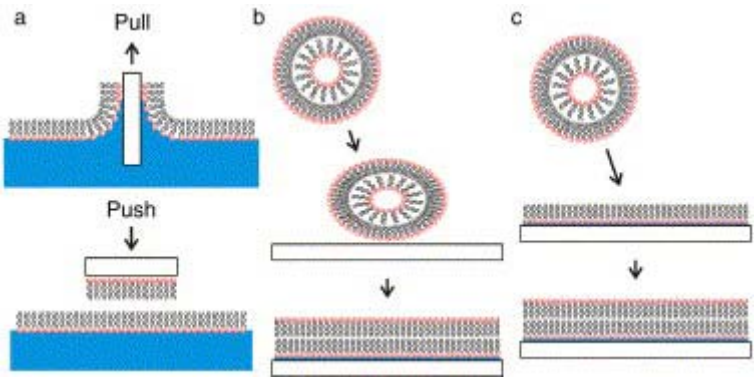

Figure 2.5: "Common techniques for the formation of supported lipid bilayers. (a)The Langmuir-Blodgett technique is carried out by pulling a hydrophilic substrate through a lipid monolayer and sequentially pushing it horizontally through another lipid monolayer. (b) Vesicles in solution adsorb and spontaneously fuse to the surface to form a solid supported lipid bilayer. (c) A combination of the Langmuir-Blodgett and vesicle fusion processes." [28]

Each of the three modes of deposition has its own specific advantages and disadvantages. The transfer of amphiphilic molecules from the air-water interface to a solid substrate dates back nearly a century [35]. Though this method is useful to development asymmetric bilayers [36], it is challenging to integrate transmembrane proteins into such a bilayer, if it is even achievable at all. The reason that this may be unachievable is that with this technique, segments of the protein within the monolayer are uncovered and left revealed to the air during transfer where they may be rendered permanently denatured [34], thus leaving the protein useless.

A simple and adaptable mode of producing *solid supported phospholipid bilayers* has to do with the adsorption and fusion of *small unilaminar vesicles* (or SUVs) on to

solid supports. These SUVs can actually be prepared by any number of different ways. In the first mode, the extrusion of *multilaminar* vesicles takes place through a porous polycarbonate membrane that is exposed to high pressure [37-40]. The second mode requires the sonication and ultracentrifugation of an aqueous lipid suspension [41]. The next mode of operation after forming the SUVs would be to use a gentle process, such as detergent removal by dialysis, to incorporate transmembrane proteins into SUVs. Many factors such as cleanliness, ionic strength, osmotic pressure, pH, size, surface charge, surface roughness and vesicle composition all affect the adsorption and fusion of SUVs to solid supports [44, 45]. Initially, vesicles from the bulk solution will adsorb onto the substrate and eventually these vesicles fuse with each other [45]. The process of how the vesicles rupture and fuse to the substrate forming planar supported bilayers depends on the individual chemistries of the lipids [46]. It should be noted that the presence of divalent cations, such has Ca^{2+} and Mg^{2+}, accelerate adsorption [36]. There are three known ways of enhancing fusion of SUVs [47]. These thee modes are: heating of the preparation; creating an osmotic gradient across the vesicle membrane [44]; and the addition of fusigenic agents such as polyethylene glycol [48]. Mathematical modeling of bilayer formations has agreed well with experiments despite the fact that the mechanism of bilayer formation due to the adsorption and fusion of SUVs is not fully understood [49].

Supported phospholipid bilayers can be also be made from a combination of vesicle fusion and Langmuir-Blodgett monolayer transfer [34]. In this mode, SUVs are fused to an already deposited monolayer of phospholipid. Asymmetric bilayers are readily formed using this method. [50] Also, the insertion of transmembrane proteins into solid supported bilayers is readily achieved. [34]

1.1.2.3 Self-Assembled Monolayers (SAMs)

A well-defined hydrophobic surface is provided for by methyl-terminated alkanethiols on gold. This assists in the formation of a *hybrid bilayer membrane* [51-53]. The *hybrid bilayer membrane* is simply composed of a metal (typically gold) supported alkanethiol SAM and a monolayer of phospholipid [54]. This is illustrated in Figure 2.6.

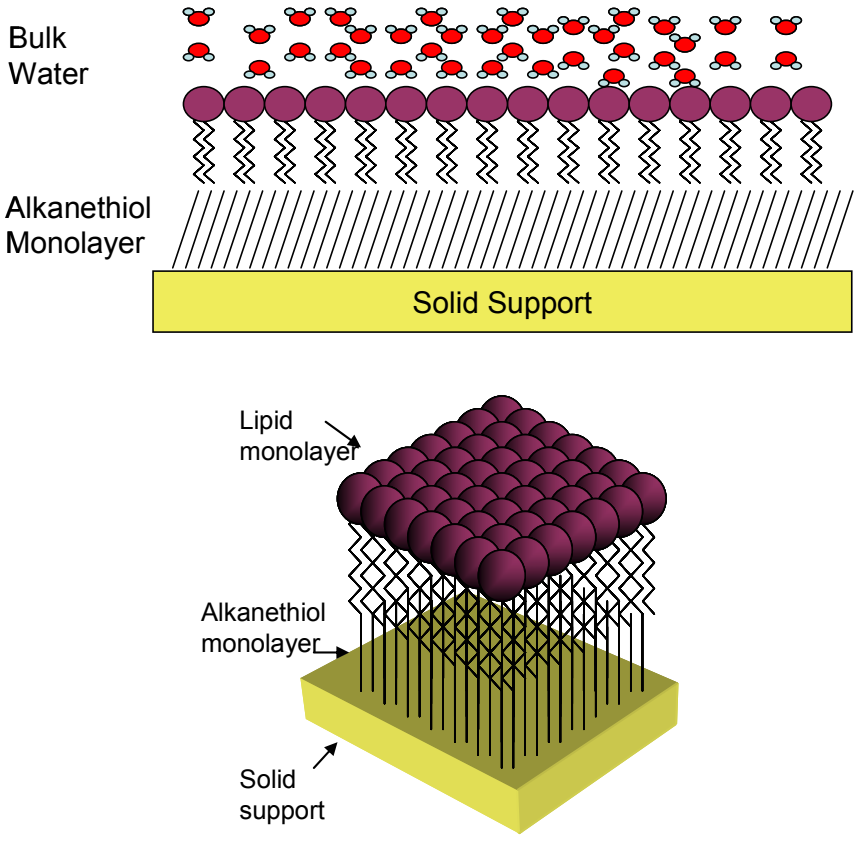

Figure 2.6: "Schematic illustration of a hybrid bilayer." [28]

Hybrid bilayer membranes can be formed any number of ways using a range of alkanethiols that self-assemble on gold surfaces. Octadecanethiol is a popular choice for producing the alkanethiol layer because it has the ability to form closely packed and well-ordered monolayers. Other methods exist for alkanethiol layer production, including one that requires a Langmuir-Blodgett transfer. However, there are two basic modes for producing the phospholipid leaflet to an alkanethiol SAM surface. These two modes are vesicle fusion and lipid transfer from an air-water interface. Lipid transfer from an air water interface requires horizontal transfer using a Langmuir trough. [28]

Hybrid bilayer membranes can also be formed from the fusion of ghost cells to alkanethiol SAMs [55 - 57]. Some of the contents of a cell membrane can be reconstituted from ghost cell fusion onto a sensor platform. Natural mixtures of proteins, lipids, receptors, as well as cellular membranes from genetically modified cells may well be studied using this type of procedure. However, since transmembrane proteins cannot penetrate further then the alkanethiol SAM, it is not apparent how they interact with this type of surface [34].

The use of various alkanethiols, lipids, and membrane additives such as sterols and proteins can alter the physical properties of a *hybrid bilayer membrane*. The properties of *hybrid bilayer membranes* can also be changed by altering the composition of the vesicles used to form the lipid layer. Investigations of binding kinetics and multivalent interactions can be enhanced by the incorporation of ligand-conjugated lipids into the membranes. [34]

Studying active peptides and transmembrane proteins with small or nonexistent peripheral domains facing the electrode requires only a slight modification of the

underlying SAM layer. Ethylene oxide spacer units at the base of the alkanethiol can be used to accomplish this [58].

Choosing a *hybrid bilayer membrane* platform for sensor applications has several advantages. The primary advantage is the direct coupling of a metallic surface to the phospholipid monolayer which allows for the detection of non-labeled analytes by direct electrical measurement [59], surface plasmon resonance [51], or quartz microbalance detection [60]. Due to the strong interactions between the alkanethiol SAM layer and the underlying substrate, hybrid phospholipid membranes are often more stable than *solid supported lipid bilayers.* When formed using an air-water interface, at least some of their original physical and chemical properties remain despite the fact that they may have dried and rehydrated after formation [61].

Though the inflexibility and close packing of the underlying alkanethiol SAM layer provides many benefits, there are also certain constraints based on this type of system. A normal leaflet of phospholipid bilayers is usually more flexible in structure then a rigid alkanethiol SAM layer [57]. This results in an environment that is less fluid for *hybrid bilayer membranes*. The packing density of the underlying SAM layer can also have consequences in the insertion of proteins [57], thus hindering the proper functioning of a protein. Clearly, *hybrid bilayer membranes* cannot easily contain transmembrane proteins with both large extra- and intracellular domains. [34]

1.1.2.4 Planar Supported Lipid Bilayers

Phospholipid vesicles self-assemble on solid supports (typically glass) into fluid planar bilayers [61]. As with *solid supported lipid bilayers* discussed above, the lateral

fluidity associated with lipid membranes in vesicles and in living cells is retained in the lipid molecules in *planar supported lipid bilayers*. Furthermore, if the appropriate components are present, the *planar supported lipid bilayers* mimics a true cell membrane because living cells recognize components displayed on the surface of *planar supported lipid bilayers* [62]. Again, as with solid supported lipid bilayers, there is a thin layer of water is trapped between the support and the headgroups of the lower leaflet of the bilayer [64]. This water layer is approximately 1-2 nm thick. The water maintains the lateral fluidity of both leaflets of the membrane by providing a lubricating layer. A poorly understood combination of hydration, van der Waals and electrostatic forces traps the bilayer at the surface. The planar supported bilayer is stable for an indefinite period as long as the entire system remains hydrated. [62]

1.1.2.5 *Polymer Cushioned Lipid Bilayers*

Solid supported phospholipid bilayers, as seen in Figure 2.7, and *hybrid bilayer membranes* have difficulty imitating the appropriate environment for transmembrane proteins, particularly those proteins which portray large peripheral domains [63]. Adequate mobility of the lipid molecules is provided for by a 1-2 nm thick water layer that exists between the solid support and a phospholipid bilayer [30, 31]. However, if the transmembrane protein contacts the substrate at any point, it will not be protected by the underlying layer of water and may denature or become immobilized. The motivation for the development of polymer supported bilayer systems is the desire to properly imitate the innately complicated nature of two-dimensionally fluid plasma membranes [63].

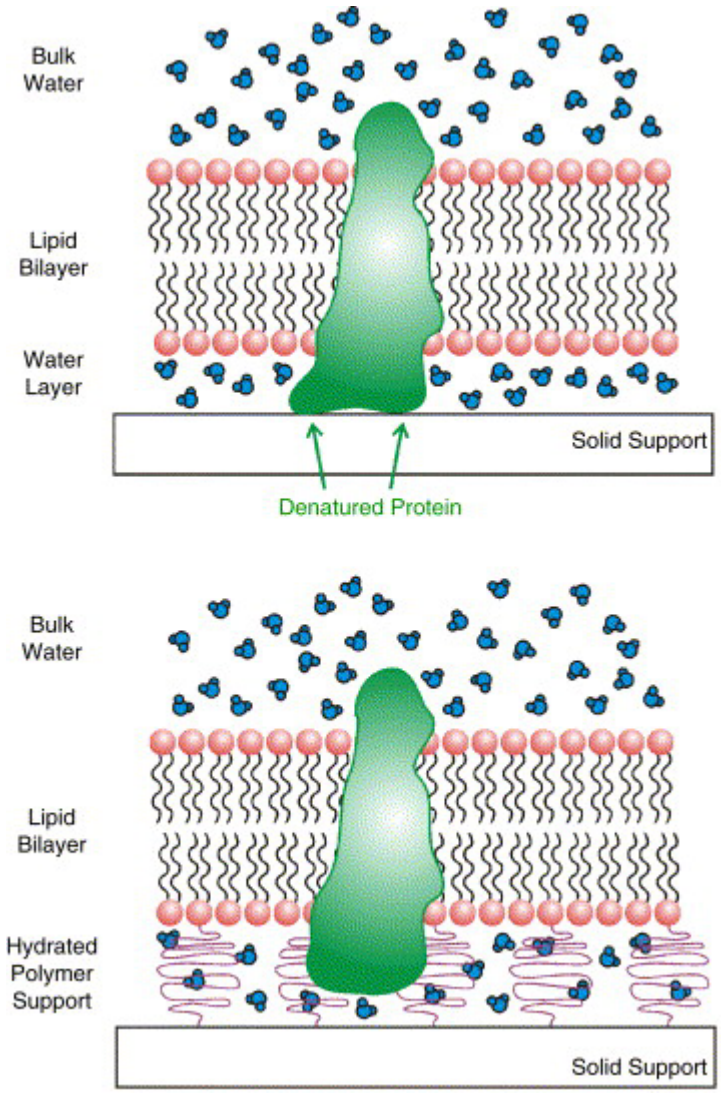

Figure 2.7: "Polymer Supported Bilayer: Peripheral domains of transmembrane proteins can become immobilized and denatured on a solid support. A polymer cushion helps shield the protein from the substrate." [28]

Including polymer layers to a membrane system permits the investigation of transmembrane proteins by a range of surface techniques while simultaneously decoupling the membrane from the surface. According to theory, transmembrane proteins should resist nonspecific adsorption into these systems. Another potential advantage of

polymeric supports is the ability to avoid nonspecific adsorption of aqueous proteins from solution which characteristically happens at defect sites in *solid supported lipid bilayers* which do not have polymer cushions. [28]

The well-defined shape of erythrocyte cells is due to the cellular membrane being supported by the cytoskeleton, which also happens to support the lipid bilayer. A sound polymer cushion motif should function much like a cytoskeleton. The balancing of surface forces requires careful consideration for the fabrication of the support system [67]. An unstable system may result in physisorbed systems where there are only weak interactions between the polymer support and phospholipid bilayer. This may be overcome by taking a few steps. First would be the covalent binding of the polymer layer directly to substrate. Next, either anchor lipids or alkyl side chains capable of inserting into the phospholipid bilayer, are used to tether the underlying polymer layer to the membrane. It would be advantageous for the polymer support to be not extensively cross-linked, nor too highly charged, hydrophilic as well as soft [64].

A number of types of polymer cushions have been explored for supporting phospholipid bilayers. Two classes of polymers are emerging as the prevalent choice for cushion materials: polyelectrolytes and lipopolymers. Polyelectrolyte material can be directly adsorbed from solution by means of layer-by-layer deposition to a diverse assortment of substrates. This provides a good way to manage the resulting film thickness. On metallic surfaces, these polyelectrolytes can be adsorbed to charged SAMs. "Mercaptoundecanoic acid on gold is capable of adsorbing alternating layers of polydiallyldimethylammonium chloride (PDDA) and polystyrene sulfonate sodium salt (PSS) for use as a polymer cusion [65, 66]." [28]

1.1.2.6 Nanotechnology

An important application of phospholipids in nanotechnology is the creation of *nanotube vesicle networks* (or NVNs) [67]. NVNs are networks of connected surface-immobilized vesicles. These networks can be created by mechanical fission, micropipet-assisted formation, or micropipette writing. [28]

The use of mechanical fission to form NVNs is limited to schemes that are not geometrically difficult since it offers the least control over vesicle size. This mode involves the use of a small carbon fiber that has been coated with bovine serum album (BSA) in order to separate a surface immobilized giant unilaminar vesicle (GUV) into two vesicles. Homofission is accomplished by depressing the carbon fiber through the GUV [68]. The two vesicles are coupled together by a nanotube of phospholipid material from vesicles. These can then be separated by lateral motion of the carbon fiber. NVNs are easily separated up to a few hundred micrometers using this mode [69].

An applied DC voltage that pulsates between a carbon reference electrode and a tapered micropipette tip is required for the formation of NVNs using micropipette-assisted formation [70]. When performed in aqueous solution, the breach and removal of a GUV by the micropipette tip results in phospholipid nanotube formation down the length of the micropipette. A vesicle can be placed at its intended position once positive pressure has been applied to the micropipette tip, thus filling it with solution. A complicated network can be assembled using this process. Both mechanical force and applied DC voltage must be used to remove the final vesicle. Materials can also be injected into NVNs using this method. In order to do this, the micropipette tip must be filled with the solution that is to be injected into the NVN. Then it must be used to form a

vesicle connected by a nanotube to the network. If the vesicle is not immobilized and allowed to be released into solution, it will move back due to surface tension and release its contents within the NVN [71].

Micropatterned gold discs that have been functionalized to present neutravidin on the surface can be used for micropipette writing of NVNs [72]. First, a GUV is drawn into a micropipette tip. This GUV must present biotin at its surface. Next positive pressure is applied to form a small vesicle at the tip of the micropipette. Finally, this vesicle is coupled with one of the micropatterned gold circles. The vesicles are held in place by the ligand-receptor interaction of biotin and neutravidin. While the vesicles are held in place, the micropipette is drawn away, leaving a phospholipid nanotube. An involved network can be generated on a micropatterned surface by repeating this process of vesicle formation and immobilization several times [72].

Individual fluorescent beads may move through the nanotubes from one compartment to the next by applying positive pressure to one of the vesicle compartments [69]. NVN technology has also been applied to investigate how small vesicles fuse to outer membrane of a cell and release their contents, which is a process known as exocytosis [73]. Also, enzymatic reactions (employing as few as 15 enzymes) have been studied inside NVNs [74]. In time, observing stochastic processes at the single molecule level may be achieved through the use of NVNs.

The current study describes the use of FTIR spectroscopy to monitor the relative stability of polymer supported membranes. The impact of surface physico-chemical properties of the polymers is explored by varying both the base polymer and chemical modification of the polymers. Lipid (DPPC) and protein-lipid conjugate interactions with

surfaces formed by linear polymers and close-packed polymer beads were studied as possible adhesion layers to show a proof of concept for the biosensor element construction.

2.0 Materials and Methods

2.1 Preparation of Polystyrene (PS) Layers

The linear polystyrene layers used in these experiments were formed through the method of evaporative formation. As such, 25 μL of a 0.025 mg/mL solution of PS in toluene was deposited on the diamond ATR surface. This solution was then exposed to a gentle stream of nitrogen gas until all of the solvent was evaporated, leaving a thin-film of PS.

2.2 Preparation of Polyvinyl Chloride (PVC) Layers

The formation of PVC layers on a diamond ATR surface was carried out much the same way as the PS layers, the exception being that it was a 2.5 mg/mL solution of PVC in tetrahydrofuran. As before, this solvent was left to evaporate under nitrogen gas, forming a thin-film of PVC.

2.3 Preparation of Random Close-Packed Nanoparticle Layers

A polystyrene "latex" nanosphere dispersion in water was acquired from Alfa Aesar (100 nm diameter, 2.5 wt %, Stock # 42712, Lot # H25Q22, CAS # 9003-53-6). This dispersion was diluted in water ten-fold and one-hundred fold into weight percents

of 0.25% and 0.025% respectively. The process of evaporative formation was then used to form a randomly close-packed layer of PS nanospheres.

2.4 *Preparation of Supported Multi-Bilayer*

For studies involving just phospholipid and no bound myoglobin, a 10 μM dispersion of DPPC (Avanti Polar Lipids) in PBS buffer was created via sonication for 60 seconds. Twenty five microliter aliquots of this dispersion were then evaporated leaving a multibilayer on the ATR surface.

In order to study the stability of protein-conjugated lipid layers on multiple surfaces, N-glutarylphosphatidylethanolamine must first be synthesized. Essentially, it is simply 1,2-dipalmitoyl-*sn*-phosphoethanolamine (DPPE) with a five carbon linker group attached to DPPE's lone nitrogen atom. This linker group will later be reacted with to form a myoglobin linked phospholipid.

The synthesis of N-glutarylphosphatidylethanolamine (N-glutaryl-PE) is described here. To form the anhydride of glutaric acid, 10.6 mg of glutaric acid and 8.1 mg 1-ethyl-3-(3-dimethylaminopropyl)carbodiimide (ECDI) were combined in 2 mL methylene chloride in a 25 mL round bottom flask with a Teflon cap. The flask was capped after nitrogen had been used to purge any remaining air and water vapor. The flask was then stirred at room temperature for 48 hours with a magnetic stir bar. A solution of DPPE (26.28 mg) in 2 mL chloroform and 15 μL of triethylamine were added to the glutaric anhydride/ECDI solution. The reaction mixture was acidified by adding 5 mL chloroform and 4 mL of 0.02 M phosphate/0.02 M citrate buffer (pH 5.5) with vigorous shaking. The aqueous phase was separated by low-speed centrifugation and

discarded. The organic phase was dried over anhydrous sodium sulfate. The desired N-glutaryl-DE was purified by silica-gel column chromatography. The dried chloroform solution was introduced into 1 x 20 cm silica-gel column (Fisher 100-200 mesh) and fractions were eluted by passing through the column 50 mL chloroform effluent solutions containing successively, 0, 10, 20, 30 and 50% methanol. Literature states that most of N-glutaryl-PE is found in the 30% effluent. [75]

For the "gas flow" experiments a controlled flow of nitrogen gas was used for the evaporative formation of thin-films on a diamond ATR surface. A gas flow meter (Matheson Gas Products) was used to control the gas stream at different flow rates to determine the optimum conditions for film formation. In one experiment, the flow rate was held constant for a series of formation to see how reproducible thin-film formation of the phospholipid films can be. In another experiment, different flow rates were used for evaporative formation to determine the optimal flow rate at which the phospholipid thin-film can form.

The next experiment was designed to see how stable a phospholipid multi-layer is on a number of different surfaces. These surfaces include diamond, PS, PVC, and PS nanospheres. This was done by replacing the buffer above the phospholipid multi-layer a number a times. IR spectra were taken between buffer exchanges to observe the absorption. If the phospholipid absorption decreases it is because the layers are being washed off.

There was also an experiment performed in order to study multibilayer formation as a function of ionic strength dependence. In this experiment sodium chloride was introduced into the protein-conjugated phospholipid dispersion in concentrations of 150

mM and 300 mM. The process of evaporative formation was then used to create multibilayers. Once formed, the multibilayers were rehydrated with buffer and an initial spectrum was taken. From this point, the buffer that had been added was replaced with fresh buffer and an additional spectrum was taken. This process was repeated until a total of ten spectra were acquired. All spectra were normalized to the initial spectrum.

2.5 *FTIR Spectroscopy*

All FTIR spectra were recorded with a Digilab (Randolf, MA) FTS 7000 FTIR spectrometer equipped with a liquid nitrogen-cooled mercury cadmium telluride (MCT) detector and a DuraSample*IR* II ATR (SensIR Technologies). Spectra were collected over the range 4000 cm^{-1} to 400 cm^{-1} with a resolution of 4 cm^{-1}. Each spectrum was produced by the coaddition of 256 scans.

3.0 Results and Discussion

In addition to the bare diamond ATR surface, three polymer adhesion layers were investigated. (1) Polystyrene is a compound made from the aromatic monomer styrene. The majority of commercial polystyrene molecules consist of a backbone of carbon atoms with phenyl groups attached to half of the carbon atoms. Free radical initiator residues terminate each end of the chain. Minor variants include chains terminated by anionic or cationic initiator residues. All commercial polystyrene products are atactic; meaning that the placement of the phenyl groups on either side of the chain is essentially random. [76]

(2) Polyvinyl Chloride (PVC), the vinyl chloride monomer polymerizes via addition polymerization to form polyvinyl chloride. The polymer exhibits limited crystallinity, though this property is not often considered as important in defining its performance. It tends to be atactic or regionally syndiotactic, surrounded by extended atactic runs. When exposed to temperatures above 100°C, polyvinyl chloride decomposes, creating free radicals that further attack the polymer chain. For this reason, the degradation of polyvinyl chloride is autocatalytic and can occur very quickly. In addition to destroying the properties of the original polymer, degradation releases hydrogen chloride which can attack the internal metal surfaces of processing equipment. [76]

(3) Nanoparticles are small structures with dimensions less then 100 nm. Polystyrene nanoparticles are widely used materials and are available in a wide range of sizes with narrow size distributions. They can be purchased surfactant free as well as modified with various surfactants such as linkers, dyes, biomolecules, and covalently bound functional groups. Availability of these particles has led to several uses ranging from applications in photonics, nanotechnology, and life science to roles in the behavior of colloidal suspensions. [77]

Poly(styrene-divinylbenzene) is structurally related to polystyrene. Essentially, it is just the cross linked version of linear polystyrene. The divinyl benzene is what actually forms the cross-link in the cross-linked bead. This cross linked structure can have different charges placed throughout or on the surface of the bead. Aminomethyl groups can be attached to the aromatic portion of poly(styrene-divinylbenzene) and add a

positive charge. Sulfuric acid can be used to react with a bead surface. This sulfonation results a negative charge being attached.

Polymers such as these can adsorb fervently on surfaces, frequently reaching saturation at very low concentrations. If the volume of an adsorbed polymer is the same as its volume in solution, then the amount of polymer adsorbed at full surface coverage but without overlap is quantitatively similar to cylinders lying flat and close-packed on the surface. Therefore a reasonable estimate of the minimum film thickness can be achieved.

3.1 Estimation of Minimum Film Thickness (PVC and PC)

Using the density, the thickness of the thin-films formed on the ATR surface can be determined. As stated earlier, the concentrations of PVC and PC used were 25 mg/mL and 0.025 mg/mL respectively. The density of PVC is 1.38 g/cm^{-3}. Since the surface of the ATR is circular, the thin film can be thought of as a very short cylinder with height "h" and area "A" being equal to "πr^2" with "r" equal to 4.0 mm. Density is of course mass per unit volume (D = m/v). Substituting "$h\pi r^2$" for volume the following equation results:

$$D = \frac{m}{h\pi r^2}$$

Solving for "h," the equation becomes,

$$h = \frac{m}{D\pi r^2}$$

The mass "m" is determined by multiplying the 25 μL aliquots used experimentally by the concentration of PVC used, which results in 62.5 μg PVC. By

substituting these values into the equation, one determines the thickness of the PVC layer to be 900 nm.

A second method of determining the thickness of the PVC film was used to verify the previously resulting thickness. In this second method the PVC molecules were estimated to be rigid cylinders having a width of 0.0335 nm (r = 0.168 nm) and a height, "h," of 774 nm. Multiplying the height by "πr^2" gives a volume of an individual molecule at 275 nm^3. In a 25 μL aliquot of PVC there is calculated to be 1.71 x 10^{14} molecules, giving a total volume of PVC at 4.70 x 10^{16} nm^3. As stated earlier, the ATR surface is also cylindrical and has a volume "V" equal to "$h\pi r^2$." Solving for "h," the equation for the volume of a cylinder becomes:

$$h = \frac{V}{\pi r^2}$$

By substituting the calculated volume for "V," the height becomes 935 nm, which is in substantial agreement with the first estimation.

By using a density of 1.05 g/cm^{-3} to determine minimum film thickness, one also finds that the height of the polystyrene (PS) films used were no thinner then 2.3 nm.

3.2 Estimation of Nanosphere Film Thickness

The regular arrangement of circles that gives the highest packing density, $\pi/\sqrt{12} \approx 0.9069$, is where the centers of the circles are arranged in a hexagonal lattice. When considering a plane with spheres placed on it, the two most common arrangements are face centered cubic and hexagonal close packing. In both arrangements, the average packing density is $\pi/\sqrt{18} \approx 0.74048$. [78, 79]

Given polystyrene spheres with a diameter of 1.0 x 10^{-7} m and an ATR surface with a diameter of 4 x 10^{-3} m (~8 x 10^{-3} m if the well is overfilled and some beads settle on the stainless steel), we calculated the number of beads needed to form a single hexagonally close packed layer to be no fewer than 6.8 x 10^{8} and most likely closer to 3.6 x 10^{9}.

The estimated minimum thickness of close packed nanospheres formed from 25 μL of a 0.025% suspension (1.14 x 10^{10} beads) to be 3-layers or about 300 nm.

3.3 FTIR of Phospholipids

The stability of polymer supported lipid multibilayer constructs was investigated by monitoring phospholipid vibrational modes after successive buffer washings.

3.3.1Methylene Vibrational Modes

The antisymmetric methylene stretch located is located between 2916 cm^{-1} and 2936 cm^{-1}. The estimated direction of the dipole moment is perpendicular to the bisector of the H-C-H angle. The symmetric methylene stretch is located between 2843 cm^{-1} and 2863 cm^{-1}. The corresponding dipole moment is then estimated to be parallel to the bisector of the H-C-H angle. [80]

3.3.2 Phosphate Vibrational Modes

There are two types of stretches unique to phosphate molecules. These are symmetric and asymmetric about the phosphate atom. The PO_2^- antisymmetric stretch vibrates at a frequency between 1200 cm^{-1} and 1260 cm^{-1}, while the symmetric modes are

located between 1085 cm^{-1} and 1110 cm^{-1}. These numbers are for typical transmision studies and the peak postion of the symmetric stretch is likely shifted to 1074 cm^{-1} when measured by ATR. For the antisymmetric stretch, the dipole moment is estimated to be perpendicular to the bisector of the O-P-O angle, whereas the symmetric stretch is parallel to the bisector of the O-P-O angle. [80]

The band peak located at 1074 cm^{-1} was chosen experimentally as it is a prominent peak due to phosphate. This peak is easy to notice and follow in the raw data.

3.4 Film Loss and Reproducibility of Film Formation

This experiment was designed to see how reproducible multibilayer formation is as a function of the nitrogen gas used to prepare such a multibilayer. After reviewing the data retrieved from the film formation experiments one can determine that there is little dependence on the flow rate of nitrogen gas used to form the thin-film. Also, the same can be said of the reproducibility in thin-film formation using a constant flow rate. It should be noted that the total absorbance at 1074 cm^{-1} in the varied gas flow experiments stayed within a range from 0.225 to 0.250. These numbers are nearly identical with data from the constant flow rate experiment. Though the exact absorbance of each thin-film formed may not be predictable, it will fall into a narrow Absorbance range. This is shown in Figure 2.8:

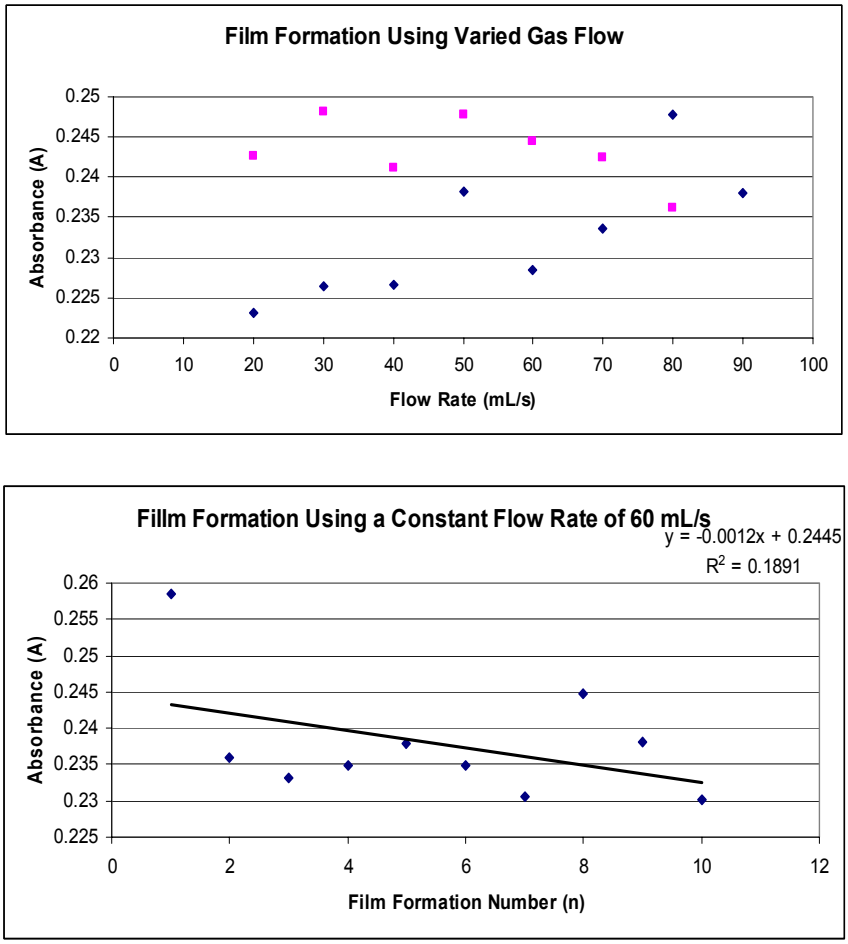

Figure 2.8: Effect of drying gas flow rate on lipid film formation. Absorbance monitored at 1074 cm^{-1}.

Sodium chloride at 150 mM or 300 mM concentrations does not appear to affect the stability of those formed bilayers. It should be noted that once the first multibilayer was formed a small amount of buffer (25 µL) was used to rehydrate the thin-film and an initial spectrum was taken to which all additional spectra were normalized against. This is represented in Figure 2.9:

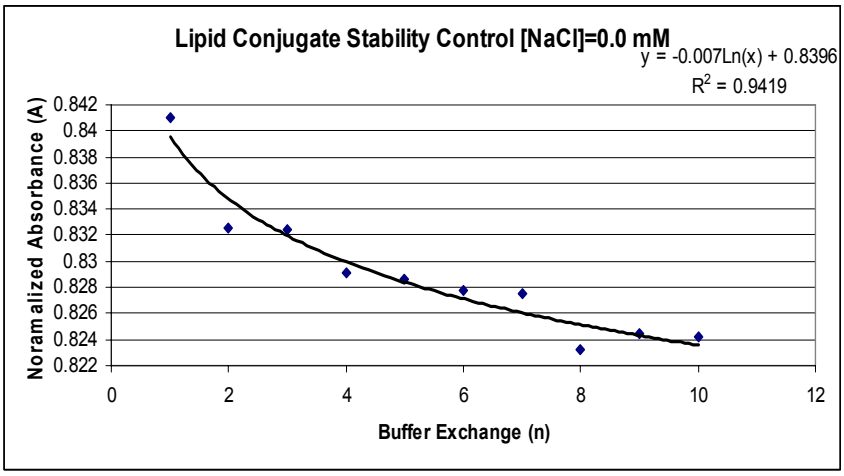

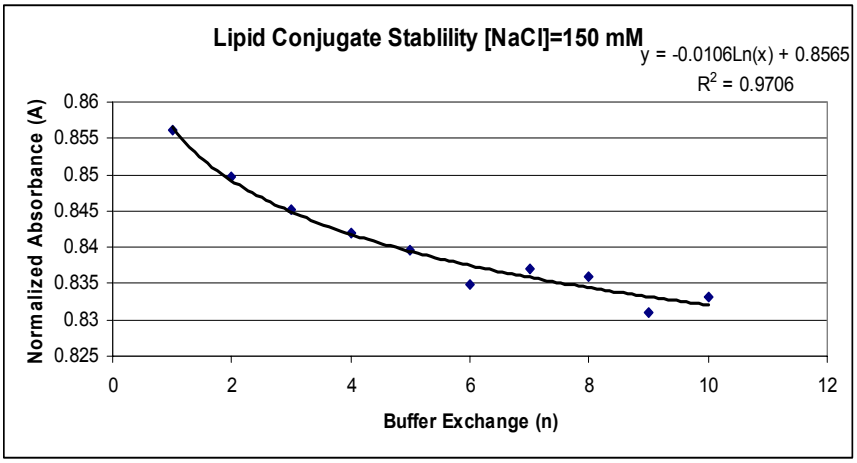

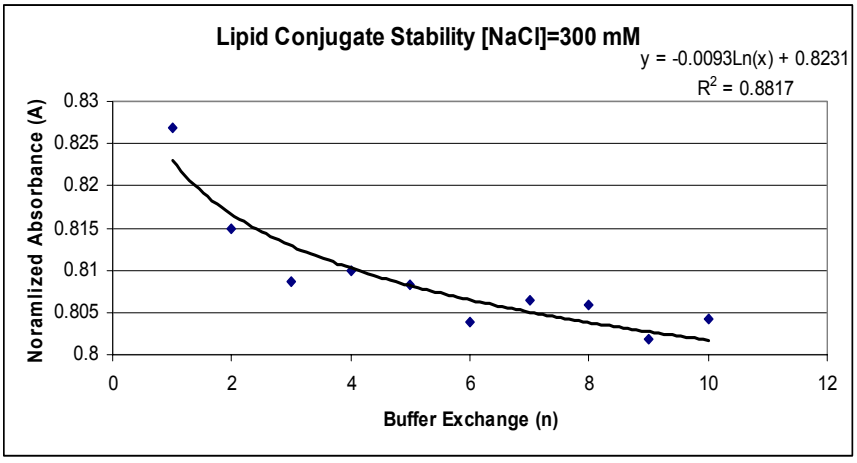

Figure 2.9: Ionic Strength Dependence of Film Stability as monitored at 1074 cm^{-1}

3.5 Stability on Various Surfaces

These experiments were designed to show how well phospholipids adhere to different surfaces. The phospholipid multibilayers were developed using evaporative formation. Once the first multibilayer was formed a small amount of buffer (25 μL) was used to rehydrate the thin-film and an initial spectrum was taken to which all additional spectra were normalized against. Among the surfaces explored are diamond, PVC, PS and PS nanoparticles. The equation in the top right hand corner of each plot represents the curve retaining the most absorbance in each plot. The resulting plots are shown in Figures 2.10 and 2.11:

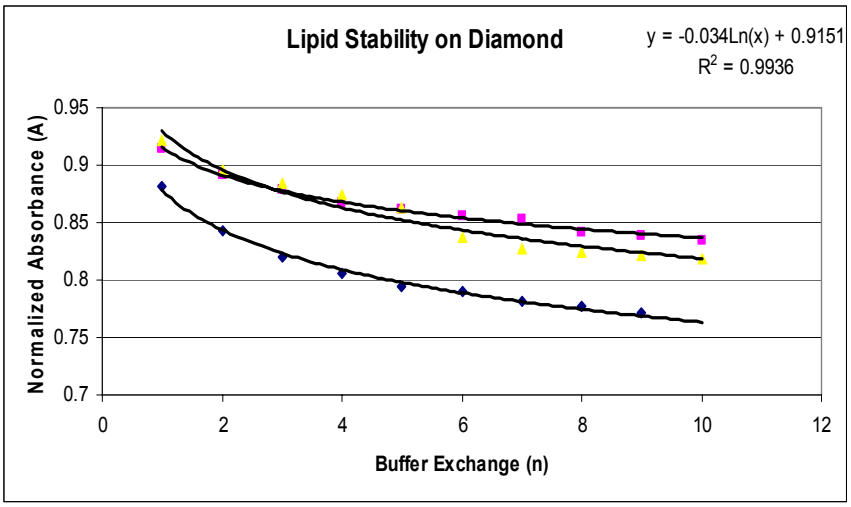

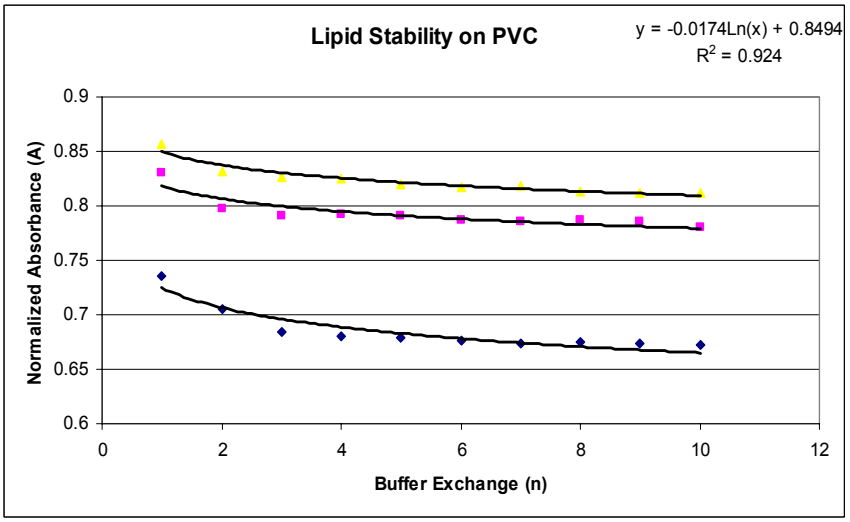

Figure 2.10: Lipid Stabilities on Various Surfaces, Monitored at 1074 cm^{-1}

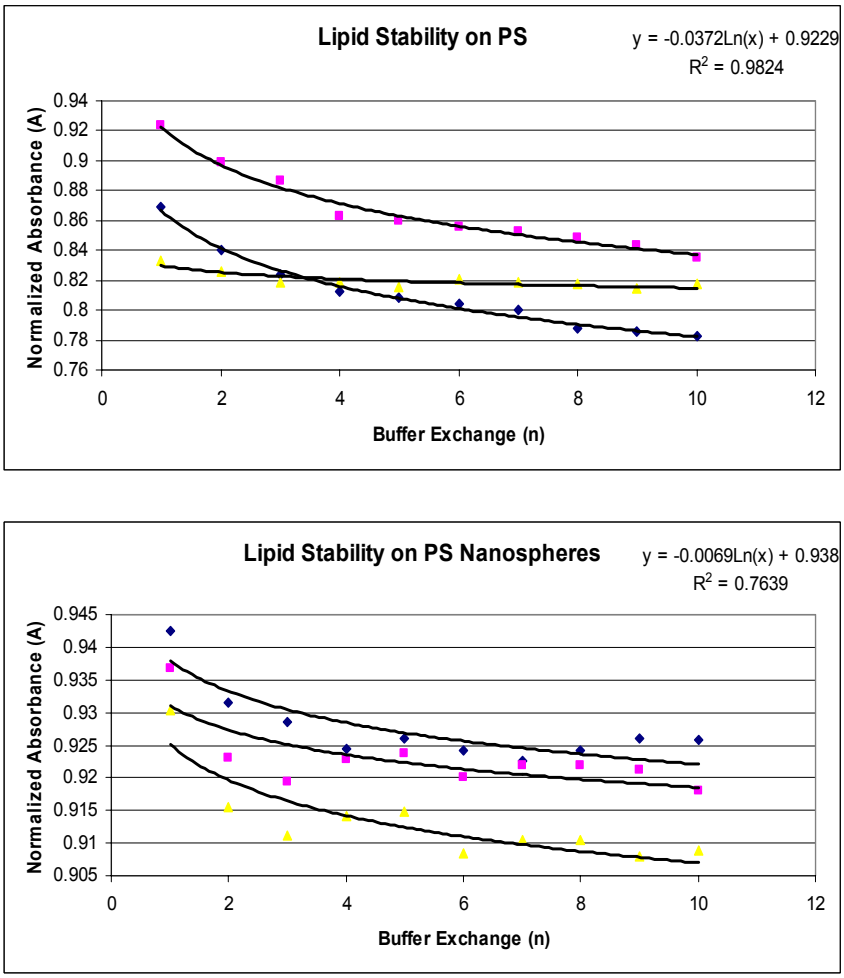

Figure 2.11: Lipid Stabilities on Various Surfaces, Monitored at 1074 cm^{-1}

3.6 Stability of Conjugated Protein-Lipid

The stability of the protein-lipid conjugate was also explored. As in previous procedures, once the multibilayer was formed a small amount of buffer (25 µL) was used to rehydrate the thin-film and a spectrum was taken. The resulting data are seen in Figures 2.12 and 2.13:

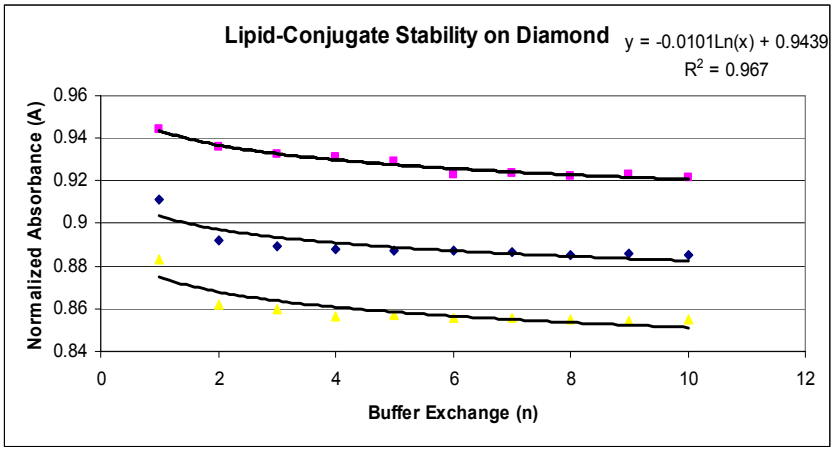

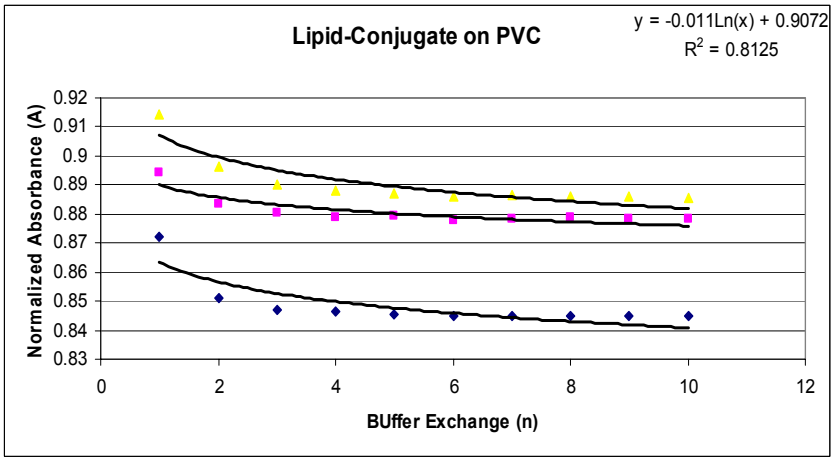

Figure 2.12: Lipid-Conjugate Stability on Various Surfaces as Monitored at 1074 cm^{-1}

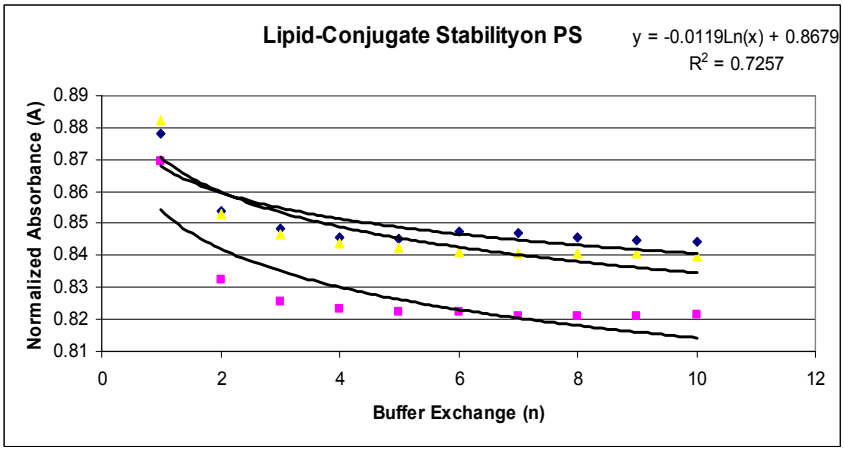

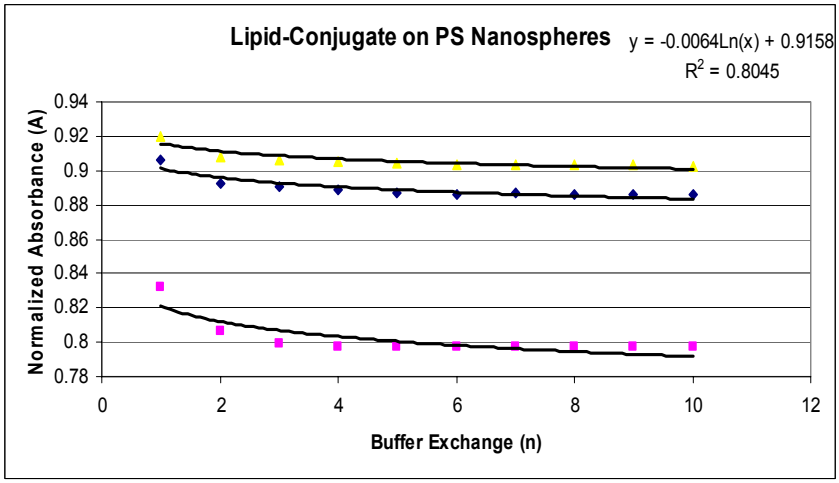

Figure 2.13: Lipid-Conjugate Stability on Various Surfaces as Monitored at 1074 cm^{-1}

So as one can see after examining the previous figures, the addition of a polymer support helps stabilize the multibilayer to the internal reflection element over a period of buffer exchanges. The PS nanospheres retained the most absorbance through 10 buffer exchanges, still leaving a normalized absorbance greater then 0.9 in one example. It is for this reason that PS nanospheres continued to be utilized in Chapter 4.

3.7 Adhesion of lipids to polymer layers

It is well established, though poorly understood, that phospholipid membranes are held in place above a solid support by a number of different forces. These forces are a combination of van der Waals, electrostatic, hydration and steric forces [81]. Using egg phosphatidylcholine bilayers supported on a glass substrate, the underlying water layer has been shown to effectively lubricate the lipids. These lubricated lipids then move freely with a lateral diffusion constant of ranging from 1 - 4 $\mu m^2/s$ [82]. It has been observed that both basic pH values and low ionic strengths adversely affect fusion of negatively charged vesicles to glass substrates [81]. Furthermore, neutral vesicles composed of zwitterionic lipids seem to fuse more readily to gold substrates displaying a charged monolayer instead of neutral layers [82].

For polymer supports and diamond, where oxides are not typically present, additional hydrophobic interactions may dominate due to their hydrophobic nature. The attractive hydrophobic interaction in water is of surprisingly long range and at small separations is much stronger than the van der Waals attraction. Hydrophobic interactions will have a significant role in adhesion of lipid bilayers to hydrophobic surfaces, even though most phospholipids are at least zwitterionic. Like the attraction between two hydrophobic surfaces, the interaction between a hydrophilic particle and a hydrophobic surface is not well described by an inverse power law or an exponential function. For both, the attractive force is longer ranged than expected from DLVO (Derjaguin, Landu, Verwey and Overbeek) theory. [83]

Although hydrophobic interaction may dominate in multibilayer formation on the diamond and polymer surfaces, the lower film stability (faster loss of adhered lipid) on the more nonpolar surfaces (Figures 2.8-2.13) suggests this type of interaction does not dominate once adhesion has occurred.

3.7.1 Van der Waals Forces

The results from repeated washings also show that van der Waals interactions may be a significant factor contributing to film stability since the polar solvent water had less of an effect as the process continued. Nonpolar molecules aggregate because of attractive *van der Waals* force. These are also known as dispersion forces [84]. These forces arise from the transient attraction of electrons of one molecule to the nuclei of another. [84] Electrons have no fixed position in the structure of an atom or molecule, but rather are distributed in a probabilistic fashion based on quantum probability, there is a non-negligible chance that the electrons are not evenly distributed and thus their electrical charges are not evenly distributed. Electrons on nearby molecules then experience an electrostatic attraction towards exposed nuclei. [86]

These van der Waals attractive forces exist in all samples, not just those composed on nonpolar molecules, although they are often weak in comparison with other types of intermolecular forces. They become dominant in the absence of other forces. [79] In general, the greater the number of electrons in a molecule or atom, the more easily polarized they become. Thus van der Waals forces become more important with increasing molecular weight and often with increased surface area of the molecule, since increased molecular weight is associated with an increased number of electrons. The

attractive forces depend not only on the number of electrons in a molecule, but also on the area of contact of a molecule with its neighbors. [86] The nanoparticles show the lowest loss of lipid with successive washings in both layers formed from pure DPPC vesicles and myoglobin-lipid conjugates. This is likely the result of the additional surface area resulting from randomly close packed beads which increases van der Waals interactions as compared to the very smooth surfaces formed by PS and PVC [87].

3.7.2 Electrostatic Interactions

Ionic interactions arise either as electrostatic attractions between opposite charges or repulsions between like charges. A lipid molecule can carry positive and/or negative charges. Also peptides and proteins can carry charges within their amino acid side chains, and at the carbon and nitrogen termini. In proteins, the charged residues are located at the surface where they interact with water molecules. In lipid molecules, the charge would be held in the polar head group, which is also exposed to water molecules. Electrostatic interactions between charged groups on a lipid or protein surface can be complicated by the presence of salts in solution. [84] Although polystyrene is a nonpolar polymer, electrostatic interactions between the polar lipid head groups and the π-electrons of the aromatic moiety are possible. However, the lack of strong ionic strength dependence for film formation and stability makes this a minor contributor at best for polystyrene adhesion layers. The nanobeads contain ~3% sulfonation to prevent bead aggregation, thus giving them a slight negative surface charge. Presumably the amine in a DPPC head group can interact with the sulfonates and stabilize membrane adhesion to the PS nanoparticles. Since, the chlorines in PVC make it a more polar polymer than PS,

electrostatic interactions may contribute to the reduction in lipid loss on the PVC surfaces.

3.7.3 Hydration and Steric Interactions

There are several types of steric interactions including steric hindrance, shielding and attraction. Steric hindrance occurs when the size of groups within a molecule prevents chemical reactions that are observed in related smaller molecules. Although steric hindrance is sometimes a problem, it can also be a very useful tool, and is often exploited to change the reactivity pattern of a molecule by stopping unwanted side-reactions (steric protection). Steric shielding occurs when a charged group on a molecule is spatially shielded by less charged (or oppositely charged) atoms, including counterions in solution (Debye shielding). In some cases, for an atom to interact with sterically shielded atoms, it would have to approach from a location where there is less shielding, thus controlling where and from what direction a molecular interaction can take place. Steric hinderance and sheilding are likely to influence only multibilayer formation on the polymer surfaces. Steric attraction occurs when molecules have shapes or geometries that are optimized for interaction with one another. In these cases molecules will react with each other most often in specific arrangements. Attractive steric interactions are extremely unlikely to play a role in multibilayer formation and stability.

Repulsive hydration forces arise whenever water molecules bind strongly to hydrophilic surface groups because of the energy needed to dehydrate these groups as the vesicle surface approaches the polymer surface. However, it is likely this would be

overcome by hydrophobic interactions which have a significant role in adhesion even though most lipid vesicles have a net surface charge.

4.0 Conclusions

The reproducibility of forming thin films had its difficulties. There seems to be no dependence on total absorbance due to the nitrogen flow rate used for evaporative formation. The addition of sodium chloride had little to no effect on the overall stability of thin-films formed. The total absorbance observed during formation varied and a normalized absorbance had to be used where data was normalized to the first hydrated spectrum observed.

As one can see from Figures 2.8 and 2.9, the phospholipid observed on diamond surface washes away quite readily when the buffer above the thin-film is replaced. This loss of lipid led to the use of a polymer supported structure to see how they affect the overall stability of the thin-film structure. Various polymers were studied, including PS, PVC and PS nanospheres. Each polymer studied aided in the stability of the phospholipid structure to some degree. Though PVC showed promise as an adhesion layer, the PS nanospheres retained normalized absorbance the best.

This work on the best adhesion layer then continued to include the conjugated lipid. Again, PS, PVC and PS nanospheres were explored as polymer support structures. All materials used resulted in an initial drop in absorbance, while eventually the normalized aborbances began to level off. Again, PVC showed promise as a supporting material, while the PS nanospheres retained the most overall absorbance. Based on this

work, the PS nanospheres has shown to be the most appropriate material to be used as a polymer support for both the lone phospholipid as well as for the protein conjugated phospholipid. This is most likely due to the electrostatic interactions between the slightly negatively charged PS nanospheres and positively charged groups located on the DPPC and DPPE used.

References:

1. Briggs, M.S., Cornell, D.G., Dluhy, R.A. and Gierasch, L.M. 1986. Conformations of signal peptides induced by lipids suggest initial steps in protein export. Science 233: 206-208
2. Cornell, D.G., Dluhy, R.A., Briggs, M.S., McKnight, C.J. and Gierasch, L.M. 1989. Conformations and orientations of a signal peptide interacting with phospholipid monolayers. Biochemistry 28: 2789-2797
3. Silvestro, L., and Axelsen, P.H. 1998. Infrared spectroscopy of supported lipid monolayer, bilayer and multibilayer membranes. Chemistry and Physics of Lipids 96: 69-80.
4. Axelsen, P.H., Braddock, W.D., Brockman, H.L., Jones, C.M., Dluhy, R.A., Kaufman, M.K. and Puga, F.J. II 1995. Use of internal reflectance infrared spectroscopy for the in-situ study of supported lipid monolayers. Appl. Spectrosc. 49: 526-531.
5. Kalb, E., Frey, S. and Tamm, L.K. 1992. Formation of supported planar bilayers by fusion of vesicles to supported phospholipid monolayers. Biochim. Biophys. Acta 1103: 307-316

6. Wenzyl, P., Fringeli, M., Goette, J. and Fringeli, U.P. 1994. Supported phospholipid bilayers prepared by the 'LB/vesicle method': a Fourier transform infrared attenuated total reflection spectroscopic study on structure and stability. Langmuir 10: 4253-4264.

7. Brian, A.A. and McConnell, H.M. 1984 Allogeneic stimulation of cytotoxic T cells by supported planar membranes. Proc. Natl. Acad. Sci. USA. 81: 6159-6163.

8. Tamm, L,K. 1988. Lateral diffusion and fluorescence microscope studied on a monoclonal antibody specifically bound to supported phospholipid bilayers. Biochemistry 27: 1450-1457.

9. Tamm, L.K. 1991. Membrane insertion and lateral mobility of synthetic amphiphilic signal peptides in lipid model membranes. Biochim, Biophys. Acta 1071: 123-148.

10. Tamm, L.K. and McConnell, H.M. 1985. Supported phospholipid bilayers. Biophys. J. 47: 105-113.

11. Gilmanshin, R., Creutz, C.E. and Tamm, L.K. 1994. Annexin IV reduces the rate of lateral lipid diffusion and changes the fluid phase structure of the lipid bilayer when it binds to negatively charged membranes in the presence of calcium. Biochemistry 33: 8225-8232.

12. Nabadryk, E. and Breton, J. 1891. Orientation of intrinsic proteins in photosynthetic membranes. Polarized infrared spectroscopy of chloroplasts and chromatophores. Biochim. Biophys. Acta 635: 515-524.

13. Nabadryk, E., Gingold and M.P. Breton, J. 1982. Orientation of gramicidin A transmembrane channel: infrared dichroism study of gramicidin in vesicles. Biophys. J. 38: 243-249.

14. Cabiaux, V., Phalipon, A., Kaczorek, M., Collier, R.J. and Ruysschaert, J.M. 1990. Structure and interaction with model membranes of a CNBR peptide of diphtheria toxin B fragment. J. de Physiologie 84: 273-277.

15. Goormaghtigh, E., De Meutter, J., Szoka, F.C. Jr., Cabiaux, V., Parente, R.A. and Ruysschaert, J.M. 1991. Secondary structure and orientation of the amphipathic peptide GALA in lipid structures. An infrared spectroscopic approach. Eur. J. Biochem. 195: 421-429.

16. Martin, I., Defrise-Quertain, F., Decroly, E., Vandenbranden, M., Brasseur, R. and Ruysschaert, J.M. 1993. Orientation and structure of the NH2-terminal HIV gp41 peptide in fused and aggregated liposomes. Biochim. Biophys. Acta 1145: 124-133.

17. Challou, N., Goormaghtigh, E., Cabioaux, V., Conrath, K. and Ruysschaert, J.M. 1994. Sequence and structure of the membrane-associated peptide of glycophorin-A. Biochemistry 33: 6902-6910.

18. Lins, L Brasseur, R., Rosseneu, M., Yang, C.Y., Sparrow, D.A., Sparrow, J.T., Gotto, A.M. Jr. and Ruysschaert. J.M. 1994. Structure and orientation of apo B-100 peptides into a lipid bilayer. J. Protein Chem. 13: 77-88.

19. Luneberg, J., Martin, I., Nubler, F., Ruysschaer, J.M. and Herrmann, A. 1995. Structure and topology of the influenza virus fusion peptide in lipid bilayers. J. Biol. Chem. 270: 27606-27614.

20. Brauner, J.W. and Mendelsohn, R., Prendergast, F.G. 1987. Attenuated total reflectance Fourier transform infrared studies of the interaction of melittin, two fragments of melittin, and δ-hemolysin with phosphatidylcholines. Biochemistry 26: 8151-8158.

21. Ter-Minassian-Saraga, L., Okamura, E., Umemura, J. and Takanaka, T. 1988. Fourier transform infrared total reflection spectroscopy of hydration of dimystritoylphosphatidylcholine multibilayers. Biochim. Biophys. Acta 946: 41-423.

22. Bechinger, B., Zasloff, M. and Opella, S.J. 1992. Structure and interactions of magainin antibiotic peptides in lipid bilayers: a solid state nuclear magnetic resonance investigation. Biophys. J. 62: 12-14.

23. Cross, T.A. and Opella S.J. 1994. Solid-state NMR structural studies of peptides and proteins in membranes. Curr. Opin. Struct. Biol. 4: 574-581.

24. Opella, S.J. 1994. Solid-state NMR structural studies of proteins. Ann. Rev. Phys. Chem. 45: 659-683.

25. Ludlam, C.F.C., Arkin, I.T., Liu, X.M., Rothman, M.S., Rath, P., Aimoto, S., Smith, S.O., Engelman, D.M. and Rothschild, K.J. 1996. Fourier transform infrared spectroscopy and site-directed isotope labeling as a probe of local secondary structure in the transmembrane domain of phospholamban. Biophys. J. 70: 1728-1736.

26. Muller P., Rudin D.O., Ti Tien H. and Wescot W.C. 1962. Reconstitution of Cell Membrane Structure *in vitro* and its Transformation into an Excitable System Nature 194: 979-980.

27. Muller P., Rudin D.O., Ti Tien H. and Wescot W.C. 1963, Methods for the Formation of Single Bimolecular Lipid Membranes in Aqueous Solution. J. Phys. Chem. 67: 534-535.

28. Castellana, E.T. and Cremer, P.S. 2006. Solid Supported Lipid Bilayers: From biophysical studies to sensor design. Surface science reports 61: 429-444.

29. Montal, M. and Mueller, P. 1972. Proc. Natl Acad. Sci. USA. Formation of Bimolecular Membranes from Lipid Monolayers and a Study of their Electrical Properties. 69: 3561-3566

30. Tamm, L.K. and McConnell, H.M. 1985. Supported Phospholipid Bilayers. Biophys. J. 47: 105-113.

31. Johnson, S.J., Bayerl, T.M., McDermott, D.C., Adam, G.W., Rennie, A.R., Thomas, R.K. and Sackman, E. 1991. Structure of an Adsorbed Dimyristoylphosphatidylcholine Bilayer Measured with Specular Reflection of Neutrons. Biophys. J. 59: 289-294.

32. Brian, A.A. and McConnell, H.M. 1984. Proc. Natl Acad. Sci. USA. Allogeneic Stimulation of Cytotoxic T Cells by Supported Planar Membranes 81: 6159-6163.

33. McConnell, H.M., Watts, T.H., Weiss, R.M. and Brian, A.A. 1986. Supported Planar Membranes in Studies of Cell-Cell Recognition in the Immune System. Biochim. Biophys. Acta 864: 95-106.

34. Kalb, E., Frey, S. and Tamm, L.K., 1992. Formation of Supported Planar Bilayers by Fusion of Vessicles to Supported Phospholipid Monolayers. Biochim. Biophys. Acta 1103: 307-316.

35. Langmuir, I. 1920. The Mechanism of the Surface Phenomena of Flotation. Trans. Faraday Soc. 15: 62-74.

36. Johnson, S.J., Bayerl, T.M., McDermott, D.C., Adam, G.W., Rennie, A.R., Thomas, R.K. and Sackmann, E. 1991. Structure of an Adsorbed Dimyristoylphosphatidylcholine Bilayer Measured with Specular Reflection of Neutrons. Biophys. J. 59: 289-294.

37. Hope, M.J., Bally, M.B., Webb, G. and Cullis, P.R. 1985. Production of Large Unilamellar Vesicles by a Rapid Extrusion Procedure. Characterization of Size Distribution Trapped Volume and Ability to Maintain A Membrane Potential. Biochim. Biophys. Acta. 812: 55-65.

38. Mayer, L.D., Hope, M.J. and Cullis, P.R. 1986. Vesicles of Variable Sizes Produced By A Rapid Extrusion Procedure. Biochim. Biophys. Acta. 858: 161-168.

39. Nayar, R., Hope, M.J. and Cullis, P.R. 1989. Generation of Large Unilamellar Vesicles from Long-Chain Saturated Phosphatidylcholines by Extrusion Technique. Biochim. Biophys. Acta. 986: 200-2006.

40. Frisken, B.J., Asman, C. and Patty, P.J. 2000. Studies of Vesicle Extrusion. Langmuir 16, 928-933.

41. Barenholz, Y., Gibbes, D., LItman, B.J., Goll, J., Thompson T.E. and Carlson F.D. 1977. A Simple Method for the Preparation of Homogeneous Phospholipid Vesicles. Biochemistry 16: 2806-2810.

42. Mimms, L.T., Zampihi, G, Nozaki, Y., Tanford, C. and Reynolds, J.A. 1981. Phospholipid Vesicle Formation and Transmembrane Protein Incorporation Using Octyl Glucoside. Biochemistry 10: 833-840.

43. Roessner, C.A., Struck, D.K. and Ihler, G.M. 1983. Injection of DNA into Liposomes by Bacteriophage Lambda. J. Biol. Chem. 258: 643-648.

44. Reimhult, E., Hook, F. and Kasemo, B. 2003. Intact Vesicle Adsorption and Supported Biomembrane Formation from Vesicles in Solution: Influence of Surface Chemistry, Vesicle Size, Temperature, and Osmotic Pressure Langmuir 19: 1681-1691.

45. Johnson, J.M., Ha, T., Chu, S. and Boxer S.G. 2002. Early Steps of Supported Bilayer Formation Probed by Single Vesicle Fluorescence Assays. Biophys. J. 83: 3371-3379.

46. Hamai, C., Yang, T.L., Kataoka, S., Cremer, P.S. and Musser, S.M. 2006. Effect of Average Phospholipid Curvature on Supported Bilayer Formation on Glass by Vesicle Fusion. Biophys. J. 90: 1241-1248.

47. Gritsch, S., Nollert, P., Jahnig, F. and Sackmann, E. 1998. Impedance Spectroscopy of Porin and Gramicidin Pores Reconstituted into Supported Lipid Bilayers on Indium-Tin-Oxide Electrodes. Langmuir 14: 3118-3125.

48. Gerquand, A., Mazeran, P.E., Pantigny, J., Proux-Delrouyre, V., Laval, J.M. and Bourdillon, C. 2003. Two-Step Formation of Streptavidin-Supported Lipid Bilayers by PEG-Triggered Vesicle Fusion. Fluorescence and Atomic Force Microscopy Characterization. Langmuir 19: 1700-1707.

49. Zheng, Z.M., Stroumpoulis, D., Parra, A., Petzold, L. and Tirrell, M., J. 2006. A Monte Carlo Simulation Study of Lipid Bilayer Formation on Hydrophilic Substrates from Vesicle Solutions. Chem. Phys. 124:

50. Crane, J.M., Kiessling, V. and Tamm, L.K. 2005. Measuring Lipid Asymmetry in Planar Supported Bilayers by Fluorescence Interference Contrast Microscopy. Langmuir 21: 1377-1388.

51. Plant, A.L., Brigham-Burke, M., Petrella, E.C. and Oshannessy, D.J. 1995. Phospholipid/Alkanethiol Bilayers for Cell-Surface Receptor Studies by Characterization of Biomimetic Surfaces. Anal. Biochem. 226: 342-348.

52. Plant, A.L. 1993. Self-Assembled Phospholipid/Alkanethiol Biomimetic Bilayers on Gold. Langmuir 9: 2764-2767.

53. Rao, N.M., Plant, A.L., Silin, V., Wight, S. and Hui S.W. 1997. Characterization of Biomimetic Surfaces Formed from Cell Membranes. Biophys. J. 73: 3066-3077.

54. Meuse, C.W., Niaura, G., Lewis, M.L. and Plant, A.L. 1998. Assessing the Molecular Structure of Alkanethiol Monolayers in Hybrid Bilayer Membranes with Vibrational Spectroscopies. Langmuir 14: 1604-1611.

55. Rao, N.M., Silin, V., Ridge, K.D., Woodward, J.T. and Plant, A.L. 2002. Cell Membrane Hybrid Bilayers Containing the G-Protein-Coupled Receptor CCR5. Anal. Biochem. 307: 117-130.

56. Hubbard, J.B., Silin, V. and Plant, A.L. 1998. Self Assembly Driven by Hydrophobic Interactions at Alkanethiol Monolayers: Mechanisms of Formation of Hybrid Bilayer Membranes. Biophys. Chem. 75: 163-176.

57. Glazier, S.A., Vanderah, D.J., Plant, A.L., Bayley, H., Valincius, G. and Kasianowicz, J.J. 2000. Langmuir 16: 10428-10435

58. Plant, A.L. 1999. Supported Hybrid Bilayer Membranes as Rugged Cell Membrane Mimics. Langmuir 15: 5128-5135.

59. Kastl, K., Ross, M., Gerke, V. and Steinem, C. 2002. Kinetics and Thermodynamics of Annexin A1 Binding to Solid-Supported Membranes: A QCM Study. Biochemistry 41: 10087-10094.

60. Meuse, C.W., Krueger, S., Majkrzak, C.F., Dura, J.A., Fu, J., Connor, J.T. and Plant, A.L 1998. Hybrid Bilayer Membranes in Air and Water: Infrared Spectroscopy and Neutron Reflectivity Studies. . Biophys. J. 74: 1388-1398.

61. Boxer, S.G. and Cremer, P.S., 1999. Formation and spreading of lipid bilayers on planar glass supports. J. Phys. Chem. B 103: 2554-2559.

62. Boxer, S.G., 2000. Molecular transport and organization in supported lipid membranes, Current Opinion in Chemical Biology 4: 704-709.

63. Wong, J.Y., Majewski, J., Seitz, M., Park, C.K., Israelachvili, J.N. and Smith, G.S. 1999. Polymer-Cushioned Bilayers. I. A Structural Study of Various Preparation Methods Using Neutron Reflectometry. Biophys. J. 77: 1445-1457.

64. Tamm, L.K. and McConnell, H.M. 1985. Supported Phospholipid Bilayers Biophys. J. 47: 105-113.

65. Zhang, L.Q., Longo, M.L. and Stroeve, P. 2000. Mobile Phospholipid Bilayers Supported on a Polyion/Alkylthiol Layer Pair. Langmuir 16: 5093-5099.

66. Ma, C., Srinivasan, M.P., Waring, A.J., Leher, R.I., Longo, M.L. and Stroeve, P. 2003. Supported Lipid Bilayers lifted from the substrate by Layer-by-Layer polyionn Cushions on Self-Assembled Monolayers. Colloids. Surf. B 28: 319-329.

67. Karlsson, A., Karlsson, R., Karlsson, M., Cans, A.S., Stromberg, A., Ryttsen, F. and Orwar O. 2001. Networks of Nanotubes and Containers. Nature 409: 150-152.

68. Braha, O., Gu, L.Q., Zhou, L., Lu, X.F., Cheley, S. and Bayley, H. 2000. Simultaneous Stochastic Sensing of Divalent Metal Ions. Nat. Biotechnol. 18: 1005-1007.

69. Karlsson, A., Karlsson, M., Karlsson, R., Sott, K., Lundqvst, A., Tokarz, M. and Orwar, O. 2003. Nanofluidic Networks Based on Surfactant Membrane Technology. Anal. Chem. 75: 2529-2537.

70. Karlsson, M., Sott, K., Cans, A.S., Karlsson, A., Karlsson, R. and Orwar, O. 2003. Micropipet Writing Technique for Production of Two-Dimensional Lipid Bilayer Nanotube-Vesicle Networks on Functionalized and Patterned Surfaces. Langmuir 19: 3904-3910.

71. Karlsson, M., Sott, K, Davidson, M., Cans, A.S., Linderholm, P., Chiu, D. and Orwar, O. 2002. Formation of Geometrically Complex Lipid Nanotube-Vesicle Networks of Higher-Order Topologies. Proc. Natl Acad. Sci. USA 99: 11573-11578

72. Sott, K., Karlsson. M., Pihl. J., Hutig. J., Lobovkina. T. and Orwar. O. 2003. Micropipet Writing Technique for Production of Two-Dimensional Lipid

Bilayer Nanotube-Vesicle Networks on Functionalized and Patterned Surfaces. Langmuir 19: 3904-1910.

73. Karlsson, A., Sott, K., Markstrom, M., Davidson, M., Konkoli, Z. and Orwar, O. 2005. Controlled Initiation of Enzymatic Reactions in Micrometer-Sized Biomimetic Compartments. J. Phys. Chem. B 109: 1609-1617.

74. Cans, A.S., Wittenberg, N., Karlsson, R., Sombers, L., Karlsson, M., Orwar, O. and Eqing, A. 2003. Artificial Cells: Unique Insights into Exocytosis Using Liposomes and Lipid Nanotubes. Proc. Natl Acad. Sci. USA 100: 400-404.

75. V.T. Kung and C.T. Redemann. 1986. Synthesis of Carboxyacyl Derivatives of Phosphatidylethanolamine and Use as an Efficient Method for Conjugation of Protein to Liposomes. Biochim. Biophys. Acta 862: 435-439.

76. Peacock, A. and Calhoun, A. 2006. Polymer Chemistry. Hanser. Munich.

77. Himmelhaus, M. and Takei, H. 2002. Self-Assembly of Polystyrene Nanoparticles into Patterns of Random-Close-Packed Monolayers via Chemically Induced Adsorption. Phys. Chem. Chem. Phys. 4: 496-506.

78. Reis, G.E. 1975 *Dense Packings of Equal Circles within a Circle,* Math. Mag. 48: 33-37.

79. Conway, J.H. and Sloane, N.J.A. 1993.*Sphere Packings, Lattices and Groups,* 2nd ed. New York: Springer.

80. Mantsch, H.H. and Chapman, D., Infrared Spectroscopy of Biomolecules. 1996. Wiley-Liss. New York

81. Morrison I.D. and Ross, S. Colloidal Dispersions: Suspensions, Emulsions, and Foams. 2002. New York: Wiley-Interscience.

82. Cremer, P.S. and Boxer, S.G. 1999. Formation and Spreading of Lipid Bilayers on Planar Glass Supports. J. Phys. Chem. B 103: 2554-2559.

83. Ayres, P.R., 2008. *Investigating Bacterial Interactions with Polymer Surfaces using Attenuated Total Reflectance Fourier Transform Infrared Spectroscopy*. University of Denver, Denver

84. Cha, T., Guo, A. and Zhu, X.Y. 2006. Formation of Supported Phospholipid Bilayers on Molecular Surfaces: Role of Surface Charge Density and Electrostatic Interaction. Biophys. J. 90: 1270-1274

85. Baker, A.D. and Engel, R. 1992. Organic Chemistry. St. Paul: West Publishing Company.

86. Garrett, R.H. and Grisham, C.M. Biochemistry, 3rd ed. 2007. Brooks/Cole. USA

87. Branan, N., *Infrared Biosensors for Biological Agent Detection.* 2006 University of Denver, Denver

Chapter 3: Thermotrophic Phase Behavior of Nanoparticle Supported Bilayers

1.0 Introduction

1.1 Equilibrium Phases

Phospholipids have several phase transitions. The most notable phases are the subgel phase "L_c", the gel phases (L_β and $L_{\beta'}$ – untilted and tilted chains respectively), a sawtoothed "ripple" phase "$P_{\beta'}$", and the liquid crystalline phase "L_α" See Figure 3.1 for a schematic description of these phases. The phase transition from $L_c \rightarrow L_{\beta'}$ is known as the subphase transition, while $L_{\beta'} \rightarrow P_{\beta'}$ is the pre-transition, and $P_{\beta'} \rightarrow L_\alpha$ is the main transition. [1]

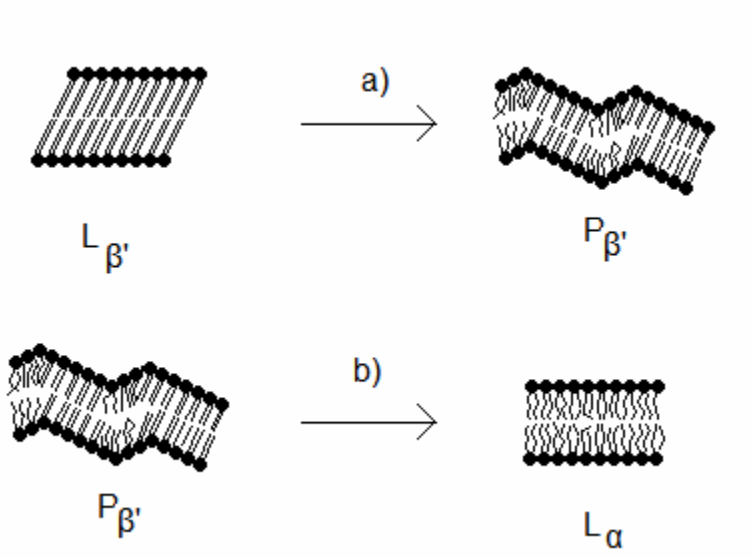

Figure 3.1: Schematic of the a) Pretransition and b) Main Transition.

Different physical characteristics of the phospholipids involved will impact the properties of said phospholipids. For example, the transition temperature of the main phase will vary according to the chain length of the phospholipid involved. For chains with fewer carbons, fewer phases are found. The richest polymorphisms are found with carbon chains between 15 and 22 units long. [1]

Studies of 1,2-dipalmitoyl-*sn*-glycero-3-phosphocholine (DPPC) (Figure 3.2) show that cooling from the L_α phase does not result in the original $P_{\beta'}$ phase. Instead, a long lived metastable phase, (known as $P_{\beta'}^{mst}$) is formed. [2, 3] This metastable phase differs in structure from the original $P_{\beta'}$ rippled phase. [4] A typical $P_{\beta'}$ phase has a wavelength of about 150 angstroms [5-9], while the metastable $P_{\beta'}^{mst}$ phase has a wavelength of about 300 angstroms [10]. The difference in enthalpy between these transitions is about 5% lower for the metastable rippled phase to liquid crystal phase ($P_{\beta'}^{mst} \rightarrow L_\alpha$) than the $P_{\beta'} \rightarrow L_\alpha$ transition [2].

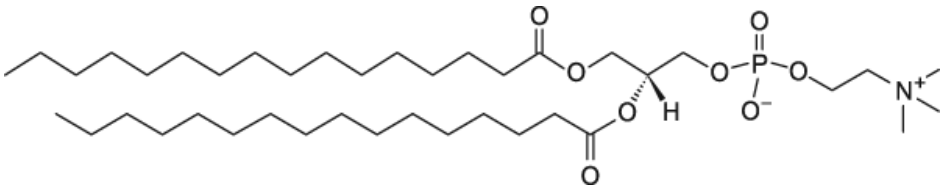

Figure 3.2: 1, 2-Dipalmitoyl-sn-Glycero-3-Phosphocholine (DPPC)

1.2 FTIR Acyl Chain Conformation

The symmetric and antisymmetric methylene stretching modes found in lipid hydrocarbon chains can be found near 2850 and 2920 cm^{-1} respectively. These modes are

also designated $_{s}\upsilon_{CH2}$ and $_{as}\upsilon_{CH2}$, respectively. Though both bands can be used for monitoring chain-melting phase transitions, the asymmetric band is not as pure as the symmetric band for such observations. The overlap that occurs in the antisymmetric stretching modes is due to methyl groups as well as Fermi resonance from the first overtones of methylene scissoring vibrations. As long as the dominant source of methylene vibrations are due to lipid hydrocarbon chains, the symmetric methylene stretch mode will continue to serve to characterize chain-melting phase transitions. [11]

During the process of hydrocarbon chain melting, a 1.5 – 2.5 cm^{-1} increase in frequency of the symmetric methylene stretch can be observed. The magnitude of the increase in frequency found can vary due to the structure and length of the hydrocarbon chain, the nature of the lipid head group, any additives that may be present, as well as the nature of the phase transition itself [12, 13]. Thus, these changes in frequency and band width of the symmetric methylene stretching mode is only useful for the detection and/or monitoring of lipid hydrocarbon chain phase transitions and not for the assigning of type of chain-melting phase. However, the assigning of chain-melting phases can be achieved through the use of other coincident infrared spectroscopic changes. [11]

Another approach to the detection of lipid hydrocarbon chain-melting phase transitions deals with methylene wagging regions. [14, 15] The all-trans polymethylene chains couple to produce band progressions, of which the intensities depend on the length of the all-trans segments involved. The introduction of gauche conformers results in the reduction of the average length of the residual all-trans polymethylene segments. This weakens the coupling of the methylene wagging mode and the band progression disappears when the lipid hydrocarbon chains are melted. It should be noted that the

disappearance of this band is not always indicative of a lipid hydrocarbon chain-melting phase transition. This is because the methylene wagging modes may couple to fundamental vibrational modes located within the polar head group to which the methylene chain is attached. This coupling is then very dependant on the nature of the polar head group. It should also be noted that unlike the methylene symmetric stretching modes, as well as other modes, the methylene wagging mode is intrinsically weak and requires the subtraction of the solvent and/or other reference spectra for data processing procedures. [11]

1.3 Polystyrene Nanospheres

1.3.1 Particle Characteristics

Polystyrene is a compound made from the aromatic styrene. Poly(styrene-divinylbenzene) is structurally related to polystyrene. Essentially, it is just the cross linked version of linear polystyrene. The divinyl benzene is what actually forms the cross-link in the cross-linked bead. This cross linked structure can have different charges placed throughout or on the surface of the bead. Aminomethyl groups can be attached to the aromatic portion of poly(styrene-divinylbenzene), adding a positive charge. Sulfuric acid can be used to react with a bead surface. This sulfonation results a negative charge being attached. Negative charges can also be attached by adding carboxylate groups.

1.3.2 Uses

Polystyrene nanoparticles have become widely used in several research fields. They are now commercially available in a wide variety of narrow size distributions.

Also, they can come with a variety of different surfactants, including linkers, dyes, biomolecules and covalently bound functional groups. Applications of these nanoparticles range from photonics, nanotechnology, life sciences, colloidal suspensions, phase transitions, to crystallization of "model" atoms. [16]

One of the more fascinating applications of polystyrene nanoparticles involves *in vivo* investigations. Recent investigations include the use of fluorescent polystyrene beads for selective cellular imaging. This is done by coupling biologically active molecules, such as proteins or nucleic acids to fluorescent polystyrene beads [17, 18]. Also, the coupling of antibodies to polystyrene nanoparticles leads to uptake by antigen-presenting cells. [19].

Randomly packed layers of PS nanoparticles also serve as a platform for biomolecular reactions. Patterning of these platforms could lead to improved dosing of biomolecules and provide better site control. This in turn, can lead to the PS nanoparticles playing an important role in both the quantification and qualification of biomolecular species. [16]

Polystyrene nanoparticles can also serve as photonic band-gap (PBG) materials [20]. PBG materials have periodic refractive indices as a function of space [21]. The electromagnetic waves propagating through a structure containing periodic refractive indices will encounter forbidden zones, much as in the same way that an electron will have a periodic function of potential within a semi-conductor material [22]. A Potential application of polystyrene nanoparticles acting as a PBG material are a new type of surface electromagnetic wave sensor that makes use of a one-dimensional PBG material in place of a metal film as used in surface plasmon resonance [20].

2.0 Materials and Methods

2.1 *Preparation of Random Close-Packed Nanoparticle Layers*

A polystyrene "latex" nanosphere dispersion in water was acquired from Alfa Aesar (100 nm diameter, 2.5 wt %, Stock # 42712, Lot # H25Q22, CAS # 9003-53-6). This dispersion was diluted in water one hundred-fold into a weight percent of 0.025%. The process of evaporative formation was then used to evaporate 25 μL aliquots to form a randomly close-packed layer of PS nanospheres.

2.2 *Preparation of Supported Multi-Bilayer*

Lipid vesicles were fused onto a diamond ATR surface or the close-packed nanobeads through the process of evaporative formation. A gentle stream of nitrogen gas was used to evaporate the water solvent, leaving a thin-film of lipid multi-layers. A small amount of PBS buffer (25 μL) was then used to rehydrate the sample.

2.3 *FTIR Spectroscopy*

All FTIR spectra were recorded with a Digilab (Randolf, MA) FTS 7000 FTIR spectrometer equipped with a liquid nitrogen-cooled mercury cadmium telluride (MCT) detector and a DuraSample*IR* II ATR (SenseIR Technologies). Spectra were collected over the range 4000 cm^{-1} to 400 cm^{-1} with a resolution of 4 cm^{-1}. Each spectrum was produced by the coaddition of 256 scans.

2.4 Data Analysis

Since transition temperatures and relative cooperativity are often difficult to measure visually, statistical software such as Origin must be employed to determine those values. There are four parameters to be obtained. These are simply "P_1, P_2, P_3 and P_4," with wavenumber as a function of temperature in Kelvin [24]:

$$Wavenumber = P_1 + \frac{P_2}{1 + \left(\frac{P_3}{T}\right)^{P_4}}$$

"P_1" is the minimum wavenumber for the phase transition. "P_2" is the magnitude of the phase transition and is also the net change in wavenumbers representing the change in number of trans-to-gauche rotamers. "P_3" is the transition temperature and represents the point where half of the molecules have undergone a phase transition. "P_4" is a measure of the relative cooperativity and describes the degree to which one lipid molecule is affected by the state of an adjacent molecule. [24]

At a given temperature, the level of disorder can be derived from the relative amount of gauche rotamers present [25, 26]. The frequency for the methylene symmetric stretch for a completely ordered system (0% gauche rotamers) of DPPC is designated ν_{min}. When the same system is completely disordered (100% rotamers) by heating, the symmetric methylene frequency is designated ν_{max}. Based on these numbers, the percentage of gauche rotamers (also known as the degree of transition or "α") can then be estimated as thus [24]:

$$\alpha = \frac{(Methylene\_Symmetric\_Stretch\_Frequency) - \nu_{\min}}{\nu_{\max} - \nu_{\min}}$$

$$k_{app} = \frac{\alpha}{1 - \alpha}$$

The DPPC bands found between 1400 cm^{-1} and 1300 cm^{-1} in the infrared spectrum are due to localized wagging vibrations of methylene groups involved in nonplanar conformers. There are four bands in this region of particular interest: 1367 cm^{-1}, 1354 cm^{-1}, 1341 cm^{-1}, and 1306 cm^{-1}. The bands at 1367 cm^{-1} and 1306 cm^{-1} are due to methylene wagging groups found in kink (gtg') sequences. The band at 1341 cm^{-1} is due to methylene wagging of end-gauche conformers. The band at 1354 cm^{-1} is due to methylene wagging of double-gauche conformers. Also in this region is a fifth band of interest located at 1378 cm^{-1} that is due to the symmetric bending of terminal methyl groups. Since this 1378 cm^{-1} band is insensitive to conformation and chain length, it can be used as an internal standard to which the wagging regions can be normalized. [27]

There are several techniques that must be employed in order to gather information from the region of the IR spectrum from 1400 cm^{-1} to 1300 cm^{-1}. First there is substantial interference from water and water vapor that must be subtracted from the region of interest. Next a baseline must be constructed by cubic spline interpolation and be subtracted from the original spectrum. Fourier deconvolution methods must then be used to obtain accurate estimates of the peak frequencies of the present absorption bands. The characteristics of the individual absorptions must then be estimated by curve-fitting Gaussian-Lorentzian functions. The integrated absorption bands can then be normalized to the methyl symmetric bending mode located at 1378 cm^{-1}. From this point, the normalized integrated intensities can be converted to conformer concentrations. [28]

3.0 Results and Discussion

3.1 Estimation of nanosphere film thickness

The regular arrangement of circles that gives the highest packing density, $\pi/\sqrt{12} \approx 0.9069$, is where the centers of the circles are arranged in a hexagonal lattice. When considering a plane with spheres placed on it, the two most common arrangements are face centered cubic and hexagonal close packing. In both arrangements, the average packing density is $\pi/\sqrt{18} \approx 0.74048$. [29, 30]

Given polystyrene spheres with a diameter of 1.0×10^{-7} m and an ATR surface with a diameter of 4×10^{-3} m (~8×10^{-3} m if the well is overfilled and some beads settle on the stainless steel), we calculated the number of beads needed to form a single hexagonally close packed layer to be no fewer than 6.8×10^{8} and most likely closer to 3.6×10^{9}.

The estimated minimum thickness of close packed nanospheres formed from 25 μL of a 0.025% suspension (1.14×10^{10} beads) to be 3-layers or about 300 nm.

3.2 Thermal Phase Transition

The thermal phase transitions of DPPC multibilayers were observed including DPPC multibilayers formed using polystyrene nanospheres as a polymer support, as well as DPPC multibilayers formed on a PS nanosphere support in the presence of divalent calcium. In order to observe the pre- and main transitions the samples were heated and subsequently cooled between ranges of approximately 20°C - 50°C. The maximum and

minimum frequencies found in each observation were used to calculate the number of gauche rotamers present.

Referring to Figure 3.3, both the heating and cooling curves of a DPPC multibilayer are represented by a solid or open red squares, respectively. The solid and open green circles represent a DPPC multibilayer formed using a PS nanosphere polymer cushion. In Figure 3.4 the green curves are identical to those found in Figure 3.3, however the solid and open blue triangles represent the heating and cooling curves of DPPC multibilayers formed on PS nanospheres in the presence of divalent calcium.

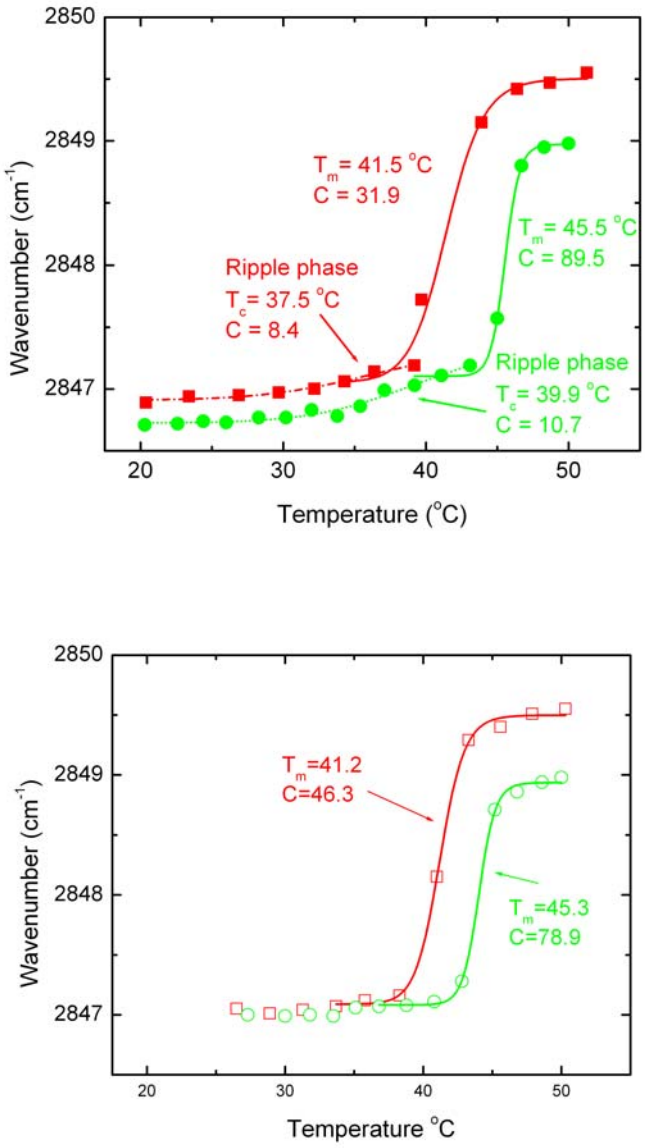

Figure 3.3: The heating (solid) and cooling (open) phase transition curves for DPPC multibilayers (red squares) formed on a PS nanosphere (green circles) surface.

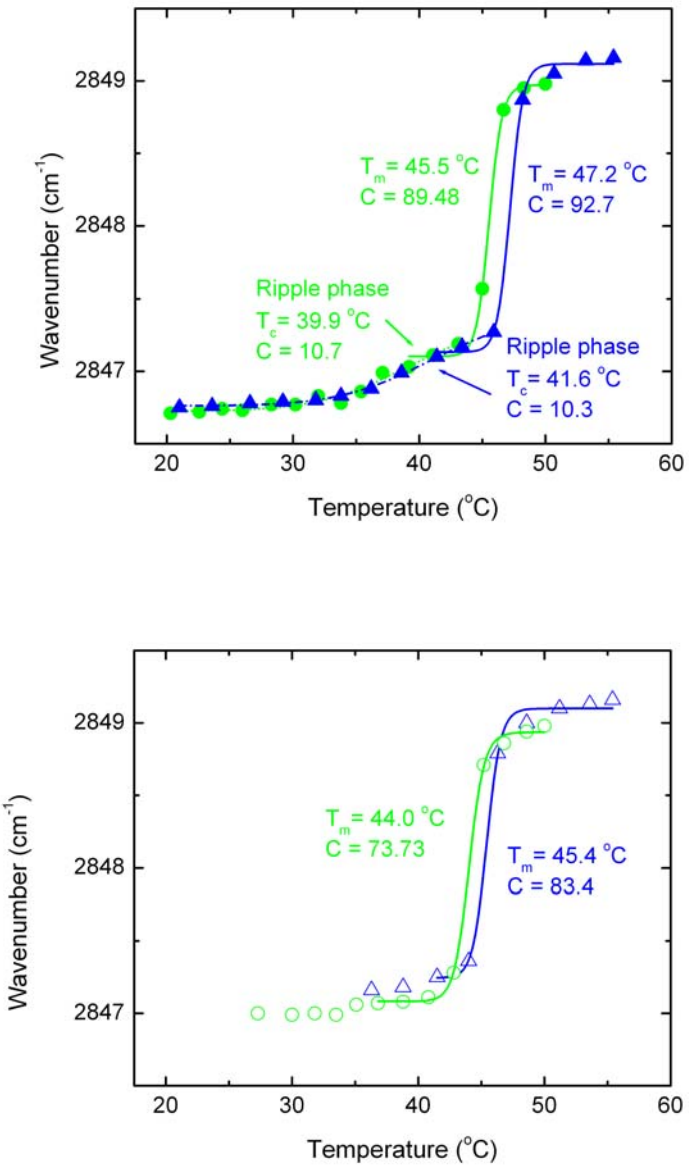

Figure 3.4: The heating (solid) and cooling (open) phase transition curves for DPPC multibilayers formed on PS nanospheres (green circles) or formed on PS nanospheres in the presence of divalent calcium (blue triangles).

Upon examination of the data represented in Figure 3.3 one can observe discontinuous increases in absorption maxima. Hysteresis between the heating and

cooling directions as seen in both the control and the PS nanosphere polymer support is minor and significantly less than that observed for vesicle suspensions when monitored in transmission mode [31]. Figure 3.4 also demonstrates discontinuous increases in absorption maxima when calcium is present. This divalent cation does induce greater hysteresis between the heating and cooling directions. This suggests an alteration of the phase transition pathway.

3.3 The Cooperative Transition

Parameter 4, "P4," as described above, is synonymous with "C," the cooperativity unit found in Figures 3.3 and 3.4. It describes a two-state process by which one phospholipid molecule is affected by an adjacent phospholipid molecule. The larger the value of "C," the more cooperative is the process of thermal phase transition. Another way of stating this is that the larger the value of "C," the more the phospholipid multilayer acts as a single unit during phase transition. The sulfonated nanobeads increase cooperativity of the main transition, $P_{\beta'} \rightarrow L_{\alpha}$. This indicates an increase in the cooperative unit size.

	Tm	C	P2 (Magnitude of Transition)	P1
Control (Heating)	41.5 +/- 0.5	32 +/- 7	2.66 +/- 0.02	2846.89 +/- 0.04
Control (Cooling)	41.2 +/- 0.1	46 +/- 5	2.54 +/- 0.05	2847.01 +/- 0.03
On Nanobeads (Heating)	45.5 +/- 0.1	90 +/- 12	2.27 +/- 0.06	2846.71 +/- 0.04
On Nanobeads (Cooling)	45.3 +/- 0.1	79 +/- 12	1.99 +/- 0.05	2846.99 +/- 0.04
On Nanobeads with Calcium (Heating)	47.2 +/- 0.1	93 +/- 13	2.41 +/- 0.5	2846.75 +/- 0.04
On Nanobeads with Calcium (Cooling)	45.4 +/- 0.2	83 +/- 18	2.00 +/- 0.08	2847.16 +/- 0.06

Table 3.1: Lipid Phase Transition Parameters

Calcium was originally employed to determine if it increased vesicle fusion to the close-packed nanobead surface. An increase in vesicle fusion and change in phase behavior was not observed beyond the usual increase in melting temperature found for lipids in the presence of divalent cations.

3.4 Thermodynamic Properties of the Transition

A two-state transition model rests on the assumption that the initial and final states have measurably different thermodynamic properties and that no thermodynamically stable intermediates are present. The Gibbs potential of lipid bilayers is:

$$G = H - TS = W_s + U_g + U_{vw} - T(S_g + S_{pk})$$

where G, H, S and T are the Gibbs potential, enthalpy, entropy and absolute temperature, respectively. W_s accounts for steric and hydrophobic interactions imposed on the headgroup packing. U_g and S_g are the energy and entropy contributions due to gauche bond formation. U_{vw} and S_{pk} are the energy and entropy contributions of van der Waals attraction and hard-core repulsions (excluded volume or packing). This model predicts that ΔU_{vw}, interchain van der Waals interactions energy, makes the major contribution to the transition enthalpy ΔH, while the entropy from intrachain trans-gauche isomerization, ΔS_g, makes the major contribution to the transition entropy. This is consistent with the general consensus that the lipid bilayer gel to liquid crystal phase transition is mainly entropy-driven due to trans-gauche isomerization at the expense of van der Waals interactions.

The linear portions of the sigmoidal curves shown in Figures 3.3 and 3.4 were used to generate van't Hoff plots. The degrees of transition, or "α," were calculated as described above using the data from Figures 3.3 and 3.4. The apparent equilibrium constant for each transition can then be described as:

$$K_{app} = \alpha / (1 - \alpha)$$

Once the apparent equilibrium constants were found $\ln(K_{app})$ is plotted vs 1/T. The resulting plots are color and shape coordinated with figures 3.3 and 3.4 such that the solid red squares represent the control DPPC multibilayers in the heating and cooling direction respectively and the green circles and blue triangles are respectively the presence of PS nanospheres and divalent calcium.

The steeper slopes for lipids supported on nanobeads reflects an increase in the van't Hoff enthalpy (slope = $-\Delta H_{vh}/R$). Since the enthalpy of transition is dominated by interchain van der Waals interaction energy, this is likely caused by an increase in cooperative unit size. The Gibbs potential of lipid bilayers includes a term linked to head group packing, W_s.. Interaction with the bead surface may alter W_s, and thus impact the transition thermodynamics. A connection between head group effects and cooperativity has been previously observed.

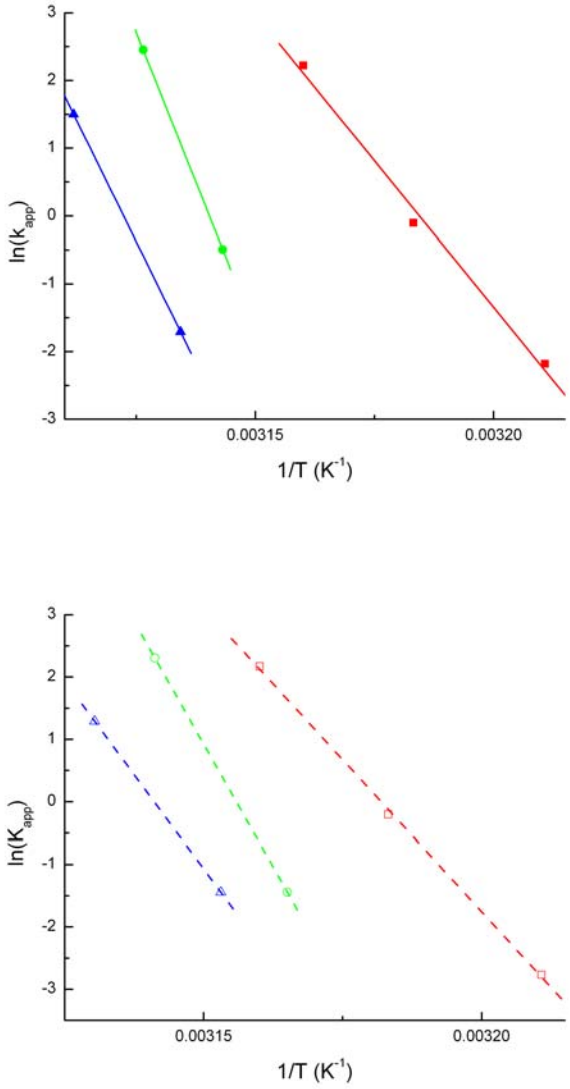

Figure 3.5: van't Hoff plots of resulting data acquired from Figures 3.3 and 3.4. The solid and dashed lines represent the heating and cooling phase transitions respectively. Red squares represent the DPPC multibilayer control, green circles represent the presence of a PS nanosphere polymer support while blue triangles represent the presence of PS nanosphere support as well as divalent calcium.

3.5 Wagging Region

The determination of percent conformation can by done by analyzing the wagging region of the infrared spectrum. Within this region are absorption bands due to the wagging motions of kink (gtg'), double gauche and end gauche rotamers as well as the symmetric methyl bend (methyl umbrella) to which the wagging modes are normalized. Using Origin software, one can determine the area due to each absorption band, and after taking into account factors such as molar absorptivity and the number of acyl chains per phospholipid molecule, use this area to determine the proportions of each rotamer species. Table 3.2 is just such data as acquired from Figures 3.6, 3.7 and 3.8.

	Kink	Double Gauche	End Gauche	Total
DPPC Control - Gel Phase	2.86 +/- 1.04	0.74 +/- 0.53	3.03 +/- 0.34	6.63
DPPC Control - Liquid Crystal Phase	3.37 +/- 0.77	2.51 +/- 0.27	2.59 +/- 0.40	8.47
Nanobeads - Gel Phase	3.16 +/- 0.92	1.45 +/- 0.19	2.18 +/- 0.18	6.79
Nanobeads - Liquid Crystal Phase	4.56 +/- 0.46	4.31 +/- 0.66	1.15 +/- 0.66	10.02
Calcium and Nanobeads - Gel phase	3.25 +/- 0.46	1.29 +/- 0.66	2.29 +/- 0.66	6.82
Calcium and Nanobeads - Liquid Crystal Phase	4.67 +/- 0.54	3.70 +/- 0.68	1.41 +/- 0.13	9.78

Table 3.2: Number of gauche rotamers found per molecule of phospholipid DPPC (Control), DPPC as formed on PS nanosphere polymer support (Nanobeads) and DPPC formed on PS nanosphere polymer support in the presence of calcium (Calcium and nanobeads).

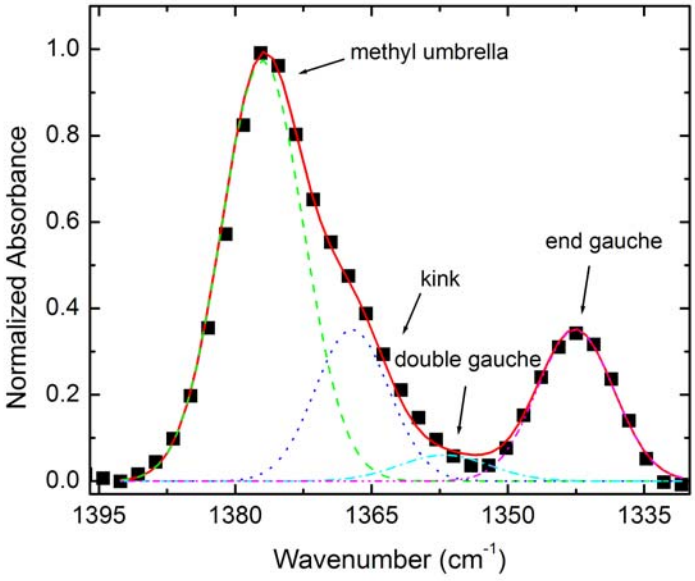

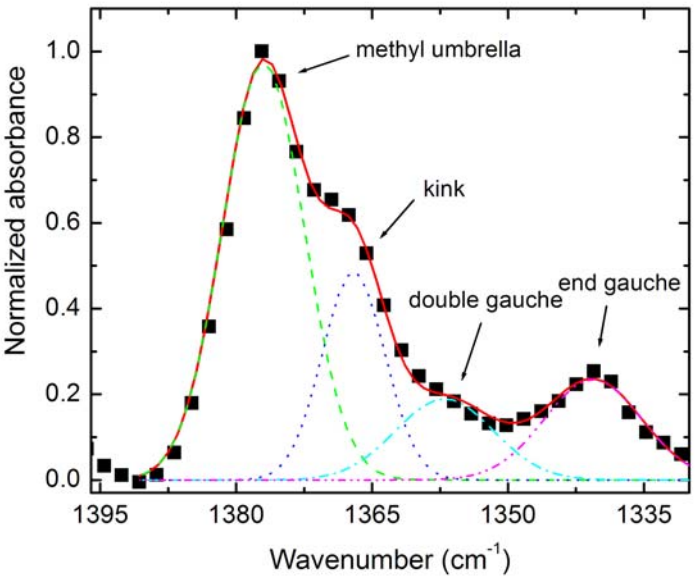

Figure 3.6: Wagging region portion of infrared spectrum for DPPC control both in the gel (top) and liquid crystal (bottom) states.

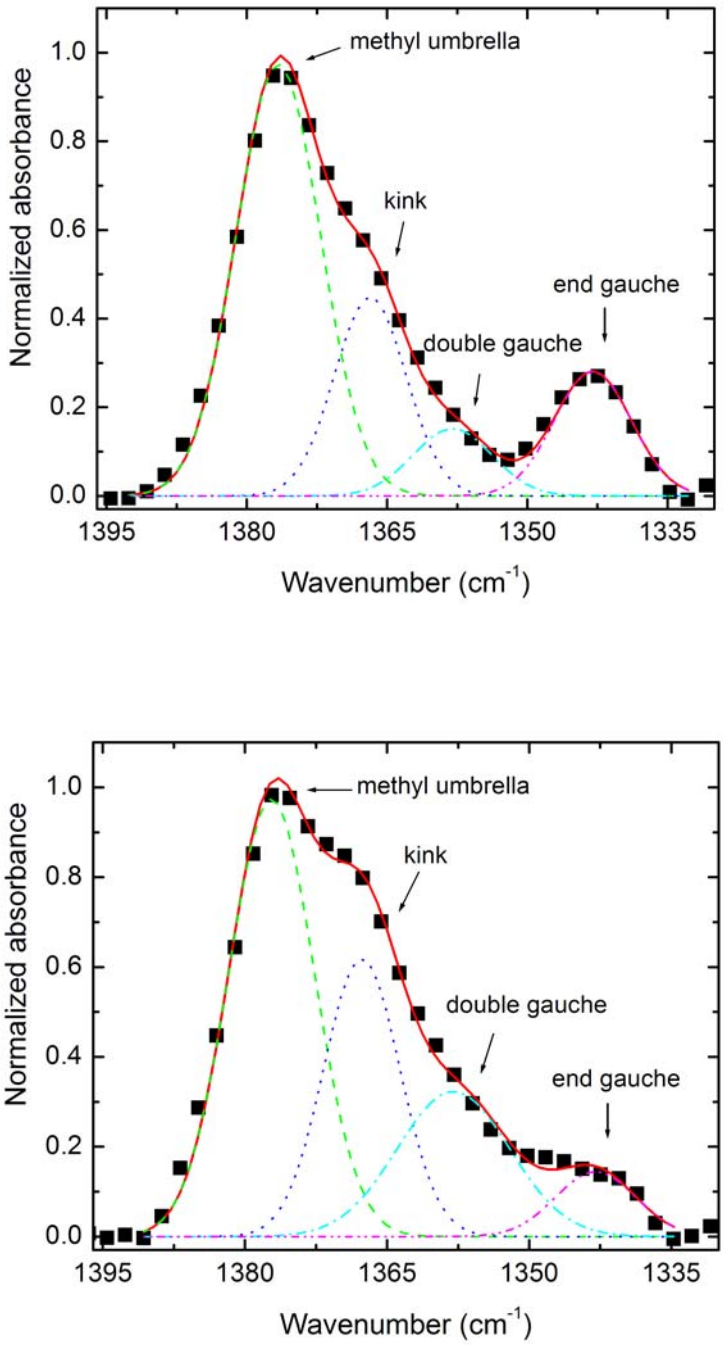

Figure 3.7: Wagging region portion of the infrared spectrum of DPPC formed on PS nanosphere polymer support both in the gel (top) and liquid crystal (bottom) states.

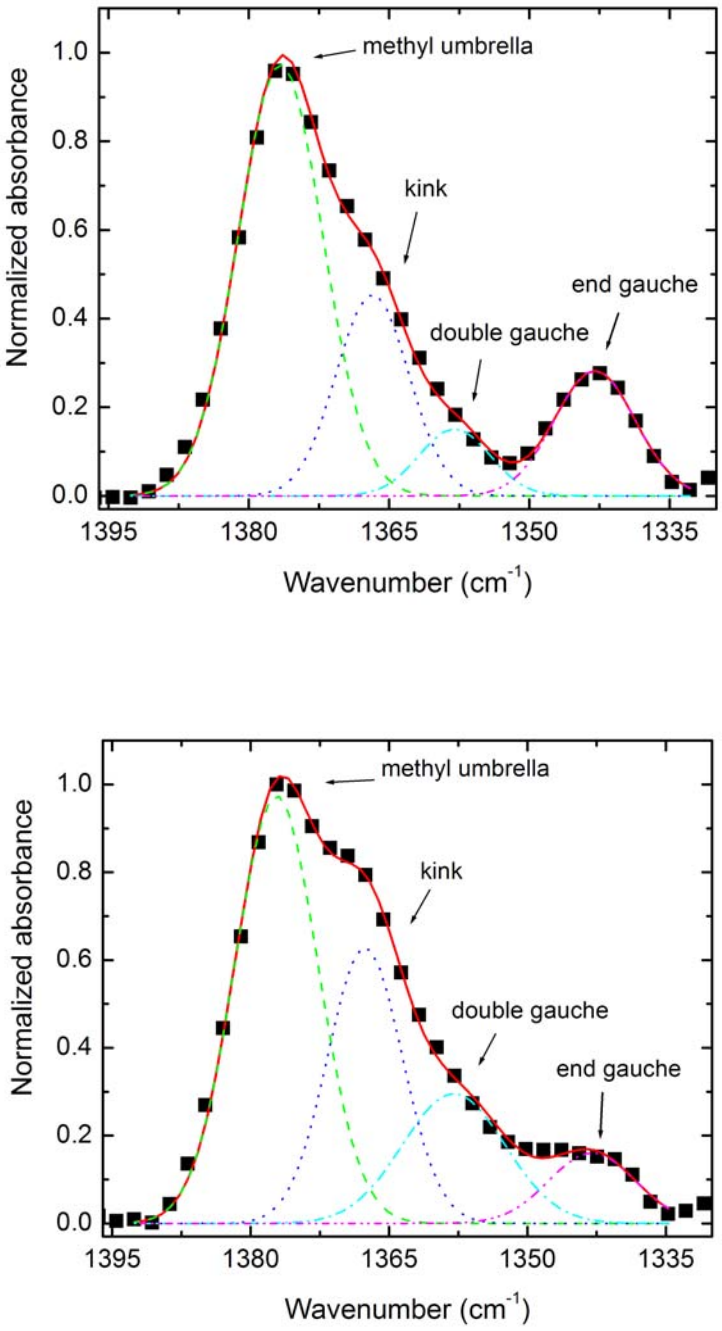

Figure 3.8: Wagging region portion of the infrared spectrum of DPPC formed on PS nanosphere polymer support in the presence of divalent calcium both in the gel (top) and liquid crystal (bottom) states.

As one can see from Table 3.2, shifting from the gel phase to the liquid crystal phase of either sample leads to an increase of approximately 2-3 total gauche rotamers. These totals result from an increase in the number of kink and double gauche rotamers resulting from the main transition. The number of end gauche rotamers decreased from the gel phases to the liquid crystal phases.

The presence of 8.5 gauche rotamers in the liquid crystal phase for the DPPC control is in very good agreement with data obtained in transmission experiments. The nanobeads increase the total gauche content above the T_m. The addition of calcium has little impact on gauche content despite its impact on the T_m. In the liquid crystal phase, the nanobeads cause an increase in kink and double gauche; however, a decrease in end gauche did occur. Calcium has only minimal impact on kink, double gauche and end gauche proportions.

4.0 Conclusions

It appears that adsorption of the multibilayer takes place on the PS nanosphere polymer support. There also appears to be no insertion of the polymer support into the multibilayer. This is most likely due to the lack of electrostatic interaction between the non-polar portion of the DPPC head group and the slight (3%) negative charge on the PS nanosphere beads as well as the relative size of the PS nanoparticle. It is almost counterintuitive that the nanobeads would increase the melting temperature so significantly and also increase gauche content. However, head group interactions impact

lipid packing in the bilayer. The interactions in the gel phase increase bilayer stability, but in the liquid crystal phase increase acyl chain mobility.

Randomly packed layers of PS nanoparticles serve as a platform for biosensors. Unpublished data from this lab have shown that stacked layers of phospholipid membrane adhere well to thin-films of PS nanospheres. These particular nanospheres have a slight negative charge on their surface due to sulfonation. This sulfonation was originally designed to keep the PS nanoparticles from coagulating. It is believed that this negative charge on the surface of the PS nanoparticles provides an electrostatic interaction with the positively charged component of the polar head group found in the phospholipid 1, 2-dipalmitoyl-*sn*-glycero-3-phosphocholine (DPPC). The contributions of electrostatic interaction versus those of the nanobead contact alone are difficult to separate.

References:

1. Koynova, R., and Caffrey, M. 1998. Phases and Phase Transitions of the Phosphatidylcholines. Biochimica Et Biophysica Acta. 1376: 91-145.
2. Tenchov, B, Yao, H. and Hatta, I. 1989. Time Resolved X-Ray Diffraction and Calorimetric Studies at Low Scan Rates. I. Fully Hydrated Dipalmitoylphosphatidylcholine (DPPC) and DPPC/Water/Ethanol Phases. Biophys. J. 56: 757-768.
3. Koynova, R., Koumanov, A. and Tenchov, B. 1996. Metastable Rippled Gel Phase in Saturated Phosphatidylcholines: Calorimetric and Densitometric Characterization. Biochimica Et Biophysica Acta. 1285: 101-108.

4. Yao, H., Matuoka, S., Tenchov, B. and Hatta, I. 1991. Metastable Ripple Phase of Fully Hydrated Dipalmitoylphosphatidylcholine as Studied by Small Angle X-Ray Scattering. Biophys. J. 59: 252, 255.

5. Tardieu, A., Luzzati, V. and Reman, F.C. 1973. Structure and Polymorphism of the Hydrocarbon Chains of Lipids: Lecithin-Water Phases. J. Mol. Biol. 75: 711-733.

6. Janiak, M.J., Small, D.M. and Shipley, G.G. 1979. Temperature and Compositional Dependence of the Structure of Hydrated Dimyristoyl Lecithin. J. Biol. Chem. 254: 6068-6078.

7. Pinto da Silva, P. 1971. Freeze Fracture of Dipalmitoyl Lecithin Vesicles. Jounal de Microscopie (Paris). 12: 185-192.

8. Verkleij, A.J. Ververgaert, P.H.J., Van Deenen, L.L.M. and Elbers, P.F. 1972. Phase Transitions of Phospholipid Bilayers and Membranes of Acholeplasma Laidlawii B Visualized by Freeze Fracturing Electron Microscopy. Biochim. Biophys. Acta, 288: 326-323.

9. Ververgaert, P.H.J., Verkleij, A.J., Elbers, P.F. and Van Deenen, L.L.M. 1973. Analysis of the Crystallization process in Lecithin Liposomes: A Freeze-Etch Study. Biochimica et Biophysica Acta, 311: 320-329

10. Sengupta, K., Raghunathan, V.A. and Katsaras, J. 2003. Structure of the Ripple Phase of Phospholipid Mulibilayers. Physical Review E. 68: 031710.

11. Chapman, D. and Mantsch, H.H. 1996. *Infrared Spectroscopy of Biomolecules.* Wiley-Liss, New York.

12. Casal, H.L., and Mantsch, H.H. 1983. The Thermotropic Phase Behavior of *n*-Methylated Dipalmitoyl Phosphatidylethanolamines. Biochim. Biophys. Acta. 735: 387-396.

13. Casal, H.L., and Mantsch, H.H., 1984. Polymorphic Phase Behavior of Phospholipid Membranes Studied by Infrared Specroscopy. Biochim. Biophys. Acta. 779: 381-402.

14. Chia, N.C., and Mendelsohn, R. 1992. CH_2 Wagging Modes of Unsaturated Acyl Chains as IR Probes of Conformational Order in Methyl Alkenoates and Phospholipid Bilayers. J. Phys Chem. 96: 10543-10547.

15. Chia, N.C., Vilcheze, C., Bittman, R. and Mendelsohn, R. 1993. Interactions of Cholesterol and Synthetic Sterols with Phosphatidylcholines and Deduced from Infrared CH_2 Wagging Progression Intensities. J. Am. Chem. Soc. 115: 12050-12055.

16. Himmelhaus, M., and Takei, H. 2002. Self-Assembly of Polystyrene Nano Particles into Patters of Random-Close-Packed Monolayers via Chemically Induced Adsorption. Phys. Chem. Chem. Phys. 4: 496-506.

17. Smith, C.L. 1994. Cytoskeletal Movements and Substrate Interactions during Initiation of Neurite Outgrowth by Sympathetic Nerurons in Vitro. J. Neurosci. 14 (1): 384-398.

18. Di, A., Krupa, B., Bindokas, V.P., Chem, Y., Brown, M.E, Palfrey, H.C., Naren, A.P., Kirk, K.L. and Nelson, D.J. 2002. Quantal Release of Free Radicals during Exocytosis of Phagosomes. Nat. Cell Biol. 4(4): 279-285.

19. Wang, X., Uto, T., Sato, K., Ide, K., Akagi, T., Okamoto, M., Kaneko, T., Mitsuru, A. and Baba, M. 2005. Potent Activation of Antigen-Specific T Cells by Antigen-Loaded Nanospheres. Immunology Letters 98: 123-130

20. Shinn, M., and Robertson, W.M. 2005. Surface Plasmon-Like Sensor Based on Surface Electromagnetic Waves in a Photonic Band-Gap Material. Sensors and Actuators B. 105: 360-364.

21. Berger, V. 1999. Photonic Crystals and Photonic Structures. Current Opinion in Solid State and Materials Science. 4: 209-216.

22. Yablonovitch, E. 1987. Inhibited Spontaneous Emission in Solid-State Physics and Electronics. Phys Rev. Lett. 58: 2059-2062.

23. V.T. Kung and C.T. Redemann. 1986. Synthesis of Carboxyacyl Derivatives of Phosphatidylethanolamine and Use as an Efficient Method for Conjugation of Protein to Liposomes. Biochim. Biophys. Acta.862: 435-439.

24. Borchman, D., Yappert, M.C. and Herrell, P. 1991. Structural Characterization of Human Lens Membrane Lipid by Infrared Spectroscopy. Investigative Ophthalmology & Visual Science 32: 2404-2416.

25. Cameron, D.G., Casal, H.G., Gudgin, E.F., and Mantsch, H.H. 1980. The Gel Phase of Dipalmitoyl Phosphatidylcholine and Infrared Characterization of the Acyl Chain Packing. Biochim. Biophys. Acta 596: 463-467.

26. Mantsch, H.H., Cameron, D.G., Umemura, J., and Casal, J.L. 1980. Fourier Transform Infrared Spectroscopy of Aqueous Systems: Applications to the Study of Biological Membranes. J. Mol. Struct. 60: 263-268

27. Casal, H.L., and McElhaney, R.N. 1990. Quantitative Determination of Hydroarbon Chain Conformational Order in Bilayers of Saturated Phosphatidylcholines of Various Chain Lengths by Fourier Transform Infrared Spectroscopy. 29: 5423-5427.

28. Lewis, R.N.A.H., McElhaney, R.N., Monck, M.A. and Cullis, P.R. 1994. Studies of Highly Asymmetric Mixed-Chain Diacyl Phosphatidylcholines that Form Mixed-Interdigitated Gel Phases: Fourier Transform Infrared and ^{2}H NMR Spectroscopic Studies of Hydrocarbon Chain Conformation and Orientational Order in the Liquid-Crystalline State. 67: 197-207.

29. Reis, G.E. 1975. *Dense Packings of Equal Circles within a Circle,* Math. Mag. 48: 33-37.

30. Conway, J.H. and Sloane, N.J.A. 1993. *Sphere Packings, Lattices and Groups,* 2nd ed. New York: Springer.

31. Kryszak, K. D., 2008. *Characterization of Nano-Confined Lipids using FTIR and EPR Spectroscopy.* University of Denver, Denver

Chapter 4: Myoglobin Based Ultrathin Layers

1.0Introduction

1.1 Myoglobin

Myoglobin was chosen as the selective biological element during this course of investigation because its ability to bind several analytes. Myoglobin is a single-chain globular protein of 153 amino acids, has a molecular weight of 16.7 kDa, and is responsible for the storage of diatomic oxygen in muscle tissue. [1] Each myoglobin protein molecule contains a single heme (iron-containing porphyrin) near its center, about which, the remaining apoprotein folds. Unlike hemoglobin, to which myoglobin is structurally related, [2] myoglobin does not demonstrate cooperative binding of oxygen. Positive cooperativity is a property of multimeric/oligomeric proteins. Instead, the binding of oxygen by myoglobin is unaffected by the oxygen pressure in the surrounding tissue. The structure of myoglobin, by high-resolution X-ray crystallography, was determined by John Kendrew and associates in 1958 [3].

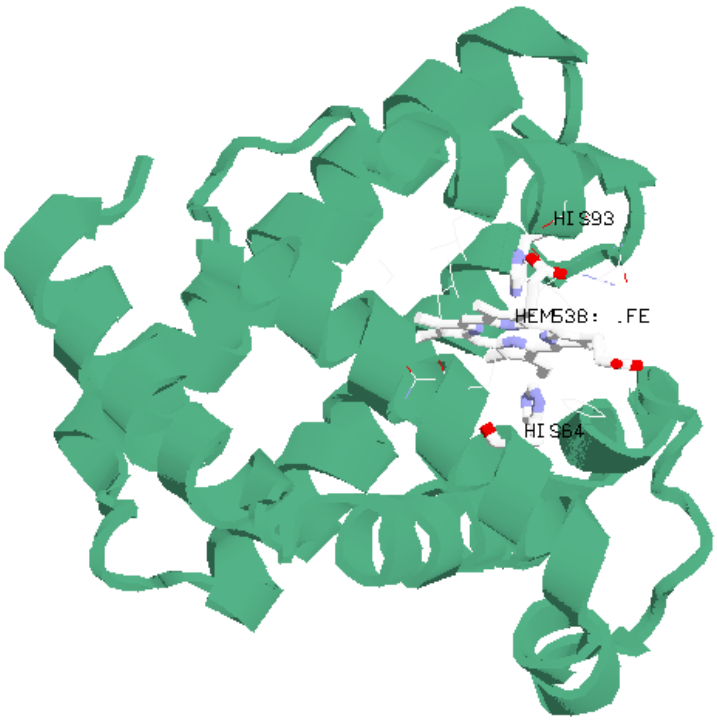

Figure 4.1: Myoglobin Structure

A porphyrin ring with an iron center is contained within myoglobin. A *proximal histidine* group is attached directly to the iron center, and a *distal histidine* group is present on the opposite face which is not bonded to the iron.

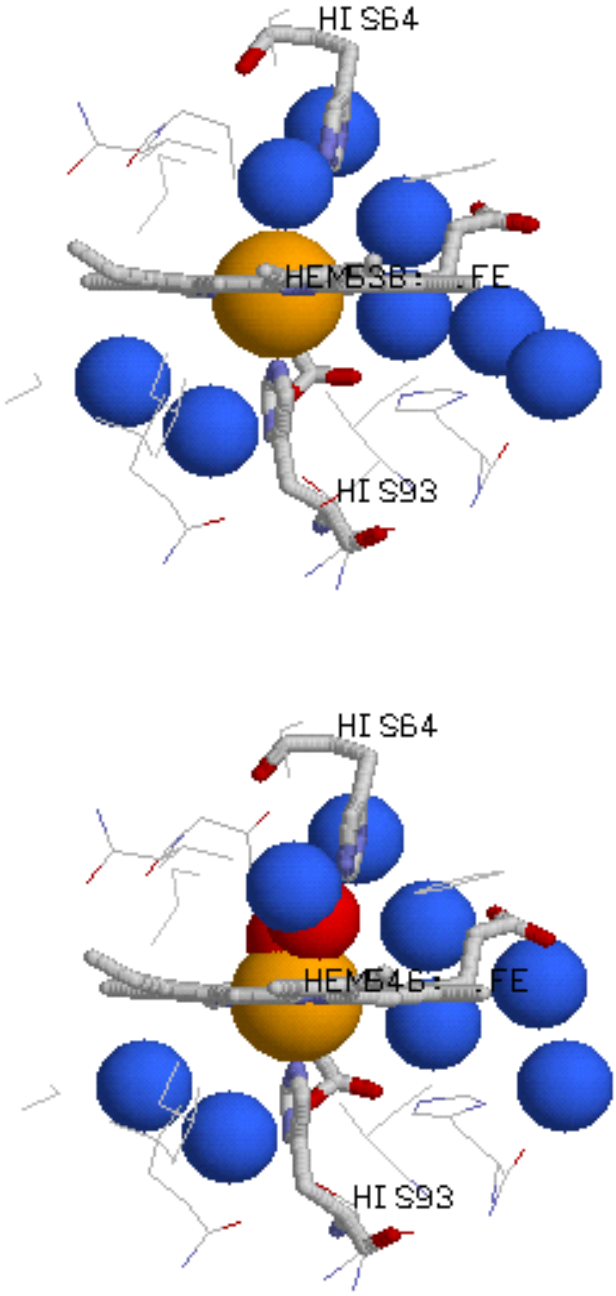

Figure 4.2: A close of up view of the iron-heme in both its deoxymyoglobin (top) and oxymyoglobin (bottom) states. Red spheres are oxygen atoms. Blue spheres are water molecules.

Many functional models of myoglobin have been studied. One of the most important is that of *picket fence porphyrin* by James Collman. This model was used to show the importance of the distal prosthetic group. As such, it serves three functions. First is that it forms hydrogen bonds with the dioxygen moiety, subsequently increasing the O_2 binding constant, while simultaneously preventing the binding of carbon monoxide. Carbon monoxide binds to iron in an end-on fashion, and is hindered by the presence of the distal histidine, which forces it into a bent conformation. Carbon monoxide binds to the heme 23,000 times better than O_2, but only 200 times better when incorporated into hemoglobin and myoglobin. Oxygen binds in a bent fashion, which corresponds well with the distal histidine. [4] Irriversible dimerization of oxymyoglobin with deoxymyoglobin species is also prevented by the distal histidine.

1.2 Sensor Element Immobilization

A process known as *immobilization* is used adhere the biological component (myoglobin) to its transducer. There are five modes of doing this. Each will be discussed below. These modes are: [5]

(i) Adsorption

(ii) Microencapsulation

(iii) Entrapment

(iv) Cross-Linking

(v) Covalent Binding

Adsorption is the first in this list of five. It is the simplest method and involves the least preparation. However, since there is weak bonding involved, this method is only considered suitable over a short lifetime. [5]

Second in the list of modes of immobilization is *microencapsulation*. Early biosensors used this method as their mode. Close contact between the biological element and the transducer can be achieved through the use of an adaptable membrane. The reliability of the biological element used is thereby retained. Also, contamination and degradation are limited. This method is stable towards changes in temperature, pH, ionic strength and chemical composition. Matter such as small molecules, gas molecules and electrons can be permeable to particular membranes. [5]

Early biosensors exploited the permeability of certain membranes. In particular they used a combination of polyethylene and cellulose acetate membranes. The polyethylene membrane was used since it was permeable to oxygen. A cellulose acetate membrane is used because it is permeable to both oxygen and glucose. For these two reasons, both types of membranes were exploited in early biosensors. [5]

Entrapment is the third mode of immobilization. In this mode the biomaterial becomes trapped when it is mixed with a monomer solution in order to form a gel. The barrier formed by polymerization affects substrate diffusion by slowing the reaction. Biological elements can also diffuse and escape through pores in the gel resulting in a loss of bioactivity. The most commonly used gel is polyacrylamide, though other gels

such as starch gels, nylon and silastic gels have been used. Polypyrroles are conducting polymers which can be useful when working with electrodes. [5]

Cross-linking is the fifth mode of immobilization. When using this mode, the selective biological element is chemically bonded to solid supports or to other supporting materials such as a gel. Bifunctional reagents such as glutaraldehyde are used in this mode. Again like in *entrapment,* there is some diffusion limitation that results in damage to the biomaterial. There is also poor mechanical strength throughout this system. Despite those limitations, this mode has proven useful to stabilize adsorbed biomaterials. [5]

The ATR-FTIR biosensor designed for these experiments uses a combination of immobilization techniques. The myoglobin, serving as the selective biological element, is covalently bound to the phospholipid DPPE. This conjugated phospholipid is then incorporated into liposomes containing the phospholipid DPPC. The resulting liposomes are then fused onto an ATR IRE leaving the conjugated DPPE adsorbed on the surface. So as one can see, the two modes of immobilization here used are a combination of *adsorption* and *cross-linking*.

1.3 Spectroscopy

Both UV-Vis and FTIR spectroscopy were used to characterize myoglobin as it was observed bound to the phospholipid 1,2-dipalmitoyl-*sn*-glycero-3-phosphoethanolamine (DPPE) in a phospholipid mixture (1:10) with DPPC. In coordination complexes such as an iron-bound heme, visible light is absorbed when

electrons move from a lower energy *d* orbital to a higher energy *d* orbital. This is known as a *d-to-d transition*. [6] Ultraviolet absorption is indicated by the excitation of a filled molecular orbital to the next higher energy orbital. Typically this consists of a transition from a nonbonding *p* or bonding π-orbital to an antibonding orbital (π* or σ*). [7]

2.0 Materials and Methods

2.1 Formation of Glutaric Acid Anhydride

In order to study the stability of lipid layers on multiple surfaces, N-glutarylphosphatidylethanolamine (N-glutaryl-PE) must first be synthesized. Essentially, it is simply 1, 2-dipalmitoyl-*sn*-phosphoethanolamine (DPPE) with a five carbon linker group attached to DPPE's lone nitrogen atom. This will later be reacted with to form a myoglobin linked phospholipid.

To form the anhydride of glutaric acid, 10.6 mg of glutaric acid and 8.1 mg 1-ethyl-3-(3-dimethylaminopropyl)carbodiimide (ECDI) were combined in 2 mL methylene chloride in a 25 mL round bottom flask with a Teflon cap. The flask was capped after nitrogen had been used to purge any remaining air and water vapor. The sealed flask was then stirred at room temperature for 48 hours with a magnetic stir bar. A solution of DPPE (26.28 mg) in 2 mL chloroform and 15 µL of triethylamine were added to the glutaric anhydride/ECDI solution. The reaction mixture was acidified by adding 5 mL chloroform and 4 mL of 0.02 M phosphate/0.02 M citrate buffer (pH 5.5) with vigorous shaking. The aqueous phase was separated by low-speed centrifugation and discarded. The organic phase was dried over anhydrous sodium sulfate. The desired N-

glutaryl-PE was purified by silica-gel column chromatography. The dried chloroform solution was introduced into 1 x 20 m silica-gel column (Fisher 100-200 mesh) and fractions were eluted by passing through the column 50 mL chloroform effluent solutions containing successively, 0, 10, 20, 30 and 50% methanol. Literature states that most of the N-glutaryl-PE is found in the 30% effluent. [8]

2.2 Conjugation of Myoglobin to Liposomes

A 1:10 mixture of DPPE:DPPC (1 μmol/mL:10μmol/mL) was made in a buffer containing 10 mM NaH_2PO_4/0.15M NaCl (pH 5) and then sonicated for 60 seconds to form liposomes. 2.5 mg/mL ECDI was added to solution and left to activate for 1 hour at room temperature. Then 50 μL of 10 mg/ml Mb was added to a 1 mL liposome suspension, plus 50 μL of 150mM NaCl was also added. The pH was adjusted to 8 with NaOH and left to react for 24 hours at 4ºC, after which, the pH was adjusted back to 7 with the use of hydrochloric acid. [8]

2.3 Preparation of nanoparticle Supported Multibilayer

Once the final Mb-attached liposomes were formed, they were then fused onto an ATR surface, as well as a reflective aluminum surface, through the process of evaporative formation. A gentle stream of nitrogen gas was used to evaporate the water solvent, leaving a thin-film of lipid multi-layers on the ATR or aluminum surface. A small amount of PBS buffer (25 μL for the diamond ATR IRE, 1 mL for the ZnSe or germanium ATR IRE) was then used to rehydrate the sample. This process was used to form films above a previously prepared layer of PS nanoparticles.

2.4 *Preparation of Random Close-Packed Nanoparticle Layers*

A polystyrene "latex" nanosphere dispersion in water was acquired from Alfa Aesar (100 nm diameter, 2.5 wt %, Stock # 42712, Lot # H25Q22, CAS # 9003-53-6). This dispersion was diluted in water one hundred-fold into a weight percent of 0.025%.

The process of evaporative formation was then used to evaporate 25 μL aliquots to form a randomly close-packed layer of PS nanospheres.

2.5 *FTIR Spectroscopy*

All FTIR spectra were recorded with a Digilab (Randolf, MA) FTS 7000 FTIR spectrometer equipped with a liquid nitrogen-cooled mercury cadmium telluride (MCT) detector and a DuraSample*IR* II ATR (SenseIR Technologies). Spectra were collected over the range 4000 cm^{-1} to 400 cm^{-1} with a resolution of 4 cm^{-1}. Each spectrum was produced by the coaddition of 256 scans.

2.6 UV/Vis Spectroscopy

Reflection-absorption UV/Vis spectroscopy was used to qualitatively analyze the myoglobin-based thin-films on a reflective aluminum surface. The thin-films were formed using the process of evaporative formation for both the randomly packed nanosphere layer and the above conjugated-phospholipid layer. Spectra were taken of the thin-film while the myoglobin was in an unbound state, as well as in the presence of 10 mM sodium cyanide or 10 mM sodium azide. The spectra were obtained using an Ocean

Optics UV/Vis spectrometer along with the dip probe. An independent light source using a tungsten filament was used in conjunction with the dip probe to acquire the data. A schematic representation of the apparatus is shown below.

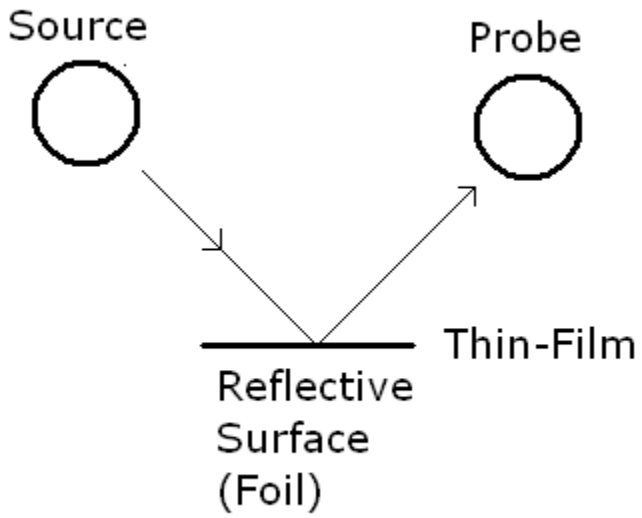

Figure 4.3: A schematic representation of how the reflection-absorption data were obtained.

UV/Vis spectroscopy was used to determine the concentration of myoglobin bound to the lipid dispersion. This was done by centrifuging the final dispersion from section 4.2 and removing the supernatant containing any unbound myoglobin. This supernatant was then diluted and subjected to UV/Vis spectroscopy as measured at 409 nM. Since the amount of myoglobin added to the dispersion initially is a known quantity, the concentration of myoglobin remaining in solution subtracted from that known quantity results in the concentration of covalently bound myoglobin.

2.7 FTIR Spectroscopy

Three different ATR crystals were used in these experiments. These are diamond, ZnSe and germanium. On each of these three crystals was deposited a randomly packed layer of PS nanoparticles on which a biomimetic membrane containing myoglobin was placed. The biomimetic membrane is formed from a 1:10 mixture of the phospholipids DPPE and DPPC. To each DPPE molecule present was attached the globular protein myoglobin, which serves as a selective biological element for recognition of binding to the anions of cyanide and azide. FTIR was used to capture spectra of the biomimetic surface in its ligand bound and ligand-free states.

3.0 Results and Discussion

Recent studies have shown biomimetic membranes formed by casting lipid vesicles on electrode surfaces may represent a new class of biosensor. Like in these electrode based systems, the optical sensors discussed here provide a biomembrane-like microenvironment. Membrane mimetic behavior coupled with ease of preparation, and long-term stability are of great importance in sensor design.

3.1 UV/Vis Spectroscopy

Reflection-absorption spectra were acquired of the myoglobin based thin-films in its unbound and ligand bound states for qualitative analysis. The unbound state displayed a local absorption maximum at 410 nm, while the cyanide and azide bound states displayed local maxima at 436 and 430 nm, respectively. These spectra show

qualitatively that indeed azide and cyanide are binding to the myoglobin-based thin-films. The thin-films retain behavior similar to myoglobin in solution.

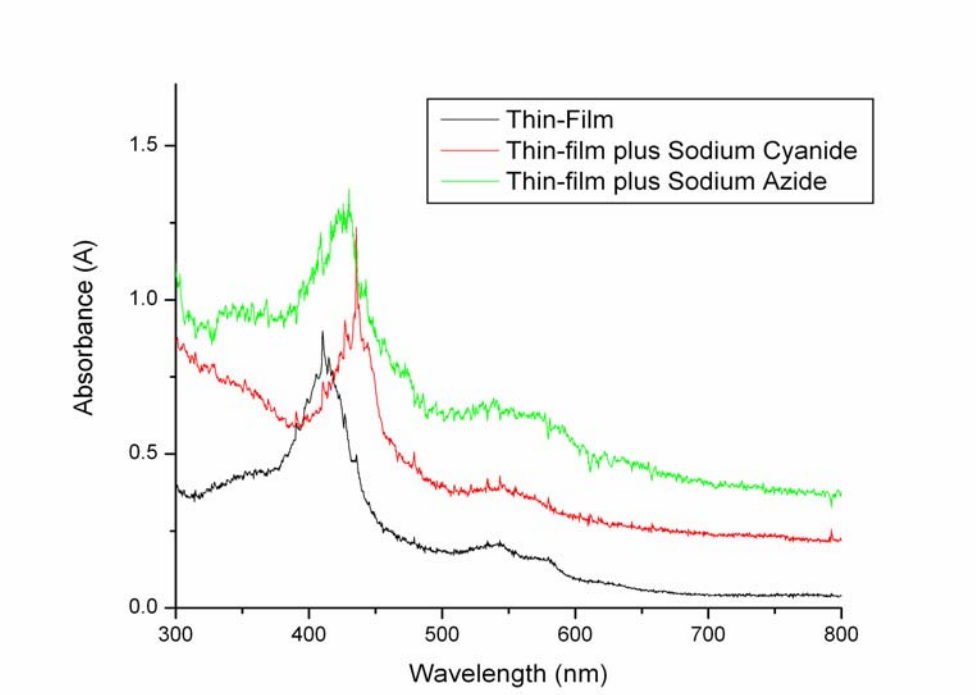

Figure 4.4: UV/Vis reflectance spectra of Myoglobin-based ultrathin layers on a reflective aluminum surface in its unbound (black), cyanide-bound (red) and azide-bound (green) states.

UV/Vis spectroscopy was also used to indirectly determine the concentration of myoglobin covalently bound to DPPE within a lipid dispersion containing DPPC. A traditional calibration curve was obtained using dilute myoglobin concentrations. The absorption of the myoglobin left in solution was measured, and a concentration of 0.03353 mg/mL was determined. This number was subtracted from 0.04762 mg/mL, which was the concentration of myoglobin originally added to the activated lipid

dispersion. This results in a difference of 0.014 mg/mL, which is the approximate concentration of myoglobin in the final lipid dispersion.

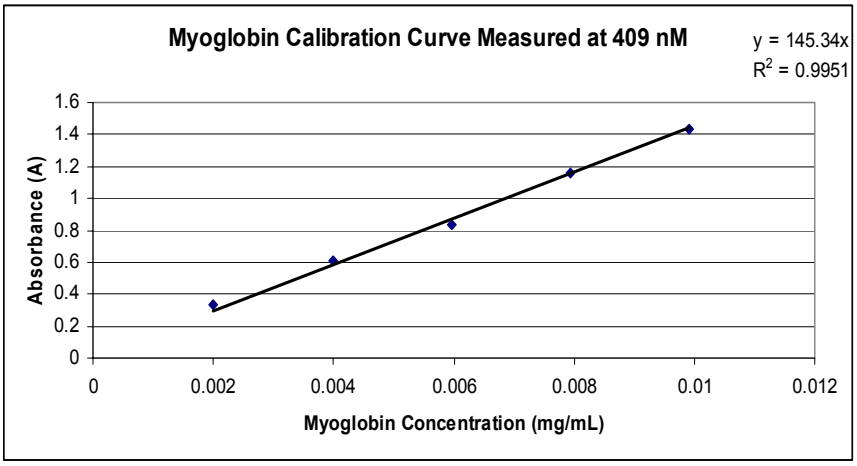

Figure 4.5: The calibration curve used to determine the concentration of myoglobin present in the supernatant resulting from the final lipid dispersion, which leads to the determination of lipid-bound myoglobin.

3.2 *FTIR Spectroscopy*

The diamond ATR internal reflection element (IRE) displays a significant absorption band between approximately 2300 cm^{-1} and 1900 cm^{-1}. As such, the diamond ATR IRE was not useful for analyzing cyanide and azide absorption due to the fact that this intense absorption obscures any absorption due to cyanide or azide. As a result, other IRE materials had to be explored. A nine-reflection zinc selenide crystal was explored as an alternative IRE, however biomimetic thin-film formation was not stable. This problem was alleviated with the use of a nine-reflection germanium IRE.

Using the germanium IRE, a myoglobin-bound biomimetic thin-film was formed

using a PS nanosphere support. Spectra were taken before and after a 10 mM solution of either sodium azide or sodium cyanide was added to the bio-mimetic thin-film. The final spectra containing the ligand-bound states were subtracted from the non-ligand-bound states to further reveal the ligand-bound absorption bands. In the case of sodium azide adsorption on the bio-mimetic thin-film, a noticeable absorption band was found at 2048.3 cm^{-1}. This absorption is due to free azide in solution. Upon further examination of this particular band one can notice another absorption band superimposed on the lower frequency side, with a local maximum at 2023.6 cm^{-1}. This lesser absorption band is close to the published value of 2023.3 cm^{-1}, which is due to heme-bound azide with iron being in a low-spin state.[9, 10] Should the iron have been in a high-spin state, the absorption would have taken place at or near 2045.6 cm^{-1}.

Using the cyanide anion as a ligand for the myoglobin-bound bio-mimetic thin-film, no significant absorption could be found due to cyanide directly or to any heme-bound cyanide. The CN^- stretch band should be found near 2078 cm^{-1}. Nowhere in any spectra obtained could a cyanide absorption band near this wavenumber be attributed. Since this was the case, other spectra were taken of thin-film formed on a PS nanosphere support that was formed with cyanide mixed into the thin-film prior to thin-film formation. Again, no significant absorptions due directly to cyanide or heme-bound cyanide could be attributed.

There were also characteristic absorption bands in the region near 1600 cm^{-1} in the azide difference spectra that are unique when compared to the same region in the cyanide difference spectra. The most prominent of these bands is at 1546.9 cm^{-1} for the azide difference spectra. This corresponds to the amide II region. Other prominent peaks

relating to the amide I region is displayed by the azide difference spectra at 1655.4 cm^{-1} and 1646.7 cm^{-1}, whereas in the cyanide difference spectra the two most prominent absorption band appear at 1610.1 cm^{-1} and 1588.9 cm^{-1}. The azide difference spectra show a similar peak at 1611.5 cm^{-1}. It should be noted that the negative peak at approximately 1732 cm^{-1} is due to slight loss of the thin-film during the course of the experiment.

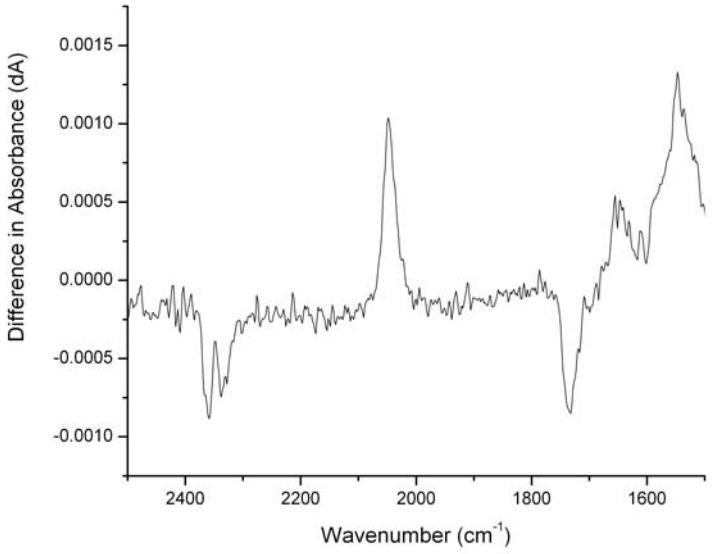

Figure 4.6: Infrared difference spectra of the azide-bound PS nanosphere supported bio-mimetic thin-film minus the unbound state.

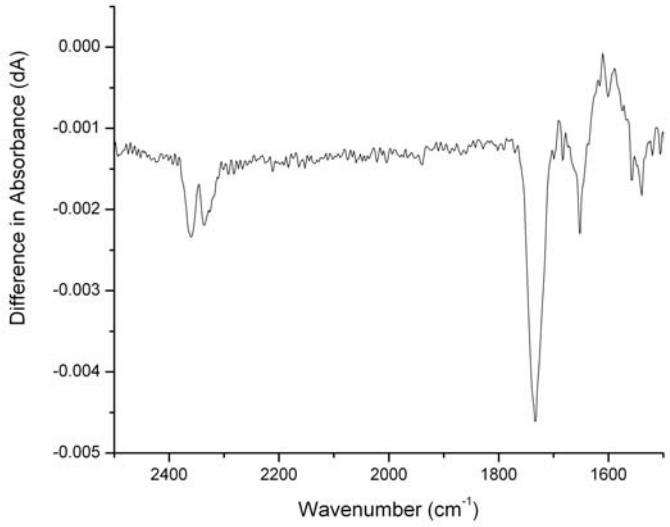

Figure 4.7: Infrared difference spectra of the cyanide-bound PS nanosphere supported bio-mimetic thin-film minus the unbound state.

4.0 Conclusions

When there was excess of ligand present as compared to the concentration of myoglobin, the presence of bound azide could still be determined by means of ATR-FTIR spectroscopy. This can be shown by the absorption band found at 2023.6 cm^{-1} which is due to heme-bound antisymmetric azide stretch in the low-spin state. The ultraviolet reflection-absorption shift between the unbound thin-film and azide-bound thin-film further demonstrates that azide is indeed binding to the myoglobin-based thin-film.

The binding of cyanide to the myoglobin-based thin-film is less conclusive. The UV/Vis reflection absorption data suggest that cyanide is binding to the thin-film. However, the ATR-FTIR data does not display any absorption due to cyanide in either a

bound or unbound state. This is most likely due to the lower extinction coefficient of cyanide versus azide.

In conclusion, the myoglobin-based ultrathin layers can be used as a model for biosensor design. It is clear that the design of this thin-film retains the native activity of the myoglobin protein. Azide can be seen binding directly to the iron-heme its infrared spectra. Though cyanide was not seen binding directly in the infrared spectra obtained, UV/Vis analysis shows that the cyanide is binding to the heme. Other molecules that can be used to study this design include CO, NO and SCN^-.

References:

1. Ordway, G.A. and Garry, D. J. 2004. Myoglobin: an essential hemoprotein in striated muscle. Journal of Experimental Biology 207: 3441–3446.
2. Lodish, H., Berk, A.,. Zipursky, L.S, Matsudaira, P., Baltimore, D. and Darnell, J. 2000. Evolutionary tree showing the globin protein family members myoglobin and hemoglobin. Molecular Cell Biology. Fourth Edition, W. H. Freeman.
3. Kendrew, J.C., Bodo, G., Dintzis, H.M., Parrish, R.G., Wyckoff, H., and Phillips, D.C 1958. A Three-Dimensional Model of the Myoglobin Molecule Obtained by X-Ray Analysis. Nature 181: 662-666.
4. Collman, J. P., Brauman, J. I., Halbert, T. R., and Suslick, K. S. 1976. Nature of Oxygen and Carbon Monoxide Binding to Metalloporphyrins and Heme Proteins. Proceedings of the National Academy of Sciences of the United States of America 73 (10): 3333-3337.

5. Eggins, B. 1996. *Biosensors: An Introduction.* Chichester: John Wiley & Sons.

6. Kotz, J.C., and Treichel, Jr., P. 1996. *Chemistry & Chemical Reactivity*. *3rd Ed.* Fort Worth: Saunders College Publishing.

7. Silverstein, R.M., Bassler G.C. and Morrill, T.C. 1974. *Spectrometric Identification of Organic Compounds. 3rd Ed.* New York: John Wiley & Sons, Inc.

8. V.T. Kung and C.T. Redemann. 1986. Synthesis of Carboxyacyl Derivatives of Phosphatidylethanolamine and Use as an Efficient Method for Conjugation of Protein to Liposomes. Biochim. Biophys. Acta. 862: 435-439.

9. Jung, C., 2000. Insight into protein structure and protein-ligand recognition by Fourier transform infrared spectroscopy. Journal of Molecular Recognition. 13: 325-351.

10. Bogumil, R., Hunter, C.L., Maurus, R., Tang, H., Lee, H., Lloyd, E., Brayer, G.D., Smith and M., Mauk, A.G., 1994. FTIR Analysis of the Interaction of Azide with Horse Heart Myoglobin Variants. Biochemistry 33: 7600-7608.

Chapter 5: Thermotrophic Phase Behavior of Triethylaminated Polystyrene Supported Bilayers

1.0 Introduction

1.1 Modified Polystyrene

Ayres (2008), decribed the substitution of polystyrene-divinylbenzene (PS-DVB) resins created by nucleophilic substitutions of chloromethylated polystyrene-divinylbenzene (Merrifield resin). Polymeric resins generated by reacting Merrifield resin with diethylamine and triethylamine were evaluated for there ability to microectract bacteria from an aqueous suspension. These crosslinked polymers did not form stable layers and were not pursue further. It was ultimately found that by using a polymer with an existing chloride moiety, poly(vinylbenzyl chloride), we were able to skip the chloromethylation step in the polymer synthesis and concentrate on the functionalization of the polystyrene base attempting to use the same chemical techniques describes for the functionalization of Merrifield resin.

In the present study, we investigated the impact of tertiary and quaternary amino polymers on the thermotropic phase behavior of lipid bilayers. The rationalization for this work is an interest in how amino groups impact membrane adhesion. This information is useful for biosensor development and has potential for nanoparticle drug delivery schemes. Cationic polymer nanoparticles can enter cells and alter cell membrane behavior.

2.0 Materials and Methods

2.1 Formation of aminated Polystyrene

The poly(vinylbenzyl chloride) was combined in conjunction with triethylamine or diethylamine (Fluka) in order to produce triethylaminated or diethylaminated polystyrene. The chloride in polyvinyl benzyl chloride provides a good leaving group for nucleophilic substitution.

2.2 Preparation of aminated Polystyrene Layers

Twenty-five microliters of a 0.025 mg/mL solution of triethylaminated or diethylaminated polystyrene in tetrahydrofuran was deposited on a diamond ATR surface. The film was dried under a gentle stream of nitrogen as described previously [1].

2.*3 Preparation of Supported Multi-Bilayer*

solution of 10 mM DPPC in PBS buffer was used to form the supported multi-bilayer. Twenty-five milliliter aliquots were deposited on a diamond ATR surface with a thin-film of triethylaminated or diethylaminated polystyrene already formed. The process of evaporative formation, as discussed in Chapter 4, was used to remove the water solvent from the DPPC in order to form a multi-bilayer supported by the polymer surface.

2.4 *FTIR Spectroscopy*

All FTIR spectra were recorded with a Digilab (Randolf, MA) FTS 7000 FTIR spectrometer equipped with a liquid nitrogen-cooled mercury cadmium telluride (MCT) detector and a DuraSample*IR* II ATR (SenseIR Technologies). Spectra were collected

over the range 4000 cm^{-1} to 400 cm^{-1} with a resolution of 4 cm^{-1}. Each spectrum was produced by the coaddition of 256 scans.

2.5 Data Analysis

The transition temperatures and relative cooperativity were obtained as decribed in Chapter 3.

3.0 Results and Discussion

3.1 Thermal Phase Transitions

In order to observe the pre- and main transitions the samples were heated and subsequently cooled between ranges of approximately ~20°C - 50°C. The thermal phase transitions of DPPC multibilayers were observed on a variety of surfaces including polystyrene (PS), poly(vinyl benzyl chloride) (PVBC), diethylaminated and triethylaminated PVBC. Figure 5.1 depicts the DPPC thermal phase transition of both the PS and PVBC surfaces. Figure 5.2 depicts the DPPC thermal phase transition of diethylaminated and triethylaminated PVBC.

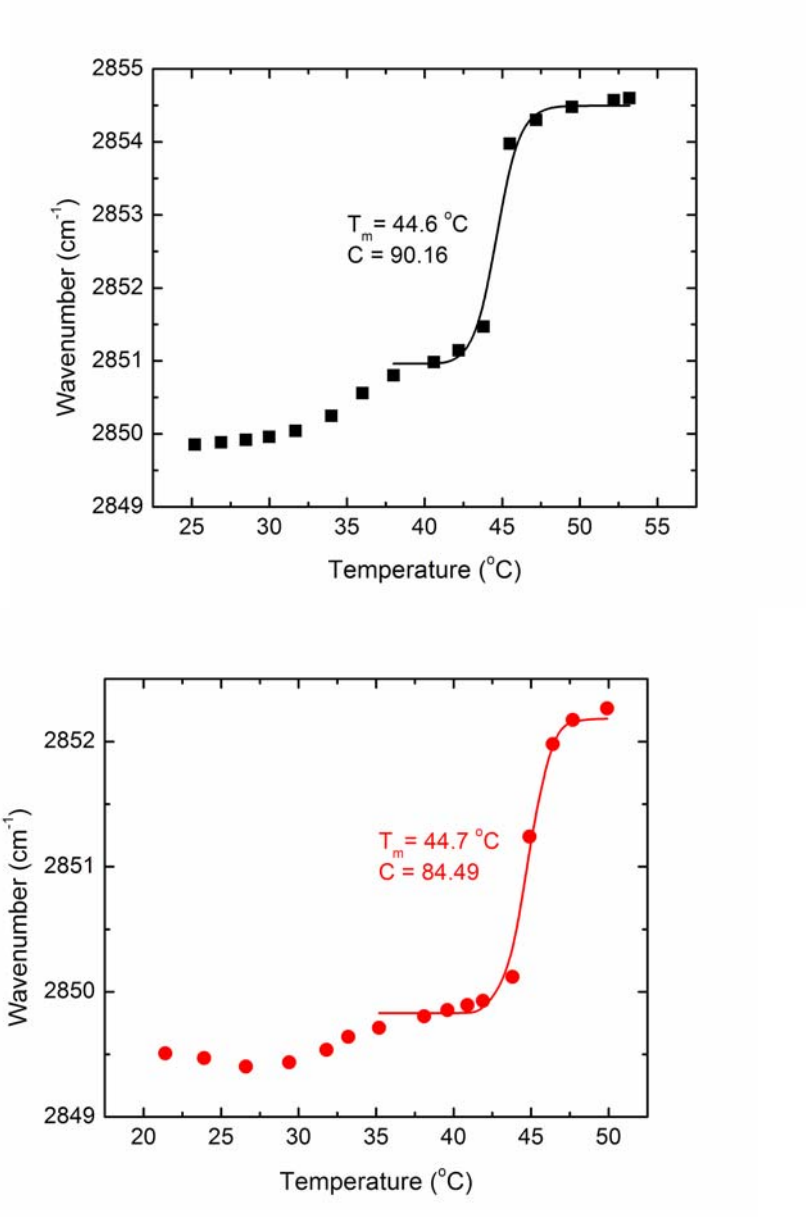

Figure 5.1: The melting phase transition curves for (Top) DPPC multibilayer on Polystyrene (PS); (Bottom) DPPC on Poly(vinyl benzyl chloride) (PVBC).

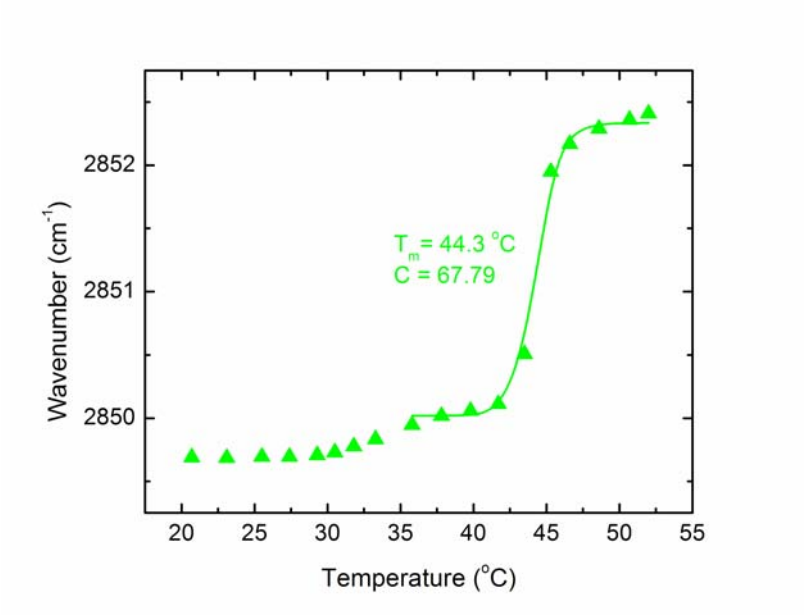

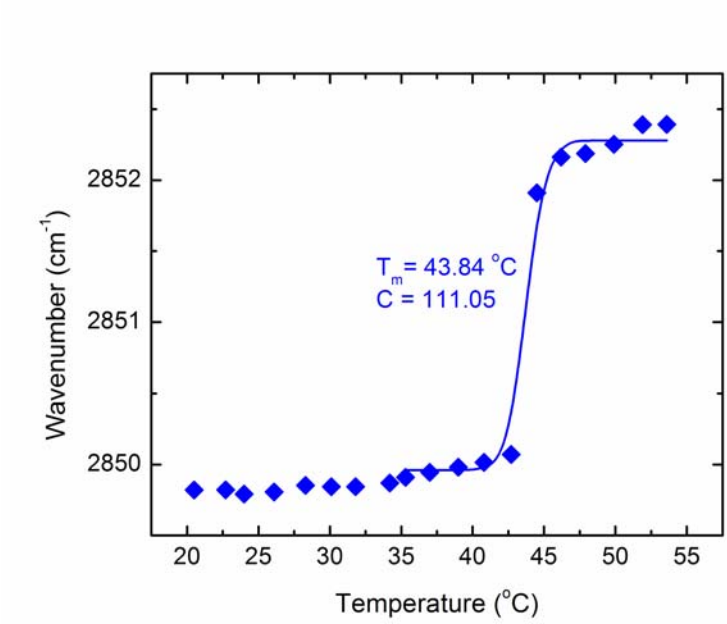

Figure 5.2: The melting phase transition curves for (Top) DPPC multibilayer on diethylaminated PVBC; (Bottom) DPPC on triethylaminated PVBC.

DPPC multibilayers on a PS surface demonstrate a maximum absorbance near 2854.5 cm^{-1}, whereas on a PVBC surface (untreated or di-/triethylaminated) the absorption maxima is no greater then 2852.5 cm^{-1}. Integration of the main transition typically begins near 2850 cm-1, but is closer to 2851 cm-1 in the case of DPPC multibilayers on a PS support. The origin of the apparent polymer effect on CH – stretching frequency is likely the result of differing head group environments [2, 3].

Although both have elevated melting temperatures, as compared to DPPC on bare diamond (44.6 °C and 44.7 °C for PS and PVBC, respectively) these are treated here as the controls to highlight the impact of the amino modification. The origin of the T_m shift for these two polymers (DPPC multibilayers on a diamond surface, T_m = 41.5°C) is not well understood. The increase in melting temperature may arise from the impact of nanostructures on the polymer surfaces (physical in nature). Although interactions between the zwitterionic lipid head group and the π-electrons of the styrene rings cannot be entirely ruled out [4].

The aminated polymers show a reduction in melting temperature. Although both diethyaminated and triethyaminated PVBC resulted in a T_m reduction of less than 1 °C, there appears to be a systematic progression to lower temperature. The tertiary amine generated from diethylamination drops the T_m a modest 0.3 °C, whereas the quaternary amine produce ~1 °C decrease.

All polymer layers studied have measurably higher cooperativity than DPPC on bare diamond (C=31.9). The cooperativity of DPPC multibilayers on PS and PVBC are similar 90.2 and 84.5, respectively. The di- and triethylaminated DVBC surfaces produced a more varied response to cooperativity, but again, both values are statistically

higher then the DPPC alone. Moreover, the triethylaminated surface produced a statistically higher cooperativity value then the diethylaminated DVBC by more then 40 units, thus showing that the triethylaminated surface produced the highest degree of cooperativity during phospholipid chain melting then any other surface examined in this dissertation. It needs to be expressed that the melting temperatures from this set of experiments (chapter 5), though similar to each other, do not quite reach the value of DPPC multibilayer on sulfonated PS nanoparticle surface of 45.5°C (Chapter 3).

The surface modification in the aminated polymers is estimated to be in the range of the 3% sulfonation seen for the nanobeads. Therefore it appears that a slight negative surface charge stabilizes the bilayers and a slight positive charge results in an almost equal reduction in membrane stability. A similar reduction in T_m occurs with monovalent cations and lipid vesicles [5].

4.0 Conclusions

The high degree of cooperativity observed for PS and PVBC surfaces is not easily explainable and at the writing of this dissertation no similar result has been found in the literature. The PS used in this present experiment was not negatively charged as with the PS nanospheres used in Chapter 3. The PS and PVDC film appear to increase the cooperative unit size in a fashion similar to the nanobeads discussed earlier, despite the lack of a charge moiety. This being said, it is difficult to imagine how particle size and shape as well as film surface architecture would produce a similar cooperative unit size. But the base polystyrene polymer does influence the phase behavior of the lipid which it

supports. The impact of charged groups appears to be separate from this larger base polymer influence.

	PS	PVBC	Ditheylaminated PVBC	Triethylaminated PVBC	Diamond	PS nanospheres
T_m	44.6 +/- 0.1	44.7 +/- 0.1	44.3 +/- 0.1	43.8 +/- 0.1	41.5 +/- 0.5	45.5 +/- 0.1
C	90 +/- 13	89 +/- 13	68 +/- 7	111 +/- 25	32 +/- 7	90 +/- 12

Table 5.1: Melting temperatures and cooperativity in the melting direction of DPPC multibilayers on varying polymer surfaces.

The di- and triethylaminated DVBC possess a positively charged nitrogen atom in addition. It is believed that the charged nitrogen atom from the di- or triethylaminated PVCB interdigitates between the phospholipid chains and interacts with the lipids phosphate group. This would leave the positively charged nitrogen atom located on the DPPC molecule to be left buried into the chain of the polymer. This is in complete distinction to Chapter 3 where the partially negative nanobeads are believed to interact with the positively charged head group of DPPC, where no intercalation is believed to take place. This intercalation may be responsible for the relatively high degree of cooperativity expressed by the triethylaminated DVBC. It should be noted that the degree of cooperativity for the diethylaminated DVBC was statistically higher then that of DPPC multibilayers on diamond, while simultaneously lower then that of DPPC on sulfonated PS nanospheres. Perhaps since the triethylaminated DVPC is allowed to penetrate further into the phospholipid membrane then the diethylaminated species, thus accounting for the higher cooperativity.

References:

1. Aryes, P.R., 2008. *Investigating Bacterial Interactions with Polymer Surfaces using Attenuated Total Reflectance Fourier Transform Infrared Spectroscopy.* University of Denver, Denver.

2. Maranas, J.K., 2005. *The influence of Environment on Dynamics of Polymers and Biological Molecules.* Abstracts of Papers, 230th ACS National Meeting, Washington, D.C., United States, Aug. 28 – Sept 1.

3. El Maghraby, G.M.M., Williams, A.C. and Barry, B.W. 2005. *Drug Interaction and Location in Liposomes: Correlation with Polar Surface Areas.* International Journal of Pharmaceutics. 292: 179 – 185.

4. Arbuzova, A., Wang, L., Wang, J., Hangyas-Mihalyne, G., Murray, D., Honig, B., and McLaughlin, S. 2000. *Membrane Binding of Peptides Containing Both Basic and Aromatic Residues. Experimental Studies with Peptides Corresponding to the Scaffolding Region of Caveolin and the Effector Region of MARCKS.* Biochemistry, 39: 10330-10339.

5. Gurtovenko, A.A. 2005. *Effect of Monovalent Salt on Cationic Lipid Membranes as Revealed by Molecular Dynamics Simulations.* Journal of Physical Chemistry B, 109: 21126 – 21134.